Aus dem Experimental and Clinical Research Center
der Medizinischen Fakultät Charité – Universitätsmedizin Berlin
und des Max-Delbrück-Zentrums für Molekulare Medizin Berlin

DISSERTATION

The role of glycoprotein 130 and the JAK/STAT-pathway in sepsis-induced muscle atrophy

Die Rolle von Glykoprotein 130 und dem JAK/STAT-Signalweg in der sepsisinduzierten Muskelatrophie

zur Erlangung des akademischen Grades
Medical Doctor - Doctor of Philosophy (MD/PhD)

vorgelegt der Medizinischen Fakultät
Charité – Universitätsmedizin Berlin

von

Lukas Zanders

Erstbetreuung: Prof. Dr. Jens Fielitz

Datum der Promotion: 23.03.2024

Table of Contents

List of Tables

List of Figures

List of Abbreviations

Abbreviation	Full Name
ADAM17	Disintegrin and Metalloproteinase Domain-Containing Protein 17
AG490	Tyrphostin AG490
AKT	Protein kinase B
AP-1	Activator protein 1
ATP	Adenosine triphosphate
ATPase	Adenosine 5'-Triphosphatase
BSA	Bovine serum albumin
CASP	Colon Ascendens Stent Peritonitis
CASPI	Colon Ascendens Stent Peritonitis with Intervention
cDNA	Complementary DNA
CIM	Critical Illness Myopathy
CIP	Critical Illness Polyneuropathy
cKO	Conditional knockout
CLP	Cecal ligation and puncture
Cntf	Ciliary neurotrophic factor
Cntfr	Ciliary neurotrophic factor receptor
CRE	Cre recombinase
Ctf1	Cardiotrophin 1
DAVID	Database for Annotation, Visualization and Integrated Discovery
DMEM	Dulbecco's Modified Eagle Medium
DMSO	Dimethyl sulfoxide
EDL	Extensor digitorum longus muscle
ELISA	Enzyme-linked immunosorbent
ERK	Extracellular Signal-Regulated Kinase
FBS	Fetal Bovine Serum
Fbxo32	F-box only Protein 32
FHRE	Forkhead Response Element
FOXO3	Forkhead Box O3
GAPDH	Glyceraldehyde 3-phosphate dehydrogenase
GLUT4	Glucose transporter 4
GO-Term	Gene Ontology Term
GP	Gastrocnemius plantaris muscle
gp130	Glycoprotein 130
HRP	Horseradish peroxidase
HUVEC	Human umbilical vein endothelial cells
ICU	Intensive Care Unit
ICUAW	Intensive Care Unit Acquired Weakness
IGF-1	Insulin-like growth factor 1

IKK-2	Inhibitor of NF-κB kinase subunit beta
IL-1β	Interleukin 1β
IL-6	Interleukin 6
IL-6R	Interleukin 6 receptor
Il11	Interleukin 11
Il11ra1	Interleukin 11 receptor subunit alpha-1
Il11ra2	Interleukin 11 receptor subunit alpha-2
Il12ra	Interleukin 12 receptor subunit alpha
Il12rb	Interleukin 12 receptor subunit beta
Il27	Interleukin 27
Il27ra	Interleukin 27 receptor subunit alpha
Il31	Interleukin 31
Il31ra	Interleukin 31 receptor subunit alpha
IRS-1	Insulin receptor substrate 1
JAK	Janus kinase
KEGG	Kyoto Encyclopedia of Genes and Genomes
KO	Knockout
Lif	Leukemia inhibitory factor
Lifr	Leukemia inhibitory factor receptor
loxP	Locus of X-over P1
LPS	Lipopolysaccharide
MAFbx	Muscle Atrophy F-box gene
MAPK	Mitogen-Activated Protein Kinase
MCSA	Myocyte cross sectional area
MHC	Myosin Heavy Chain
mRNA	Messenger Ribonucleic acid
MRC	Medical Research Council
MSC	Muscle satellite cells
MuRF1	Muscular RING (really interesting new gene) Finger 1
NF-κB	Nuclear Factor kappa light chain enhancer of activated B-cells
Osm	Oncostatin M
Osmr	Oncostatin M receptor
PBS	Phosphate buffered saline
PI3K	Phosphoinositide 3-kinase
qRT-PCR	Quantitative real-time polymerase chain reaction
RAF	Rapidly Accelerated Fibrosacroma
RAS	Rat Sarcoma Virus
rIL-6	Recombinant interleukin 6
RNA	Ribonucleic acid
RNAseq	Ribonucleic acid sequencing
SAA1	Serum amyloid A1

SCF	Skp1-Cul1-F-box protein
SDS	Sodium dodecyl sulfate
sgp130	Soluble glycoprotein 130
SHP-2	Src homology region 2 domain-containing phosphatase 2
sIL-6R	Soluble interleukin 6 receptor
siRNA	Small interfering ribonucleic acid
SOCS	Suppressor of Cytokine Signaling
SOFA	Sequential Organ Failure Assessment Score
SOL	Soleus muscle
SRE	Serum Response Element
STAT	Signal transducer and activator of transcription
TA	Tibialis anterior muscle
TBS-T	TRIS-buffered saline Tween
TF	Transcription Factor
TNFα	Tumor necrosis factor alpha
Trim63	Tripartite Motif Containing 63
TRIS	Tris(hydroxymethyl)aminomethane
UPS	Ubiquitin Proteasome System
WT	Wildtype

Abstracts

German Version

Hintergrund: Bis zu 90% septischer Patient*innen entwickeln eine Muskelschwäche, die früh im Krankheitsverlauf auftritt und mindestens 5 Jahre nach der Entlassung persistiert. Ursächlich ist eine Muskelatrophie mit reduzierter Proteinsynthese und gesteigertem -abbau. Dieser wird insbesondere durch das Ubiquitin-Proteasom-System mit der E3 Ubiquitin Ligase *Tripartite Motif Containing 63* (*Trim63)*/Muscle Really Interesting New Gene Finger 1 (MuRF1) und dem F-Box Protein *F-box only Protein 32* (*Fbxo32)*/Atrogin-1 vermittelt.
Erhöhte Plasmawerte von Interleukin 6 (IL-6) sind ein Risikofaktor für die Entwicklung einer Muskelatrophie in kritisch kranken Patient*innen, die überdies eine Beeinträchtigung muskulärer Insulin-induzierter Signalwege zeigen. In Mäusen mit Tumorerkrankungen vermittelt IL-6 Muskelatrophie über den Glykoprotein 130 (gp130)/Januskinase 2 (JAK2)/Signal Transducer and Activator of Transcription 3 (STAT3) -Signalweg. Die hier vorgelegte Studie hatte zum Ziel, die Rolle der IL-6-induzierten Signalwege in der Sepsis-assoziierten Muskelatrophie zu untersuchen.

Methodik: Aus Skelettmuskelbiopsien kritisch kranker Patient*innen wurde eine quantitative Real-Time-Polymerase Kettenreaktion durchgeführt. Aus Skelettmuskeln septischer Mäuse wurde Ribonukleinsäure (RNA) isoliert und sequenziert (RNAseq). Die Effekte des gp130/JAK2/STAT3- und des Phosphoinositolkinase 3 (PI3K)/Proteinkinase B (AKT)-Signalweges auf Protein- und messenger RNA (mRNA)-Expression, sowie Muskelatrophie wurde in C2C12 Myotuben nach Behandlung mit IL-6 und/oder Insulin untersucht. In Mäusen mit einer muskelspezifischen Deletion von *Interleukin 6 signal transducer* (*Il6st)*, dem kodierenden Gen für gp130, sowie Wildtyp Mäusen, die mit dem JAK2-Inhibitor Tyrphostin AG490 behandelt wurden, wurde mittels Ligatur und Punktion des Caecums (CLP) eine Sepsis induziert. In Muskeln wurde anschließend der Phänotyp der Atrophie, die induzierten Signalwege, die Protein- sowie mRNA-Expression analysiert.

Ergebnisse: In Muskeln kritisch kranker Patient*innen zeigte sich eine erhöhte mRNA-Expression des IL-6 Zielgens *Suppressor of Cytokine Signaling 3* (*SOCS3)*. Das RNAseq zeigte eine Aktivierung des JAK/STAT-Signalweges und eine Inhibition der

insulininduzierten Signalwege in Muskeln septischer Mäuse. IL-6 inhibierte die Insulin-induzierte AKT-Phosphorylierung und induzierte Atrophie in Myotuben *in vitro*, die durch einen Knockdown von *Il6st*, sowie die Inhibition von JAK2 oder STAT3 attenuiert wurden. Eine muskelspezifische Deletion von *Il6st* blockierte die Reduktion der AKT-Phosphorylierung in Muskeln septischer Mäuse. Tiere mit *Il6st*-Deletion zeigten eine Reduktion der sepsisinduzierten Muskelatrophie, der Aktivierung des JAK/STAT-Signalweges und des MuRF1 Proteingehalts. Die JAK2-Inhibition reduzierte die Muskelatrophie in septischen Mäusen, sowie die *Trim63*/MuRF1 und *Fbxo32*/Atrogin-1 Expression.

Fazit: Der gp130/JAK2/STAT3-Signalweg vermittelt sepsisinduzierte Muskelatrophie.

English Version

Background: Up to 90% of critically ill patients with sepsis develop intensive care unit-acquired weakness (ICUAW), which can persist for at least 5 years after discharge. Muscle atrophy occurs early in the course of the disease and is caused by a disturbed muscular protein homeostasis with impaired protein synthesis and increased breakdown, primarily via the ubiquitin-proteasome system with the E3 ligase *Tripartite Motif Containing 63* (*Trim63)*/Muscle Really Interesting New Gene Finger 1 (MuRF1) and the F-Box protein *F-box only Protein 32* (*Fbxo32)*/Atrogin-1. Increased interleukin-6 (IL-6) plasma levels are an independent risk factor for the development of ICUAW. In a murine model of cancer cachexia, the IL-6 receptor glycoprotein 130 (gp130) mediates muscle atrophy via the Janus kinase 2 / Signal transducer and activator of transcription 3 (JAK2/STAT3) signaling pathway. The aim of this study was to investigate the role of IL-6-induced signaling pathways in sepsis-induced muscle atrophy.

Methods: Quantitative Real-Time Polymerase Chain Reaction was performed to measure Suppressor of Cytokine Signaling 3 (*SOCS3)* messenger ribonucleic acid (mRNA) expression in muscles of critically ill patients. The cecal ligation and puncture (CLP) procedure was used to induce sepsis in mice. Sequencing of bulk RNA (RNAseq) isolated from muscles of septic mice was performed. The effects of the gp130/JAK2/STAT3 and insulin/Phosphoinositide 3-kinase / Protein kinase B (PI3K/AKT) pathway were investigated by analyzing myotube diameter, mRNA expression, and protein levels in C2C12 myotubes after IL-6 and/or insulin treatment with and without pathway inhibition. Mice with a deletion of the Interleukin 6 signal transducer (Il6st), encoding gp130, in myocytes (*Il6st*$^{-/-}$) were subjected to CLP. Additionally, mice were treated with the JAK2 inhibitor, Tyrphostin AG490. Muscle atrophy was investigated by morphological and molecular analyses.

Results: The mRNA expression of the IL-6 target gene Suppressor of Cytokine Signaling 3 (*SOCS3*) was increased in skeletal muscle of critically ill patients. RNAseq revealed an activation of JAK/STAT-signaling and a decrease in insulin-signaling in muscles of septic mice. IL-6-induced C2C12 myotube atrophy was attenuated by knockdown of *Il6st* and inhibition of JAK2- and STAT3. Co-treatment of C2C12 myotubes with IL-6 blocked insulin-induced AKT phosphorylation. Sepsis-induced activation of the JAK/STAT-

pathway and muscle atrophy were reduced in *Il6st*$^{-/-}$ mice. Loss of *Il6st* in myocytes resulted in lower protein content of MuRF1. Sepsis-induced muscle atrophy was attenuated by treatment with AG490. Inhibition of the JAK/STAT-pathway was accompanied by a reduction in *Fbxo32*/Atrogin-1 and *Trim63*/MuRF1 mRNA and protein contents. Sepsis-induced attenuation of AKT phosphorylation was blocked by loss of *Il6st*.

Conclusion: The gp130/JAK2/STAT3 pathway mediates sepsis-induced muscle atrophy.

1 Introduction

Skeletal muscles constitute the largest organ system within the human body, serving a multitude of pivotal roles, that range from respiratory mechanics to locomotion and preservation of skeletal integrity. The function of skeletal muscles relies on the maintenance of muscle metabolism and mass, which is regulated by a tightly orchestrated homeostasis. Skeletal muscles possess dynamic capacities to balance requirements in contractile force and metabolic efficiency. Pathologic conditions, such as critical illness, can disrupt this homeostasis leading to compromised muscle structure and function.

1.1 Anatomy and physiology of skeletal muscles

Skeletal muscles facilitate movement through contractions, which result in joint movement of bones they are attached to via tendons. Muscles are surrounded and compartmentalized by fibrous sheaths, which divide each muscle into muscle bundles and fascicles, which contain tube-shaped syncytial muscle cells called myofibers (Fig. 1, left panels). The functional units responsible for muscle contraction, known as sarcomeres, are found within these myofibers. Between the myofiber cell membrane and the surrounding basal membrane, multipotent stem cells called muscle satellite cells (MSCs) are located [1].
Sarcomeres are cylindrical units organized in cellular organelles, called myofibrils, and consist of longitudinally spanned actin filaments attached to the Z line at both ends. Within the sarcomere, thick filaments, connected to the Z line by titin molecules, are located alongside the thin actin filaments. The shortening of myosin heavy chains (MyHCs) in the thick filaments leads to the shortening of the sarcomere, resulting in muscular contraction (Fig. 1 right upper panel) [1].

Various MyHC isoforms serve specialized functions in different muscle tissues. In skeletal muscles, MyHC I (slow-twitch), MyHC IIa (fast-twitch), MyHC IIb (fast-twitch) and MyHC IIx (fast-twitch) are the predominant isoforms [2].
Skeletal muscles primarily involved in endurance exercise and postural maintenance, like the erector spinae muscles, have a higher abundance of slow-twitch / type I myofibers,

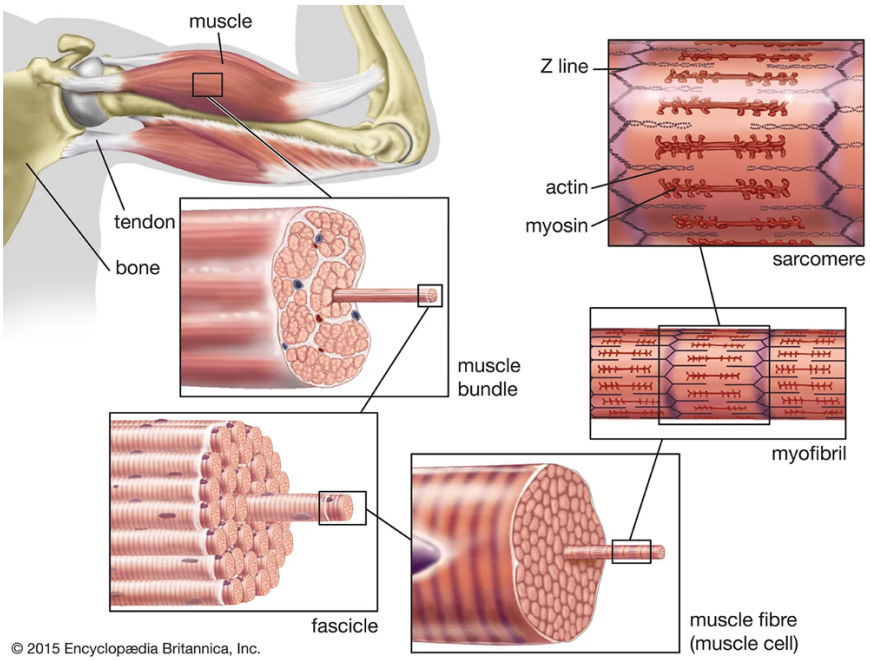

Figure 1 Muscle anatomy and histology. Left upper panel: Skeleton, biceps and triceps muscles with their according origin and insertion tendons of the human left upper extremity. **Left mid panel:** The macroscopic sub-structure of skeletal muscles with muscle fascicles separated by the fibrous perimysium. **Left lower panel, right lower panel**: The muscle fascicles contain syncytial muscle cells, termed muscle fibers. **Right mid panel**: The muscle fiber is further divided into myofibrils, that contain the functional unit of muscles, the sarcomere. **Right upper panel**: The sarcomere is confined by the Z lines containing the thin, actin containing, and thick, myosin containing filaments. Reprinted from Encyclopædia Britannica (https://www.britannica.com/science/human-muscle-system#/media /1/1346474 /46939) with permission of Encyclopaedia Britannica, Inc.

primarily containing MyHC I. Conversely, muscles composed of fast-twitch (type II) myofibers, such as the vastus lateralis muscle, are rich in MyHC IIa, b and x. The composition of fiber types within muscles varies between species and individuals and are influenced by functional demand [1, 2].

1.2 Myogenesis and skeletal muscle plasticity

During embryonic development, skeletal muscles, like other muscle tissues, originate from the mesoderm. Stem cells within the mesoderm differentiate into MSCs. These multipotent stem cells further differentiate into myoblasts, which then fuse to form myocytes, ultimately leading to the formation of myofibers. The size of the myofiber syncytium is mainly confined by the ratio of nuclei to cytoplasm, and additional myoblast fusion can increase this ratio [1, 3].

In adult skeletal muscle, muscle mass is regulated by a homeostasis between protein synthesis and degradation of sarcomeric proteins. Upon demand, myofibers adapt through hypertrophy, involving the synthesis of structural sarcomeric components. Hypertrophy relies on the asymmetric division of MSCs to maintain the stem cell pool and the nuclei-to-cytoplasm ratio in the setting of increased intracellular structural proteins and hence intracellular volume [3].

During periods of inactivity and disease, myofibers undergo atrophy, a reduction in their content of structural proteins, leading to a decrease in volume. Muscle atrophy occurs in response to muscle disuse or pathological conditions such as loss of innervation or inflammatory diseases [4-6].
Mechanistically, a disrupted protein homeostasis in myofibers results in decreased protein synthesis and increased degradation, primarily mediated by the ubiquitin-proteasome-system (UPS) [6-8].

The UPS functions through a two-step process: proteins are tagged through polyubiquitination, and the ubiquitinated proteins are then selectively degraded by the 26S proteasome. Ubiquitination is mediated through ubiquitin ligases. E1 and E2 ligases are responsible for the transfer of ubiquitin molecules to target proteins [9].
E3 ligases play a pivotal role in substrate specificity, with RING (Really Interesting New Gene) and SCF (Skp1-Cul1-F-box protein) families being prominent structural families [7, 8]. In skeletal myofibers, the main E3 ligases involved in degradation of sarcomeric proteins are Muscle RING Finger 1 (MuRF1) and F-box protein Atrogin-1 [7, 8]. These E3 ligases primarily target skeletal MyHC and are essential for muscle atrophy. Knockout (KO) of *Tripartite Motif Containing 63 (Trim63),* the encoding gene of MuRF1 or *F-box-only protein 32 (Fbxo32)*, the encoding gene of Atrogin-1, protect mice from muscle atrophy after denervation and lead to higher protein contents of different MyHC isoforms compared to wild-type (WT) controls [7, 10]. Patients with muscle atrophy show increased protein contents of these “atrogenes” (MuRF1 and Atrogin-1) in skeletal muscles.

1.3 Interleukin 6-induced intracellular signaling

Interleukin 6 (IL-6) was initially identified as a pro-inflammatory cytokine involved in the humoral immune system [11]. Over the past decades, diverse functions have been

elucidated, encompassing regenerative, hematopoietic and metabolic roles [12-14]. Notably, IL-6 is secreted by skeletal myocytes and plays key roles in the regulation of skeletal muscle integrity and plasticity [15-17].

IL-6 exerts intracellular signaling through two mechanisms: the classical pathway, where it binds to membrane-bound Interleukin 6 receptor (IL-6R), and the trans-signaling pathway, where it binds to a soluble form of IL-6R (sIL-6R). These two signaling mechanisms induce dimerization of glycoprotein 130 (gp130), while exerting distinct cellular effects. While classical IL-6 signaling primarily mediates regenerative and metabolic effects, trans-signaling promotes pro-inflammatory effects. Most tissues exert low membrane-bound IL-6R expression levels. Thus IL-6-induced cellular effects mainly rely on trans-signaling, particularly during inflammatory states. The beta receptor gp130 is ubiquitously expressed and exhibits high expression levels in skeletal muscles [18]. Endogenous inhibition of trans-signaling is primarily mediated by soluble gp130 (sgp130), which binds to circulating IL-6/sIL-6R complexes and prevents binding to membrane bound gp130 (Fig.2). Notably, sgp130 only inhibits trans-signaling [19].

Upon binding of IL-6 to IL-6R, gp130 dimerizes and can activate three signaling pathways: the Janus Kinase (JAK) / Signal Transducer and Activator of Cytokine Signaling (STAT), the Phosphoinositide 3-Kinase (PI3K) / Protein Kinase B (AKT) and the Rat Sarcoma (RAS) / Mitogen-Activated Protein Kinase (MAPK) signaling pathway (Fig. 2) [19].

However, While there are conflicting data on systemic IL-6R antibody treatment, specifically inhibiting the trans-signaling pathway increases survival in septic mice [20, 21].

1.4 Intensive Care Unit Acquired Weakness

Skeletal muscle atrophy and weakness is a common and severe complication observed in critically ill patients, affecting up to 90% of those admitted to the intensive care unit (ICU) with severe sepsis. The condition, known as Intensive Care Unit Acquired Weakness (ICUAW) is associated with increased morbidity and mortality, occurs early in the disease course and persists for at least five years after discharge [22-24].

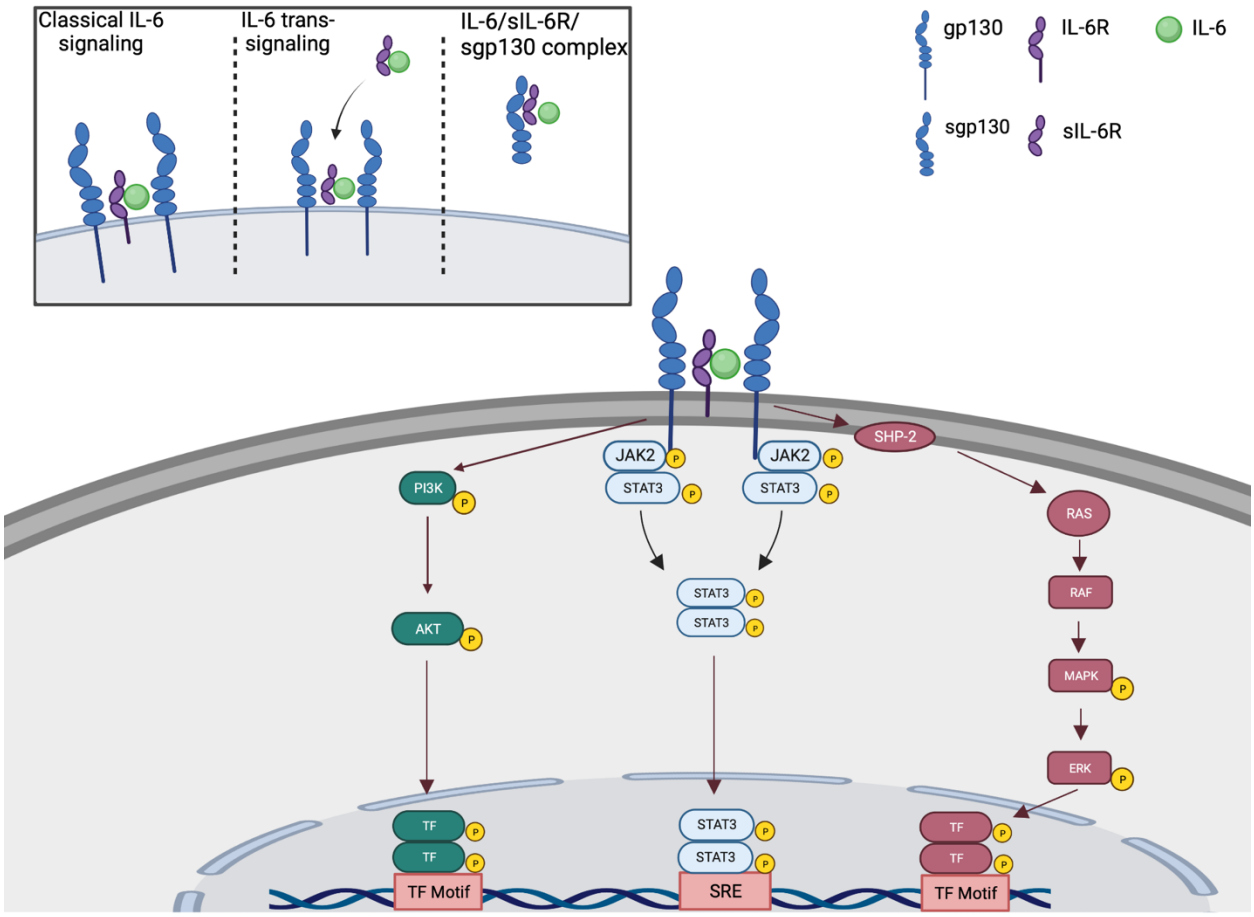

Figure 2 Signaling mechanisms and intracellular signaling pathways induced by interleukin 6. Left upper panel: IL-6 can bind to membrane bound IL-6R (left section) or soluble IL-6R (mid section), both inducing intracellular signaling in target cells. The IL-6/sIL-6R complex can be captured by circulating sgp130, preventing intracellular signaling. **Main panel:** Binding of IL-6 to its receptor IL-6R induces dimerization of gp130. This can induce the JAK/STAT, PI3K/AKT and RAS/RAF/MAPK signaling pathways, subsequently resulting in altered gene expression. Gp130: glycoprotein 130; sgp130: soluble glycoprotein 130; IL-6: Interleukin 6; IL-6R: Interleukin 6 receptor; sIL-6R: soluble Interleukin 6 receptor; PI3K: phosphoinositide-3-kinase; AKT: protein kinase B; TF: Transcription factor; JAK2: Januskinase 2; STAT3: Signal transducer and activator of Transcription 3; SHP-2: Src homology region 2 domain- containing phosphatase 2; RAS: Rat Sarcoma Virus; Raf: Rapidly Accelerated Fibrosarcoma; MAP: Mitogen-Activated Protein Kinase; ERK: Extracellular Signaling-Regulated Kinase. Created with biorender.com.

ICUAW can involve pathologies of muscles, known as Critical Illness Myopathy (CIM) and peripheral nerves, known as Critical Illness Polyneuropathy (CIP). These mechanisms can occur independently or, more commonly, together to induce ICUAW [25].

CIP is characterized by sensorimotor polyneuropathy and has been widely investigated [6]. CIM is characterized by early myofiber atrophy, primarily affecting fast twitch / type II muscle fibers [22].

Risk factors for ICUAW include disease severity indicators, such as high Sequential Organ Failure Assessment (SOFA) scores, prolonged mechanical ventilation and delayed return to physical activity, with inflammation emerging as a potentially modifiable

risk factor [5]. Diagnosing CIP or CIM is challenging due to the need for invasive diagnostic measures, complicated by the patients' frequent inability to cooperate and comorbidities, including anasarca and hypothermia, which can interfere with the diagnostic signal quality [6].

Strategies for preventing and treating ICUAW are limited, with only strict glycemic control and early mobilization showing beneficial effects [26]. The underlying mechanisms of ICUAW need further exploration to identify potential therapeutic targets.

1.5 Regulating factors of Critical Illness Myopathy

Various conditions, such as fasting, diabetes, immobility and glucocorticoid treatment, can induce muscle atrophy [6]. These conditions commonly show an induction of Atrogin-1 and MuRF1, which associates with inhibition of the PI3K/AKT signaling pathway, that typically mediates anabolic effects. Inhibition of the PI3K/AKT signaling pathway induces myocyte atrophy, which can be rescued by Insulin like Growth Factor 1 (IGF1), indicating a role for insulin-induced signaling [10, 27, 28].

Muscles of patients with CIM demonstrate signs of insulin resistance, such as missing translocation of the Glucose Transporter 4 (GLUT4) to the cell membrane and reduced mRNA expression of Insulin Receptor Substrate 1 (IRS1), a component of the insulin receptor complex (Fig. 2) [29].

Impaired insulin signaling may additionally result from interactions with pro-inflammatory pathways, as evidenced by overexpression of the interferon γ and IL-6 target genes *Suppressor of Cytokine Signalling 1 and 3* (*SOCS1* and *SOCS3)* overexpression *in vitro* leading to UPS-mediated breakdown of IRS-1 (Fig. 2) [19, 30].

Various pro-inflammatory cytokines have been associated with muscle atrophy. Elevated levels of the acute phase protein serum amyloid A1 (SAA1) were observed in plasma of critically patients [15]. Muscles of ICUAW patients and septic mice exerted increased mRNA and protein levels of SAA1, which induced myocyte atrophy via toll like receptors 2 and 4 (TLR2, TLR4) and Nuclear Factor kappa-light-chain-enhancer of activated B cells

(NF-$\varkappa$B)-signaling *in vitro.* Inhibition of NF-$\varkappa$B attenuated muscle atrophy in septic mice (Fig. 2). Notably, SAA1 induced IL-6 expression in myocytes [31].

Plasma levels of interleukin-1β (IL-1β) are elevated in septic patients, which induces atrophy in C2C12 myocytes *in vitro* [32, 33]. KO of the NLR Family Pyrin Domain Containing 3 (NLRP3) inflammasome, critical for IL-1β activation, protected mice against sepsis-induced muscle atrophy. Interestingly, the KO results in lower plasma levels of not only IL-1β but also IL-6 during sepsis [33].

These data strongly indicate a significant role of inflammation in CIM, with emerging evidence pointing to IL-6 as a central player in its pathogenesis.

1.6 Interleukin 6 in muscle plasticity

Recent findings demonstrated that IL-6 is directly secreted by myocytes and plays a pivotal role in the regulation of muscle mass [15]. Mice carrying a global deletion of the *Il6* gene exhibit signs of impaired muscle hypertrophy following functional overloading, reduced STAT3- and AKT-phosphorylation in skeletal muscle, diminished MSC proliferation, and lower numbers of nuclei within myofibers [34]. *In vitro* studies showed that proliferating MSCs rely on autocrine IL-6 stimulation for sufficient proliferation [34]. These findings suggest that IL-6 is essential for adequate muscle hypertrophy as myofibers cannot undergo hypertrophy after muscle strain without maintaining the appropriate nuclei-to-cytoplasm ratio [1].

On the other hand, IL-6 induces protein degradation in myocytes *in vitro* and *in vivo* through degradation of sarcomeric proteins [17, 35]. Transgenic mice overexpressing IL-6 develop muscle atrophy and show increased signs of UPS activation, which can be rescued by treatment with an IL-6R antibody [35].

Notably, an observational cohort study of critically ill patients elucidated increased IL-6 plasma levels as an independent risk factor for the development of CIM [5, 36].

Recombinant IL-6 (rIL-6) stimulation of C2C12 myotubes induces *Saa1* mRNA expression via NF-κB signaling and treatment with SAA1 induces IL-6 expression [31].

Additionally, IL-1β enhances the expression levels of IL-6 [33]. Other inducers of IL-6 expression in myocytes are tumor necrosis factor alpha (TNFα) and LPS (Fig. 2) [15].

Considering that these cytokines share their ability to induce IL-6 expression and muscle atrophy, it is reasonable to speculate that the induced atrophic effects are partially induced indirectly by IL-6. This speculation is further corroborated by IL-6's potential to induce muscle atrophy itself.

1.7 The JAK/STAT-signaling pathway in muscle atrophy

IL-6 induces the JAK/STAT-signaling pathway via IL-6R and gp130, which is encoded by the Interleukin 6 Signal Transducer gene (*Il6st*) [19].
Loss of gp130-mediated signaling in myocytes via a myocyte-specific KO attenuates cancer-induced muscle atrophy in a mouse model of lung cancer. *Il6st*$^{-/-}$ mice exhibited reduced activation of NF-κB- and JAK/STAT-signaling and attenuated muscle weight loss. This was associated with decreased protein contents of Atrogin-1, while no data on MuRF1 protein levels were presented [18]. In an adenocarcinoma model, muscle atrophy was attenuated by muscular overexpression of a dominant negative STAT3 allele. Conversely, overexpression of constitutively active STAT3 induced muscle atrophy in mice previously implanted with C26 cells and controls not bearing cancer cells [37].
In denervation-induced muscle atrophy, micro-array analyses unveiled IL-6-induced signaling to be upregulated in muscles. Inhibition of either JAK1/2 or STAT3 attenuated muscle atrophy in mice [4].
These studies provide comprehensive insights into the role of gp130 and JAK/STAT-signaling in denervation-induced and cancer-associated muscle atrophy. However, the applicability of these findings to models of sepsis-induced muscle atrophy is limited due to different kinetics of serum IL-6 levels observed in models of cancer cachexia and muscle denervation. While in cancer cachexia, the observed levels of IL-6 rise moderately over weeks, denervation causes mild and chronic elevations of circulating IL-6 [4, 38]. In contrast, sepsis induces a rapid and strong increase in IL-6 plasma levels within hours after induction of bacteremia [20].

The described findings suggest that mild and short-term increases in serum IL-6 levels as well as paracrine activation of MSCs, are necessary for myofiber hypertrophy [34, 39],

while prolonged and severe increases in serum IL-6 levels induce muscle atrophy [35]. However, the role of IL-6-induced signaling in sepsis-associated skeletal muscle atrophy remains unknown.

1.8 Aim and Hypotheses

The available data suggests a central role of IL-6 and its induced signaling pathways in muscle atrophy. As IL-6 serum levels have been elucidated as an independent risk factor for the development of Critical Illness Myopathy, the aim of this study was to characterize the role of IL-6 in CIM [5]. Therefore, the hypotheses of this project were:

1. Patients with ICUAW show signs of activated intracellular signaling downstream of IL-6 in skeletal muscles
2. IL-6 induces myocyte atrophy via the JAK/STAT signaling pathway *in vitro*
3. IL-6-induced signaling pathways mediate myocyte atrophy in a murine model of polymicrobial sepsis

2 Materials & Methods

2.1 Materials

Name	Component	Final concentration
Protein lysis buffer	TRIS	50 mM
	NaCL	150 mM
	Glycerol	1 M
	Triton X-100	1 % (w/v)
Laemmli loading buffer	SDS	39 mM
	TRIS	50 mM
	Bromophenol blue	250 µM
	Glycerol	800 mM
TBS-T	TRIS	20 mM
	SDS	150 mM
	Tween-20	0.1%
Acidic pre-incubation buffer	Potassium acetate	50 mM
	Calcium chloride dihydrate	18 mM
	Acetic acid	Adjust pH to 4.4
	Distilled water	
TRIS washing buffer	TRIS	100 mM
	Calcium chloride dihydrate	18 mM
	Hydrochloric acid	Adjust pH to 7.8
	Distilled water	
ATP incubation medium	Glycine	53 mM
	Calcium chloride dihydrate	29 mM
	Sodium chloride	65 mM
	Sodium hydroxide	47.5 mM
	Hydrochloric acid	Adjust pH to 9.4
	ATP	
	Distilled water	
1% calcium chloride solution	Calcium chloride dihydrate	68 mM
	Distilled Water	

Table 1. Buffers

Primer Name	Sequence (5' – 3')
Mm_*Il6st*_loxP forward	TGG CTT GAG CCT CAG CTT GGC TAG
Mm_*Il6st*_loxP reverse	GTG AAC AGT CAC CAT GTA CTC TGT ACG C
Pax7ICN forward	GCT CTG GAT ACA CCT GAG TCT
Pax7ICN forward mutant	GGA TAG TGA AAC AGG GGC AA
Pax7ICN reverse	TCG GCC TTC TTC TAG GTT CTT GCT C

Table 2. Primer sequences used for genotyping of *Il6st*$^{loxP/loxP;\ Pax7\text{-}CRE}$ mice.

Name	Sequence (5'- 3')
Hs_*SOCS3* forward	AGA CTT CGA TTC GGG ACC A
Hs_*SOCS3* reverse	AAC TTG CTG TGG GTG ACC A
Hs_*GAPDH* forward	AGC CAC ATC GCT CAG ACA C
Hs_*GAPDH* reverse	GCC CAA TAC GAC CAA ATC C
Mm_*Socs3* forward	GAA TTT CGC TTC GGG ACT AG
Mm_*Socs3* reverse	AAC TTG CTG TGG GTG
Mm_*Il6st* forward	AAA GAT GGG CCG GAA TTC
Mm_*Il6st* reverse	CAC ACA GGC ACG ACT ATG G
Mm_*Trim63* forward	CCT GCA GAG TGA CCA AGG A
Mm_*Trim63* reverse	GGC GTA GAG GGT GTC AAA CT
Mm_*Fbxo32* forward	AGT GAG GAC CGG CTA CTG TG
Mm_*Fbxo32* reverse	GAT CAA ACG CTT GCG AAT CT
Mm_*Gapdh* forward	ATG GTG AAG GTC GGT GTG A
Mm_*Gapdh* reverse	AAT CTC CAC TTT GCC ACT GC
Mm_*Myh2* forward	AAC TCC AGG CAA AAG TGA AAT C
Mm_*Myh2* reverse	TGG ATA GAT TTG TGT TGG ATT GTT
Mm_*Myh4* forward	GGG AAC ATG AAA TTC AAG CAA
Mm_*Myh4* reverse	ATA GGC AGC CTT GTC AGC AA

Table 3. Primer sequences used for quantitative real-time-PCR.

Antibody	Clonality	Dilution	Species	Manufacturer
anti-GAPDH clone 6C5	Monoclonal	1:10 000	Mouse	Merck-Millipore
anti-IRS1 #2382	Monoclonal	1:1000	Rabbit	Cell Signalling Technology, MA, USA
anti-phosphor IRS1 S636/S639 #2580	Monoclonal	1:1000	Rabbit	Cell Signalling Technology, MA, USA
anti-STAT3 #12640	Monoclonal	1:2000	Rabbit	Cell Signalling Technology, MA, USA
anti-phosphor STAT3 Y715 #9145	Monoclonal	1:1000	Rabbit	Cell Signalling Technology, MA, USA
anti-AKT #4691	Monoclonal	1:1000	Rabbit	Cell Signalling Technology, MA, USA
anti-phosphor AKT Ser473 #4060	Monoclonal	1:1000	Rabbit	Cell Signalling Technology, MA, USA
anti-MuRF1	Polyclonal	1:200	Rabbit	Marcel Nowak, MDC Berlin, Germany
anti-Atrogin 1 Ab92281	Monoclonal	1:1000	Goat	Abcam, UK
anti-gp130 Ab202850	Monoclonal	1:1000	Rabbit	Abcam, UK

Table 4. Primary antibodies used for immunoblotting.

Antibody	Clonality	Dilution	Species	Manufacturer
anti-mouse-Fc HRP #7076	Monoclonal	1:2000	Horse	Cell Signalling Technology, MA, USA
anti-rabbit-Fc HRP #7074	Monoclonal	1:2000	Goat	Cell Signalling Technology, MA, USA
anti-goat-Fc HRP ab97110	Monoclonal	1:2000	Donkey	Abcam, UK

Table 5. Secondary antibodies used for immunoblotting.

2.2 Human muscle biopsies

Skeletal muscle biopsies were obtained from a single-center observational pilot study's biobank, which involved 33 critically ill patients [22]. CIM was defined by non-excitability of muscle membranes as indicated by a compound muscle action potential after direct

muscle stimulation below 3.0 mV, as previously described [36]. The study was approved by the institutional ethics committee and institutional review board of the Charité – Universitätsmedizin Berlin, Germany. Written consent was obtained from the patients or their legal representatives prior to their inclusion in the study. Patients who were mechanically ventilated and had a Simplified Acute Physiology Score II of ≥20 on three successive days within the first week after admission to the ICU met inclusion criteria.
Muscle biopsies were obtained from the vastus lateralis muscle via open surgical excision in sedated patients on days 5 and 15 following ICU admission. Biopsies were snap-frozen in liquid nitrogen and stored at -80°C until further processing. Vastus lateralis muscle biopsies from otherwise healthy controls undergoing hip replacement surgery were used as controls.

2.3 Cell culture experiments

All cell culture experiments were conducted using the immortalized murine C2C12 myoblast cell line (ATCC, VA, USA) in passages 5 to 15. The cells were cultured in Dulbecco's Modified Eagle Medium (DMEM; Sigma-Aldrich, MO, USA) supplemented with 10% fetal bovine serum (FBS; Biochrom, Merck-Millipore, Germany) and 1% penicillin/streptomycin (Sigma-Aldrich), and maintained in a humidified incubator at 37°C with 5% CO_2. Prior to experiments, 100,000 cells were seeded into each well of 6-well plates and allowed to grow until they reached near-confluence over a period of 2 days. To induce differentiation, the medium was replaced with DMEM supplemented with 2% FBS, and the medium was exchanged daily. Experiments were conducted using myotubes that had undergone 5 days of differentiation.
Myotubes were treated with recombinant mouse interleukin 6 (R&D Systems, MN, USA). rIL-6 was dissolved in 0,1% bovine serum albumin (BSA) in phosphate-buffered saline (PBS) and added to the cells to a final concentration of 10 ng/ml. The cells were subsequently incubated for the designated time periods. As solvent control, 0,1% BSA in PBS was used.
Small molecule inhibitors of JAK2 (Tyrphostin AG490, Sigma-Aldrich) and STAT3 (C188-9, Merck-Millipore, Germany and S3I-201, Selleckchem, TX, USA) were employed. The inhibitors were reconstituted in dimethyl sulfoxide (DMSO) at 1 mM and further diluted in PBS. The inhibitors were added to the cells at a final concentration of 10 µM, 60 minutes prior to treatment with rIL-6. DMSO in PBS without inhibitors served as the solvent control.

To achieve knockdown of *Il6st*, a small interfering RNA (siRNA) targeting *Il6st* (Dharmacon, Thermo Fisher Scientific, MA, USA) was used at a final concentration of 50 nM. Scrambled siRNA (Dharmacon, Thermo Fisher Scientific) served as the control. Three days differentiated C2C12 myotubes were transfected using the DharmaFECT 3 reagent (Dharmacon) in Opti-MEM® Medium (Life Technologies, Thermo Fisher Scientific). The cells were incubated for an additional 48 hours before treatment with rIL-6 or solvent, to complete five days of differentiation. Knockdown was confirmed via qRT-PCR with self-designed primers (Eurofins Scientific, Luxembourg, Table 3) and immunoblots employing a gp130 antibody (Table 4).

2.4 Animal models

All animal experiments were approved by the Landesamt für Gesundheit und Soziales, Berlin, Germany (permit No. G207/13) and conducted in accordance with the guidelines of the Charité – Universitätsmedizin Berlin and the Max-Delbrück-Center for Molecular Medicine, as well as the *Guide for the Care and Use of Laboratory Animals* by the National Institutes of Health (Publication No. 85-23, 1985). Mice were kept at a 12 hour light-dark-rhythm with free access to chow and water.

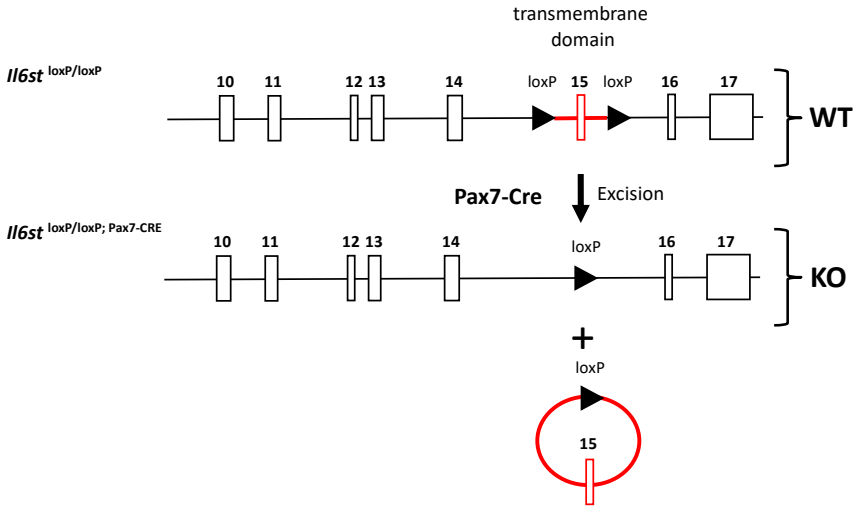

Figure 3. Schematic knockout strategy of Il6st$^{loxP/loxP;\ Pax7\text{-}CRE}$ mice. Exon 15, encoding for the transmembrane domain of gp130, was flanked by loxP sites which are recognized by the Cre recombinase. Cre is expressed under control of the Pax7 promoter, resulting in expression specifically in muscle satellite cells. Excision of the loxP-flanked regions results in a frameshift mutation and deficiency in gp130. *Il6st*: Interleukin 6 signal transducer; loxP: Locus of X-over P1; WT: wild-type; Pax7: Paired Box Protein Pax7; CRE: Cre Recombinase, KO: Knockout.

Using the Cre Recombinase (Cre) - Locus of X-over P1 (loxP) - system, a mouse line bearing a homozygous conditional *Il6st* allele (*Il6st*$^{loxP/loxP}$) was utilized. Exon 15 of the *Il6st* gene was flanked by loxP sites, which are recognized by Cre, which was expressed under control of the *Paired box protein Pax7* (*Pax7*) promoter. Excision of the region flanked by loxP sites results in a frame shift (Figure 3). The mouse line was a kind gift from Klaus Rajewski, and the detailled KO strategy and baseline characteristics have been published previously [40].

Since *Pax7* is specifically expressed in MSCs, and all skeletal myofibers originate from these multipotent stem cells, the deletion of *Il6st* results in deficiency in all MSCs and myofibers. Mice bearing the conditional knockout (*Il6st*$^{loxP/loxP;\ Pax7\text{-}Cre}$; '*Il6st*$^{-/-}$') and littermate controls without the Cre recombinase (*Il6st*$^{loxP/loxP}$; 'WT') were maintained until they reached 12 to 16 weeks of age before undergoing treatment. The knockout was confirmed through genotyping using ear punch biopsy specimens and qRT-PCR from muscle lysates (for genotyping primers, see table 1, for qRT-PCR primers, see table 3).

For *in vivo* JAK2 inhibition experiments, 40 twenty-week-old C57/BL6J mice (Jackson Laboratory, ME, USA) were used. Tyrphostin AG490 (Sigma-Aldrich) was reconstituted in DMSO at 1 mM and further diluted in PBS, with the pH adjusted to 7.3 using sodium hydroxide. Solvent control littermates were treated with DMSO in PBS. The animals received intraperitoneal injections of 500µg of Tyrphostin AG490 or the solvent, 60 minutes before CLP and every 24 hours thereafter, for a total of four injections. Inhibition of the JAK2/STAT3 signaling pathway was confirmed via immunoblotting with pSTAT3 antibodies (Table 4) and qRT-PCR with self-designed primers for *Socs3* (Table 3).

Polymicrobial sepsis was induced using the Cecal Ligation and Puncture (CLP) procedure (24 hours *Il6st* cKO experiment: WT sham: n = 4, WT CLP = 6, cKO sham: n = 4, cKO CLP: n = 4; 96 hours *Il6st* cKO experiment: WT sham: n = 6, WT CLP = 11, cKO sham: n = 6, cKO CLP: n = 16; AG490 experiment: solvent sham: n = 5, solvent CLP: n = 15, AG490 sham = 5, AG490 CLP: n = 15).

Under short-term general anesthesia with isoflurane, a longitudinal mini-laparotomy was performed (Fig. 4b) to expose the cecum (Fig. 4c). The middle section of the cecum was ligated using a Prolene 6-0 suture (Ethicon, Johnson & Johnson, NJ, USA; Fig. 4 d-g) followed by a single puncture with a 16-gauge canula (Fig. 4 h-k). A small quantity of intraluminal content was expressed from the lumen before repositioning the cecum back into the abdominal cavity. The peritoneum and skin were individually closed using a

Prolene 6-0 suture (Ethicon, Johnson & Johnson) (Fig. 4l; note that sutures were utilized instead of clamps as illustrated). As sham procedure, only laparotomy was performed without ligation and puncture of the cecum (Fig. 4 b, l).

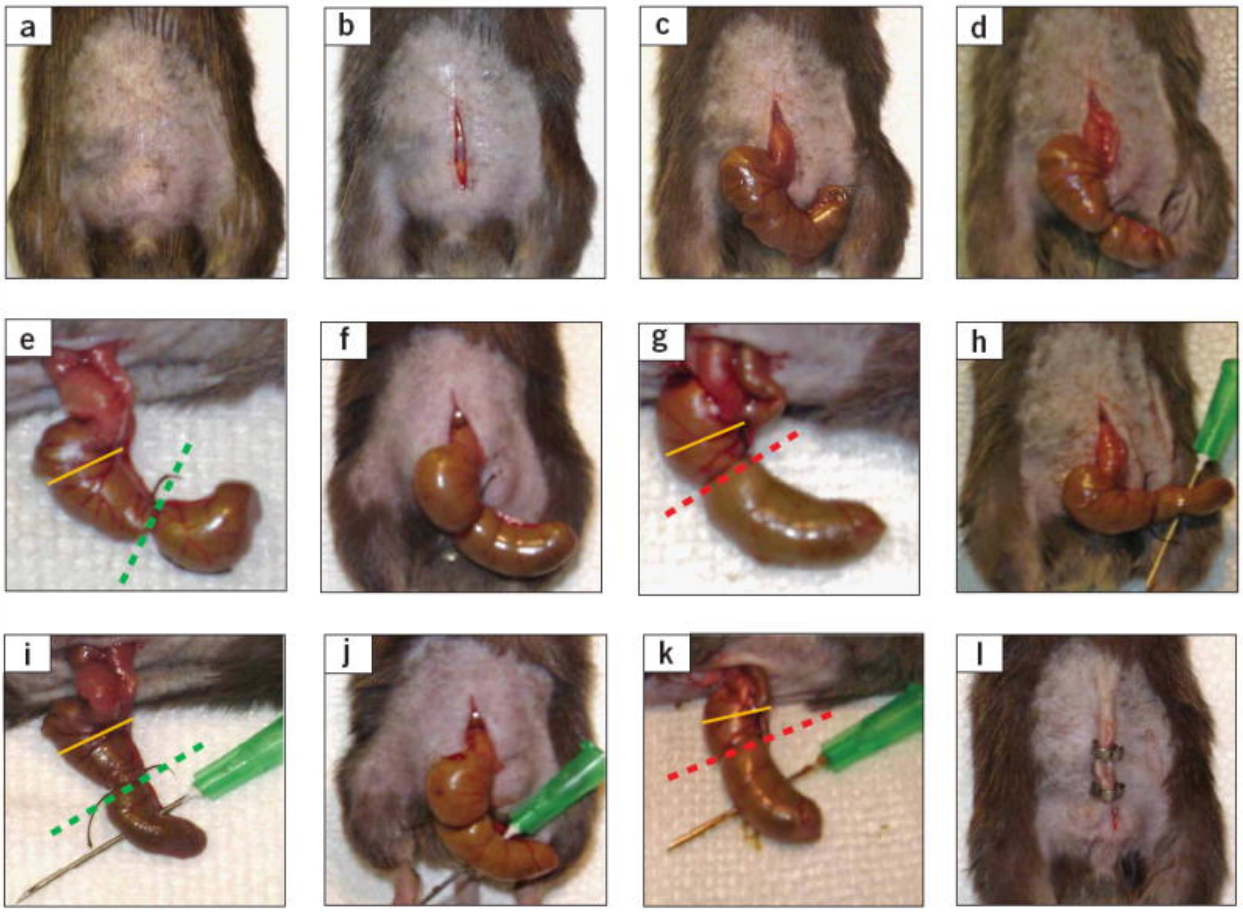

Figure 4. The cecal ligation an puncture technique. a: The abdominal wall is shaved. **b**: A longitudinal mini-laparotomy is performed. **c**: The cecum is exposed. **d,e**: Ligation of the cecum in the distal section. **f, g**: Ligation of the cecum in the mid-section. **h, i**: Puncturing of the cecum after ligation in the distal section. **j, k**: Puncturing of the cecum after ligation in the mid-section. **l**: Closure of the abdominal wall using metal clips. Taken from Rittirsch et al., Nat Protoc., 2009;4(1):31-6 [41]. Permission for usage granted by Nature Publishing Group (Permission No. 5571360097806).

After surgery, mice were rehydrated by subcutaneous injection of 2 ml of Ringer's lactate solution and placed in pre-warmed cages. Checks for survival were conducted every 12 hours. At the designated time points of 24 or 96 hours, the mice were sacrificed by neck dislocation under isoflurane anesthesia. Blood samples were collected from the retroorbital venous plexus and the heart, lungs, liver and kidneys were harvested. The tibialis anterior (TA), gastrocnemius/plantaris (GP), soleus (SOL) and hind limb extensor digitorum longus (EDL) muscles were carefully removed.

For histological analysis, muscles were embedded in gum tragacanth (Merck, Germany), snap-frozen in isopentane followed by liquid nitrogen and stored at -80°C until further processing. All other tissues were immediately snap-frozen in liquid nitrogen after removal and stored at -80°C until subsequent processing.

2.5 Bulk mRNA sequencing

Tibialis anterior muscles were obtained from WT CLP or sham-operated mice, 24h or 96 hours after surgery. Three mice were used for each condition and the harvested muscles subjected to bulk mRNA sequencing. The quality of the extracted RNA was assessed using an Agilent 2100 Bioanalyzer (Agilent Technologies, Inc., CA, USA). Subsequently, 500 ng of RNA from each sample was used for library preparation using the Illumina TruSeq Stranded mRNA Kit (Illumina Inc., CA, USA). The complementary desoxyribonucleic acid (cDNA) obtained after reverse transcription was evaluated using the Agilent 2100 Bioanalyzer. Next generation sequencing was performed using the Illumina HiSeq 4000 platform.

The quality of the sequencing was assessed using the FASTQC software (v0.11.5; Babraham Bioinformatics, UK). Alignment of the reads to the mouse genome GRCm38 was performed using the STAR aligner (v2.5.3a) [42].

Read counts were extracted using the feature Counts software (v1.5.1) [43]. Genes with at least ten reads in each muscle specimen were included in further analyses. Differential gene expression between treatment groups was conducted using the DESeq2 package for R (v1.16.1) [44]. Genes with a log2-fold change ≥2 and an adjusted p-value <0.05 were considered differentially expressed (DEGs).

The sequencing data has been deposited under EBI Annotare version 2.0 with the Project-ID E-MTAB-10960.

Voronoi Treemaps of DEGs per KEGG (Kyoto Encyclopedia of Genes and Genomes) pathway were generated using the Paver software (DECODON, Greifswald, Germany) [45, 46], which employs a space proportional algorithm. The treemaps visually represent overexpressed genes and pathways, with larger sizes indicating higher expression levels, enabling comparison with other pathways or genes. Pathway enrichment analyses were conducted using the Database for Annotation, Visualization, and Integrated Discovery (DAVID) Bioinformatics Resources 6.8 [47, 48], with BP_ALL (all biological process terms) as the output for functional annotation and visualization. Venn diagrams were

created using the VENNY2.1 tool to show the number of genes that were increased or decreased in expression. Gene ontology (GO) term and KEGG pathway analyses were performed using the DAVID tool.

2.6 Quantitative real-time PCR

Biopsies from the cohort study (section 3.2.1) and mouse muscle specimens (section 3.2.3) were homogenized using a FastPrep24™ homogenizer (MP, Fisher scientific, MA, USA) and ceramic beads (Precellys, Bartin, FR) in TRIzol™ reagent (Invitrogen, CA, USA) at 4°C. For *in vitro* experiments, cells were lysed with TRIzol™ reagent at 4°C and then harvested from the 6-well plates using a cell scraper. After transfer to vials, chloroform was added to the lysates, followed by centrifugation. The RNA-containing phase was transferred to a new vial, and nucleic acid precipitation was performed using isopropyl alcohol. After another centrifugation run, pellets were washed with ethanol, air-dried and reconstituted in water. The concentration of RNA was measured using a NanoDrop™ spectrophotometer (Thermo Scientific, MA, USA) with an absorbance ratio of 260 to 280 nm.
For cDNA synthesis, 1 µg of RNA was used for cDNA synthesis with the SuperScript II reverse transcriptase (Invitrogen, Life Technologies Corporation, CA, USA). Quantitative real-time PCR was performed with the *Power SYBR® Green PCR Master Mix* (Thermo Fisher Scientific) and self-designed primers (Eurofins, Table 3). The StepOnePlus™ thermocycler (Applied Biosystems, Thermo Fisher Scientific) was utilized, and a cDNA standard curve normalization approach was employed. The reference gene, glyceraldehyde 3-phosphate dehydrogenase (*Gapdh*), was used for data normalization.

2.7 Protein isolation and immunoblot analyses

Muscle samples were lysed in 500µl of cold protein lysis buffer (Table 1) supplemented with protease (cOmplete™ protease inhibitor cocktail, Roche Diagnostics, Germany) and phosphatase inhibitors (PhosStop™, Roche Diagnostics). The samples were homogenized using a FastPrep24™ homogenizer with ceramic beads (Precellys). The samples were centrifuged and the soluble phase transferred to new vials. Protein quantification was performed using Pierce® BCA reagent (Thermo Fisher Scientific). The samples were stored at -80°C until further usage.

For immunoblot analyses, Laemmli buffer was added and the proteins denatured at 95°C for 10 minutes. 100 µg protein was loaded into 10 or 15% Sodium dodecyl sulfate (SDS) -Polyacrylamide gels, depending on the size of the protein of interest. For immunoblotting of GAPDH, IRS-1, pIRS1, STAT3, pSTAT3, AKT and pAKT nitrocellulose membranes (GE Healthcare, Germany) were used. PVDF membranes (GE Healthcare) were used for immunoblots of MuRF1, Atrogin1 and gp130. After protein transfer, the membranes were blocked with 5% skimmed milk or 5% BSA in TBS-T for one hour at room temperature. Primary antibodies (Table 4) were dissolved in 5% skimmed milk or 5% BSA in TBS-T, and the membranes were incubated with the antibodies at 4°C for 12 hours. Following incubation, the membranes were washed with TRIS-buffered saline Tween (TBS-T) and incubated with horseradish peroxidase-linked antibodies (HRP; table 5) in 5% skimmed milk or 5% BSA in TBS-T for one hour at room temperature. Chemiluminescence substrate (SuperSignal® West Pico, Thermo Fisher Scientific) was applied to the membranes for HRP-reaction, and chemiluminescence films (GE Amersham, UK) were used for signal detection. Films were developed with an Agfa CP1000 developer machine (Agfa-Gavaert NV, Belgium) and digitalized using a flat-bed scanner.
Densitometry was performed on digitalized immunoblot films using the ImageJ software v1.6.0_24 (National Institutes of Health). The pictures were inverted, and the intensity values of protein bands were measured individually. To normalize for background noise, the intensity of areas not containing bands were measured and subtracted from each band.

2.8 C2C12 myocyte diameter measurements

Phase contrast images of myotubes were captured using a Leica CTR 6500 microscope equipped with a Leica DFC 360 FX camera (Leica Microsystems, Germany). The imaging was conducted on living cells before and at 24-hour intervals following the start of treatment with rIL-6. Blinding of treatment groups was carried out by a person not involved in subsequent analyses.
For each well, five random areas were photographed. For myotube diameter measurements, 100 myotubes from each treatment group were measured in the middle and both distal sections using the ImageJ software v1.6.0_24 (National Institutes of Health). The means of the three measurements were used for further analyses.

2.9 Histologic staining and measurement of myocyte cross sectional areas

Muscle cross sections measuring 5 µm were obtained from the TA, GP, and SOL muscles of mice from the 96 hour sepsis experiments using a cryostat microtome (CM3050S, Leica Microsystems). The sections were stained with metachromatic adenosine 5'-triphosphatase (ATPase) staining to facilitate fiber type identification.
Metachromatic ATPase staining was achieved by subjecting the sections to acidic pre-incubation buffer (Table 1) for a duration of 8 minutes followed by 3 consecutive washing steps in TRIS washing buffer for 2 minutes each. Subsequently, the slides were incubated in Adenosine triphosphate (ATP) incubation medium for 25 minutes and then immersed in 1% calcium chloride solution. Following this, the slides were stained with 0.1% Toludine Blue for 1 minute, washed with water, consecutively dehydrated in 95% and 100% ethanol, cleared with 100% xylol and embedded using Vitro-Clud® embedding medium (R. Langenbeck, Germany)

Ten random sections of the tissue slides were photographed using a Leica CTR 6500 microscope and a Leica DFC 425 camera. To ensure blinding for treatment and genotype, a person not involved in subsequent analyses performed sample blinding. After verifying the quality of the sections for perpendicular orientation of the myocytes, individual cells were manually marked at the sarcolemma. Fast twitch / type II and slow twitch / type I myofibers were analyzed separately. A total of 500 myocyte cross sectional areas (MCSA) of each genotype and treatment group were measured using the ImageJ software version 1.6.0_24. To control for perpendicular section of myofibers, minimal Feret's diameters were measured as control (data not shown). Quantification of fiber type distribution was performed by counting slow-twitch/type I and fast twitch/type II myofibers in 10 sections per animal.

2.10 Measurement of plasma IL-6 concentrations

Blood samples were collected from mice by puncturing the retroorbital plexus using Pasteur pipettes and heparin-coated vials (Sarstedt, Germany). The collected samples were immediately centrifuged at 1500 rpm for 20 minutes at 4°C. Following centrifugation, the plasma fraction was carefully transferred into new tubes and stored at -80°C until further processing.

Quantification of circulating IL-6 was performed using an IL-6 enzyme-linked immunosorbent assay (ELISA; R&D Systems, MN, USA).
Each sample was analyzed in technical duplicates. After a 2-hour incubation of samples with the pre-coated 96-well plate at room temperature, the wells were washed, and 100 µl of mouse IL-6 Conjugate was added to each well. Following another incubation and washing step, 100 µl of substrate solution was added and incubated for 30 minutes. The reaction was stopped and absorbance of each well was measured using a SPECTRAmax M5 plate reader (Molecular Devices, CA, USA) at a wavelength of 450 nm with a wavelength correction at 540 nm. A standard curve was generated using the absorbance measurements of a IL-6 2:1 standard serial dilution, and sample concentrations were calculated accordingly. As CLP-treated animals frequently showed measurements out of range, the according plasma samples were diluted in PBS at a 2:1 dilution to facilitate accurate measurements.

2.11 Statistical analyses

All cell culture experiments were conducted in triplicates and repeated three times. Two tailed t-tests were employed for normally distributed data, such as mRNA expression, immunoblot densitometry, and myocyte diameter measurements in cell culture experiments, and MCSA measurements in mouse data. The normal distribution of the data was assessed through visual inspection of dot plots and the Shapiro-Wilk test.
For non-normally distributed data, the non-parametric Mann-Whitney U test was employed. This test was used for analyzing mRNA expression, western blot densitometry, IL-6 ELISA data from human and mouse samples. Survival analyses were performed using the log-rank test, and the outcomes were visualized using Kaplan-Meier curves.

Differences were considered statistically significant at $p<0.05$. Unless otherwise stated, values are presented as mean ± standard deviation (SD) for cell culture experiments and mean ± SEM for human and mouse samples.
Statistical analyses and graph creation were performed using GraphPad Prism® 8.0 software (GraphPad Software, CA, USA). Figure layouts were generated using Adobe Illustrator CS6, version 16.0.0 and Adobe Photoshop CS6, version 13.0 (Adobe Inc., CA, USA).

3 Results

3.1 The JAK/STAT signaling pathway is active in muscles of critically ill patients

Muscle tissue samples were available from 8 critically ill patients without signs of CIM at day 5 and 6 patients at day 15. From critically ill patients with CIM, 17 samples were available at day 5 and 13 on day 15. As controls, 6 muscle samples were available from otherwise healthy controls undergoing hip replacement surgery.

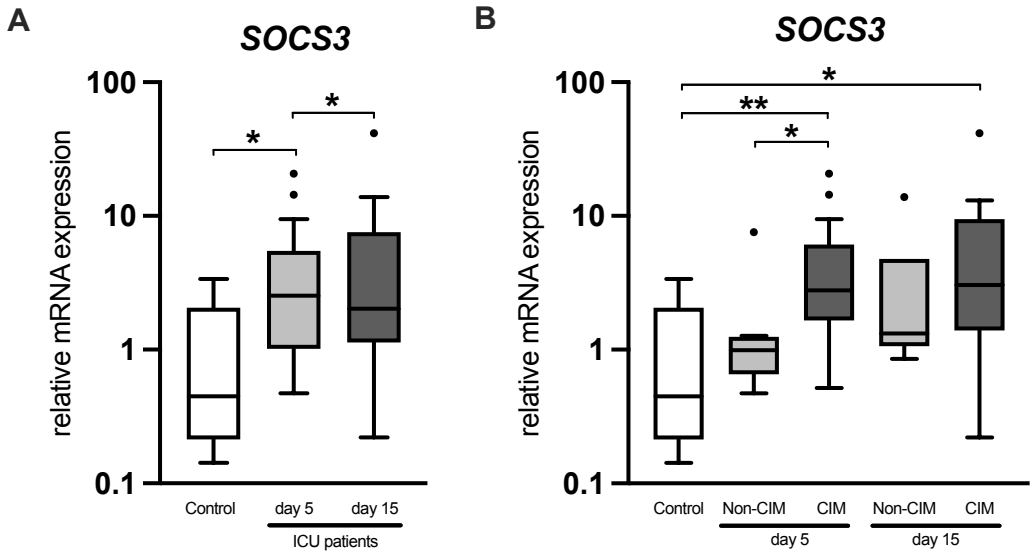

Figure 5. *Suppressor of Cytokine Signaling 3* mRNA expression in muscles of critically ill patients. *SOCS3* mRNA contents were investigated in lateral vastus muscle biopsies from critically ill patients on days 5 (n = 25) and 15 (n = 19) after admission to the intensive care unit. Otherwise healthy controls underground hip replacement (n = 6) were used as controls. **A**: *SOCS3* mRNA content according to the day of tissue sampling. **B**: *SOCS3* mRNA content according to diagnosis of critical illness myopathy (day 5 non-CIM: n = 8, day 5 CIM: n = 17, day 15 non-CIM: n = 6, day 15 CIM: n = 13). *SOCS3*: Suppressor of Cytokine Signaling 3; mRNA: messenger ribonucleic acid; ICU: Intensive Care Unit; CIM: Critical Illness Myopathy. * $p < 0.05$; ** $p < 0.01$ as determined by Mann-Whitney U test. Values are Median, boxes indicate the 25th and 75th percentile, whiskers indicate 1.5 interquartile ranges. Adapted from Zanders et al., J Cachexia Sarcopenia Muscle. 2022 Feb;13(1):713-727 with permission under a Creative Commons Attribution 4.0 International License [49].

Critically ill patients exhibited a 5.63-fold and 4.51-fold increase in *SOCS3* mRNA expression after 5 and 15 days, respectively, in comparison to healthy controls (Fig. 5A). Higher levels of *SOCS3* mRNA expression were observed in patients with CIM on day 5 when compared to critically ill patients without (Fig. 5B). Muscles from critically ill patients without signs of critical illness myopathy did not demonstrate a significant increase in *SOCS3* mRNA expression when compared to healthy controls (Fig. 5B).

3.2 Sepsis induces interleukin 6 signaling in murine skeletal muscle

C57BL/6J mice were subjected to CLP or sham surgery and TA muscles were harvested 24 or 96 hours later (n = 3 per group).

In CLP-operated mice, RNAseq from TA muscle revealed 736 significantly upregulated genes after 24 hours and 1546 after 96 hours, compared to the sham-operated controls (Fig. 6). 714 downregulated genes were observed after 24 hours and 1509 after 96 hours in CLP-treated animals compared to sham-treated controls. In a pooled analysis combining data from both timepoints, 1036 upregulated and 1621 downregulated DEGs were observed in muscles of septic mice (Fig. 6, 7).

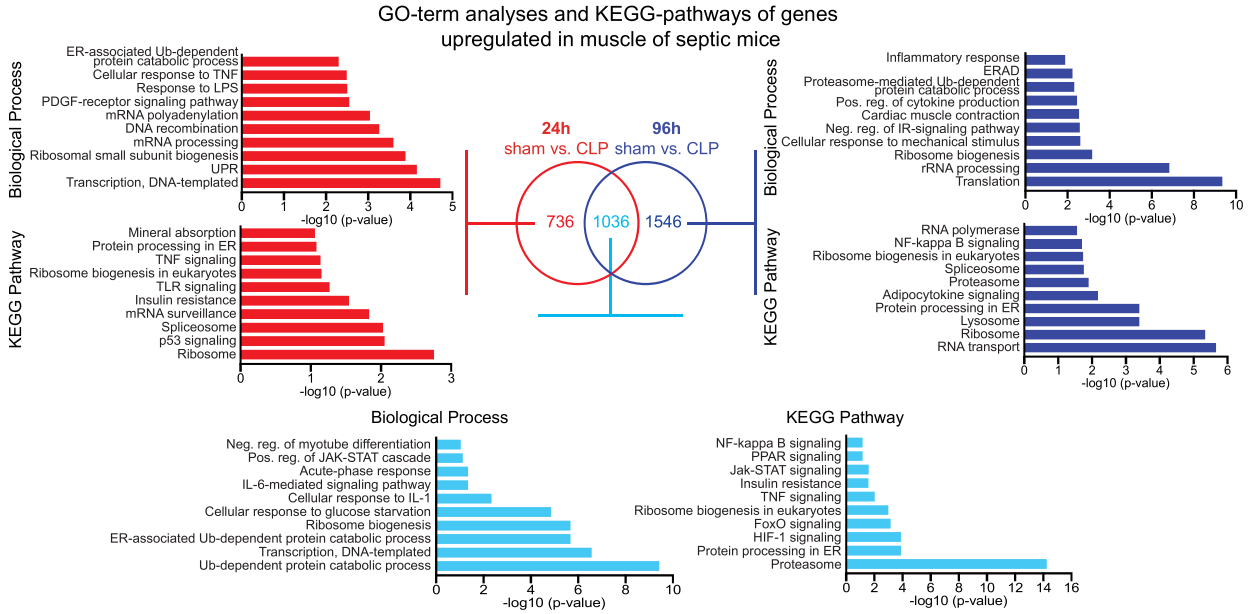

Figure 6. Analysis of upregulated differentially expressed genes (DEGs). Wild-type C57BL/6J mice were subjected to CLP or sham surgery and sacrificed 24 or 96 hours after surgery. Tibialis anterior muscles were harvested and subjected to bulk RNA sequencing (n = 3 for each group). The Venn diagram shows upregulated DEGs between sham and CLP-treated mice. The bar graphs show the results with the highest consensus between DEGs and index gene sets of GO terms or KEGG pathways, sorted by p-values determined by Wald tests. Genes were considered differentially expressed at $p < 0.01$. GO: Gene Ontology; KEGG: Kyoto Encyclopedia of Genes and Genomes, CLP: Cecal Ligation and Puncture. Reprinted from Zanders et al., J Cachexia Sarcopenia Muscle. 2022 Feb;13(1):713-727 with permission under a Creative Commons Attribution 4.0 International License [49].

GO-term analyses were conducted to examine biological processes, and KEGG-pathway analyses were performed. In the combined analysis of both timepoints, the results revealed the GO terms ‘positive regulation of JAK/STAT cascade’, ‘IL-6 mediated

signaling pathways', as well as 'insulin resistance' and 'cellular response to glucose starvation' among the results with highest matching ranks. Additionally, an upregulation of the terms 'proteasome' and 'Ub-dependent protein catabolic process' was observed (Fig. 6).

KEGG pathway analyses unveiled a downregulation of 'PI3K/Akt signaling' and 'insulin signaling' at both time points (Fig. 7).

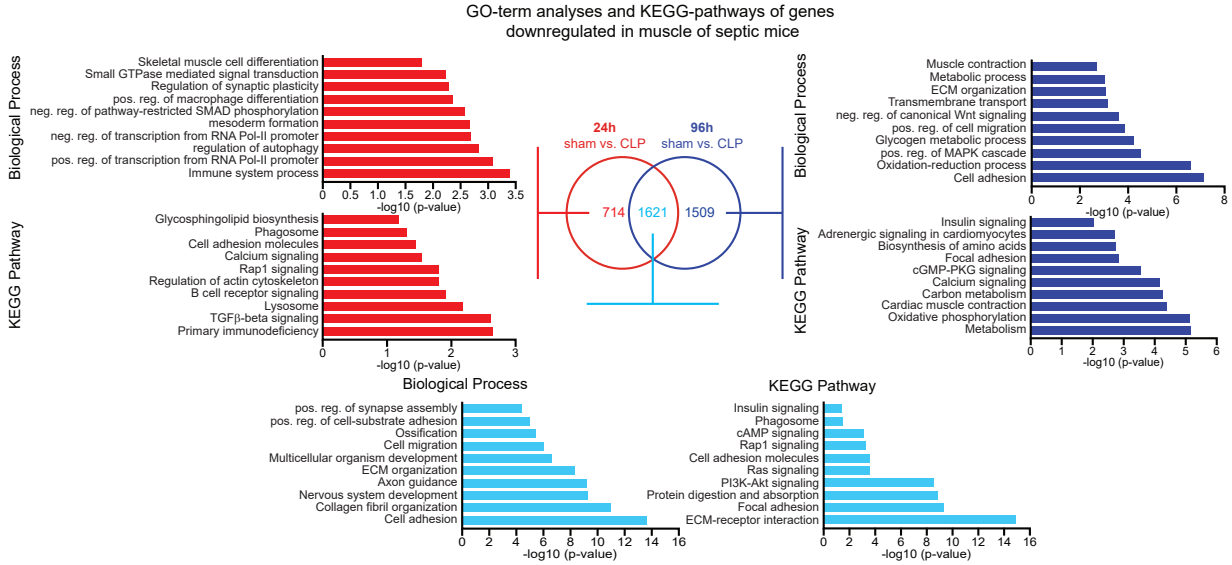

Figure 7. Analysis of downregulated differentially expressed genes (DEGs). Sepsis was induced via the CLP method in C57BL/6J wild-type mice. Animals (n = 3 per group) were sacrificed after 24 or 96 hours and tibialis anterior muscles of three mice per group subjected to bulk RNA sequencing. The Venn diagram depicts the downregulated DEGs at 24 and 96 hours as well as the analysis from both timepoints combined. The bar graphs show the GO terms and KEGG pathways with the highest consensus between DEGs and genes contained the respective gene sets, sorted by the p-values as determined by Wald tests. Genes were considered differentially expressed at $p < 0.01$. GO: Gene Ontology; KEGG: Kyoto Encyclopedia of Genes and Genomes, CLP: Cecal Ligation and Puncture. Reprinted from Zanders et al., J Cachexia Sarcopenia Muscle. 2022 Feb;13(1):713-727 with permission under a Creative Commons Attribution 4.0 International License [49].

To further focus on IL-6-induced signaling, GO-term analyses related to IL-6 signaling were performed. Components of GO-Terms 7259 'Positive regulation of JAK-STAT cascade' and 70102 'IL-6-mediated signaling pathway' were subsequently analyzed. Notable upregulated genes within these gene sets included *Il6ra*, *Stat3*, as well as the STAT3-target genes *Icam1* and *Gab1* [49-51].

To investigate the involvement of other members of the IL-6 cytokine family and their respective receptors, analyses of the components and their receptors were conducted. A

strong up-regulation of *Il6* and *Il6r*, as well as the *Interleukin 12 receptor (IL-12R)* gene were observed. The other members were either marginally deregulated (*Cardiotrophin 1* (*Ctf1*), *Ciliary neurotrophic factor* (*Cntf*), *Leukemia inhibitory factor receptor (Lifr*), *Oncostatin M* (*Osm*), *Oncostatin M receptor* (*Osmr*), *Interleukin 11* (*Il-11*), *Interleukin 11 receptor subunit alpha-1* (*Il-11ra1*), *Interleukin 11 receptor subunit alpha-2* (*Il-11ra2*), *Interleukin 27* (*Il-27*), *Interleukin 27 receptor subunit alpha* (*Il-27ra*), *Interleukin 31* (*Il-31*), *Interleukin receptor subunit alpha* (*Il-31ra*)) or down-regulated (*Cardiotrophin receptor* (*Cntfr*), *Leukemia inhibitory factor* (*Lif*), *Interleukin 12 subunit alpha* (*Il-12a*)) (Fig. 8).

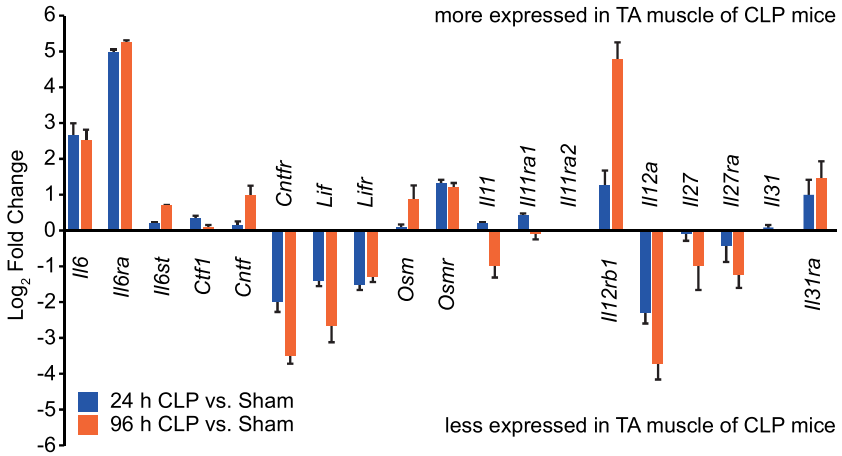

Figure 8. mRNA regulation of members of the IL-6 cytokine family and their receptors in CLP-treated mice. Sepsis was induced by CLP in C57BL/6J mice and animals sacrificed after 24 or 96 hours. Sham operated littermates were used as controls. Tibialis anterior muscles from three animals per group were harvested and subjected to bulk RNA sequencing. Depicted are the changes of CLP vs sham treated animals of the members of the IL-6 cytokine family and their respective receptors. Values are presented as mean ± SD. *Il6*: Interleukin 6; *Il6ra*: Interleukin 6 Receptor Subunit alpha; *Il6st*: Interleukin 6 Signal Transducer; *Ctf1*: Cardiotrophin 1; *Cntf*: Ciliary Neurotrophic Factor; *Cntfr*: Ciliary Neurotrophic Factor Receptor; *Lif*: Leukemia Inhibitory Factor; *Lifr*: Leukemia Inhibitory Factor Receptor; *Osm*: Oncostatin M; *Osmr*: Oncostatin M Receptor; *Il11*: Interleukin 11; *Il11ra1*: Interleukin 11 Receptor Subunit alpha 1, *Il11ra2*: Interleukin 11 Receptor Subunit alpha 2; *Il12rb1*: Interleukin 12 Receptor Subunit beta 1, *Il12a*: Interleukin 12A; *Il27*: Interleukin 27; *Il27ra*: Interleukin 27 Receptor Subunit alpha; *Il31*: Interleukin 31; *Il31ra*: Interleukin 31 Receptor Subunit alpha. Reprinted from Zanders et al., J Cachexia Sarcopenia Muscle. 2022 Feb;13(1):713-727 with permission under a Creative Commons Attribution 4.0 International License [49].

3.3 Interleukin 6 induces atrophy in murine C2C12 myocytes

Five days differentiated C2C12 myotubes were treated with 10 ng/ml rIL-6 for up to 96 hours. Following 24 hours of IL-6 treatment, an 11.1% relative reduction in myocyte diameter was observed, which remained consistent at 48 (9.7%), 72 (7.1%) and 96 hours

(9.0%). No significant alterations in myotube size were detected between these time points. No changes in *Fbxo32* or *Trim63* mRNA expression were observed between rIL-6 treatment and controls (Fig. 9C, D).

3.4 Interleukin 6 induces the JAK/STAT3 signaling pathway in murine C2C12 myocytes

Following treatment with rIL-6 for 5, 10, 30 and 60 minutes, the phosphorylation of STAT3 at Tyr705 was increased 1.2-fold at 5 minutes, followed by 2.1-fold at 10 minutes, 3.0-fold at 30 minutes, and 1.5-fold at 60 minutes (Fig. 9A).
After 24 hours, a 2.28-fold increase in *Socs3* mRNA expression was observed compared to the control group. After 48 and 72 hours of treatment, *Socs3* mRNA expression levels showed a 1.85-fold and 1.27-fold induction, respectively, while not meeting statistical significance at 72 hours (Fig. 9B).

3.5 Interleukin 6-induced myocyte atrophy is mediated by the gp130/JAK/STAT signaling pathway

Following transfection with siRNA targeting *Il6st* for 48 hours, a significant reduction in *Il6st* mRNA expression and gp130 protein content were observed after 48 hours (Fig. 10A, B). Upon treatment with rIL-6, an 11.8-fold induction of STAT3 phosphorylation was observed after 30 minutes. Knockdown of *Il6st* attenuated this response to 8.0-fold (relative reduction: 32.2 %; Fig. 10B). Furthermore, the knockdown of *Il6st* resulted in a reduction in *Socs3* mRNA expression from 3.58- to 3.16.fold (relative reduction; 11.7%; Fig. 19C).

In myocytes transfected with scrambled siRNA, treatment with rIL-6 led to a 28.4% reduction in myocyte diameter. Knockdown of *Il6st* attenuated this atrophic effect to 8.3% (relative reduction: 70.8%; Fig. 10D).

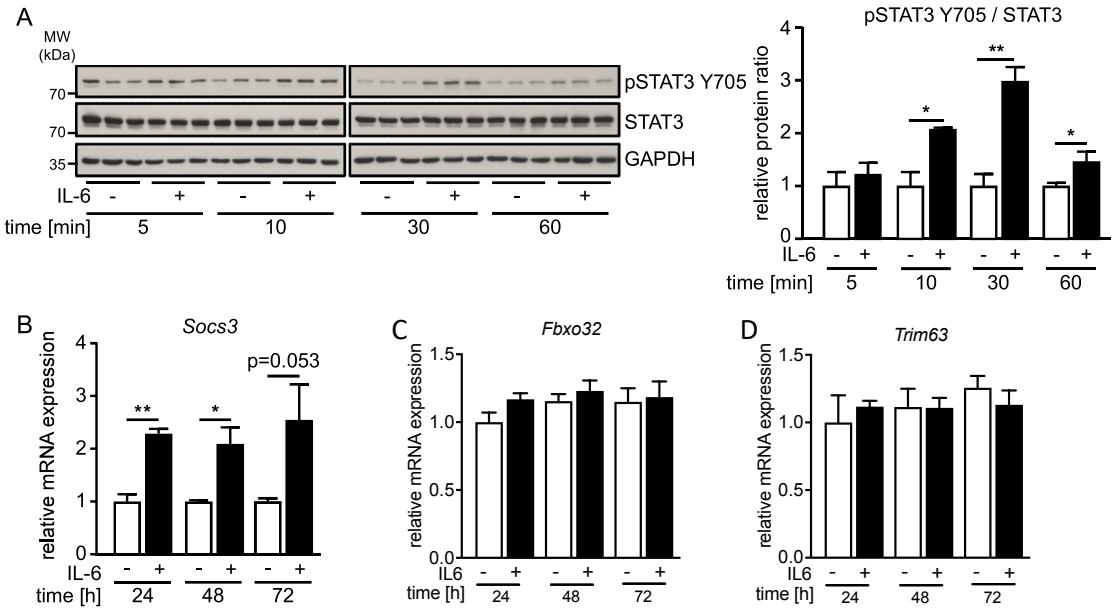

Figure 9. Interleukin 6 induces the JAK/STAT signaling pathway in myotubes. C2C12 myoblasts were differentiated into myotubes for 5 days and subsequently treated with 10 ng/ml recombinant murine Interleukin 6 for the given timepoints (n = 3 per group). **A**: Immunoblots of cell lysates using primary antibodies targeting GAPDH, STAT3 and pSTAT Y705 and densitometry analyses of the shown immunoblot. **B**: *Socs3* mRNA expression as determined by RT-qPCR. **C**: mRNA expression of *Fbxo32* as determined by RT-qPCR. **D**: *Trim63* mRNA expression as determined by RT-qPCR. * $p < 0.05$, ** $p < 0.01$ as determined by Mann-Whitney U test. Bar graphs show mean ± SD. pSTAT3 Y705: phospho-Signal Transducer and Activator of Transcription 3 at tyrosine 705; STAT3: Signal Transducer and Activator of Transcription 3; GAPDH: Glyceraldehyde-3-Phosphate Dehydrogenase; *Socs3*: Suppressor of Cytokine Signaling 3; *Fbxo32*: F-Box Protein 32; *Trim63*: Tripartite Motif Containing 63. Adapted from Zanders et al., J Cachexia Sarcopenia Muscle. 2022 Feb;13(1):713-727 with permission under a Creative Commons Attribution 4.0 International License [49].

The efficacy of JAK2-inhibition using Tyrphostin AG490 and STAT3-inhibition using C188-9 or S3I-201 was confirmed by an attenuation of IL-6-induced STAT3 phosphorylation and mRNA expression of *Socs3* (Fig. 10E, F, data for S3I-201 not shown).

The atrophic effect of rIL-6 treatment was attenuated by inhibition of JAK2 and was blocked by STAT3 inhibition (relative diameter reductions: solvent: 32.4%, AG490: 5.2%, C188-9: 0.7%).

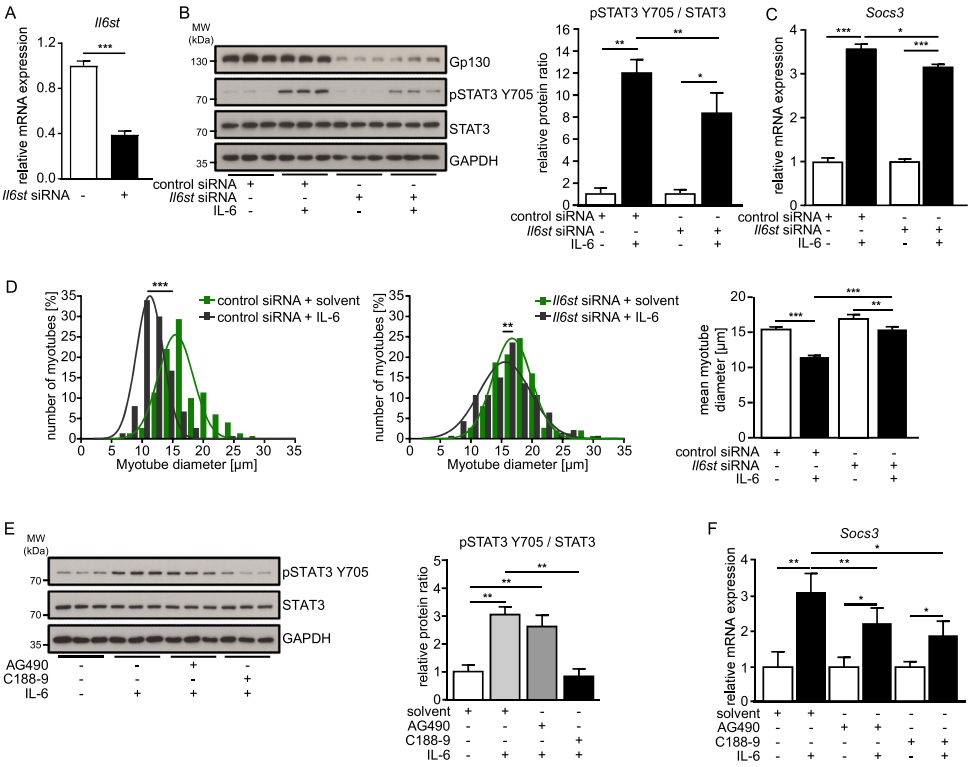

Figure 10. Effects of the gp130/JAK2/STAT3 signaling pathway on myotube atrophy after IL-6 treatment. C2C12 myoblasts were differentiated into myotubes for five days and subsequently treated with 10 ng/ml recombinant murine IL-6 with or without inhibitors for Januskinase 2 (AG490) or STAT3 (C188-9) or siRNA targeting *Il6st* (n = 3 per group). **A**: *Il6st* mRNA content in C2C12 myotubes after transfection with control siRNA or siRNA targeting *Il6st*. **B**: Immunoblots from C2C12 myotube lysates using primary antibodies targeting gp130, pSTAT3 Y705, STAT3 and GAPDH and according densitometry analyses of pSTAT Y705. **C**: *Socs3* mRNA content from C2C12 myotubes as determined by RT-qPCR. **D**: C2C12 myotube diameters of IL-6 treated C2C12 myotubes with or without transfection of siRNA targeting *Il6st*. Left and mid panel showing frequency distribution histograms, right panel showing mean diameters. **E**: Immunoblots using primary antibodies against pSTAT3 Y705, STAT3 and GAPDH and respective densitometry analyses of pSTAT3 Y705. **F**: *Socs3* mRNA content as determined by RT-qPCR from C2C12 myotubes. * $p < 0.05$, ** $p < 0.01$, *** $p < 0.001$ as determined by Mann-Whitney U tests (A, C, E, F) or two-tailed t-test (D). Bar graphs depict mean ± SD. *Il6st*: Interleukin 6 signal transducer; pSTAT3 Y705: phospho-Signal Transducer and Activator of Transcription 3 at tyrosine 705; STAT3: Signal Transducer and Activator of Transcription 3; GAPDH: Glyceraldehyde-3-Phosphate Dehydrogenase; *Socs3*: Suppressor of Cytokine Signaling 3**.** Reprinted from Zanders et al., J Cachexia Sarcopenia Muscle. 2022 Feb;13(1):713-727 with permission under a Creative Commons Attribution 4.0 International License [49].

3.6 Loss of gp130 in muscle cells attenuates sepsis-induced muscle atrophy in mice

Mice with a conditional knockout of *Il6st* (subsequently '*Il6st*$^{-/-}$') in the skeletal myocytes were subjected to CLP or sham surgery. At baseline, Il6st mRNA expression was reduced in *Il6st*$^{-/-}$ in TA and GP muscles. CLP-treated animals showed an induction of *Il6st* mRNA, which was attenuated in *Il6st*$^{-/-}$mice (Fig. 12E).

No significant differences in survival between treatment groups or genotypes were observed. One animal died within 96 hours after CLP (WT Sham: n = 6; WT CLP: n = 10; *Il6st*$^{-/-}$ sham: n = 6; *Il6st*$^{-/-}$ CLP: n = 15; Fig. 11).

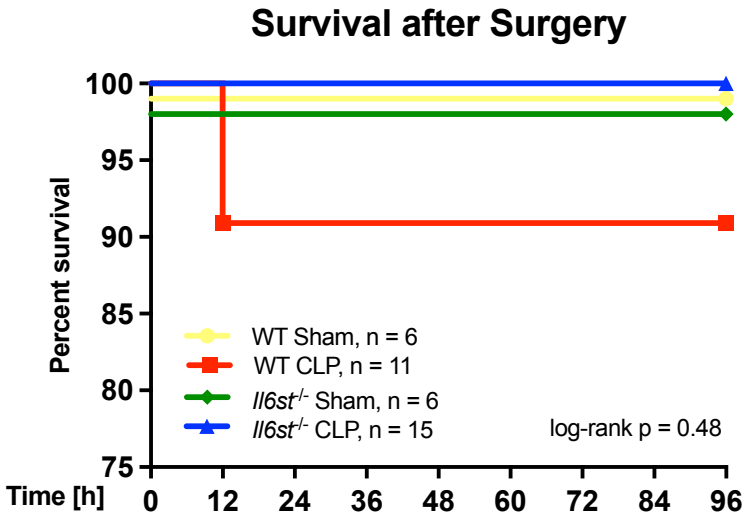

Figure 11. Survival of *Il6st*$^{-/-}$ and WT mice after CLP or surgery. Mice bearing a conditional deletion of *Il6st* in the skeletal myocyte lineage and WT controls were subjected to CLP or sham surgery. Survival was monitored for up to 96 hours and animals were subsequently sacrificed. The graph shows Kaplan-Meier-Curves for the treatment groups and the log-rank test was used for survival analyses. WT: Wild-type; *Il6st*: Interleukin 6 Signal Transducer.

IL-6 plasma levels were similar between WT and *Il6st*$^{-/-}$ animals in sham-operated controls (1.8±1.8 vs 2.4±2.4 pg/ml, p = 1.00) and septic animals (469±295 vs 351±170 pg/ml, p = 0.40).

After 96 hours of sepsis, WT mice exhibited a reduction of 22.3% and 19.7% in muscle weight in TA and GP muscle, respectively, compared to sham operated controls. A reduction in muscle weights of 13.5% and 7.7% was observed in TA and GP muscle of *Il6st*$^{-/-}$ mice, respectively (Fig. 11C, GP data not shown). This corresponded to a relative reduction in muscle weight loss of 39.46% in the TA muscle and 60.9% in the GP muscle of *Il6st*$^{-/-}$ animals. MCSAs of type II / fast twitch fibers from CLP-treated animals showed a 26.6% and 39.1% reduction in TA and GP, respectively. *Il6st*$^{-/-}$ mice showed a MCSA reduction of 6,0% in TA and 21,5% in GP (Fig. 11 D, GP data not shown). This translates to a relative reduction in MCSA loss of 77.4% in TA and 45.0% in GP muscle. Atrophy affected fast twitch/ type II fibers only, as slow twitch/type I myofibers did not exhibit

reductions in MCSA. No effect of genotype or treatment was observed on fiber type distribution.

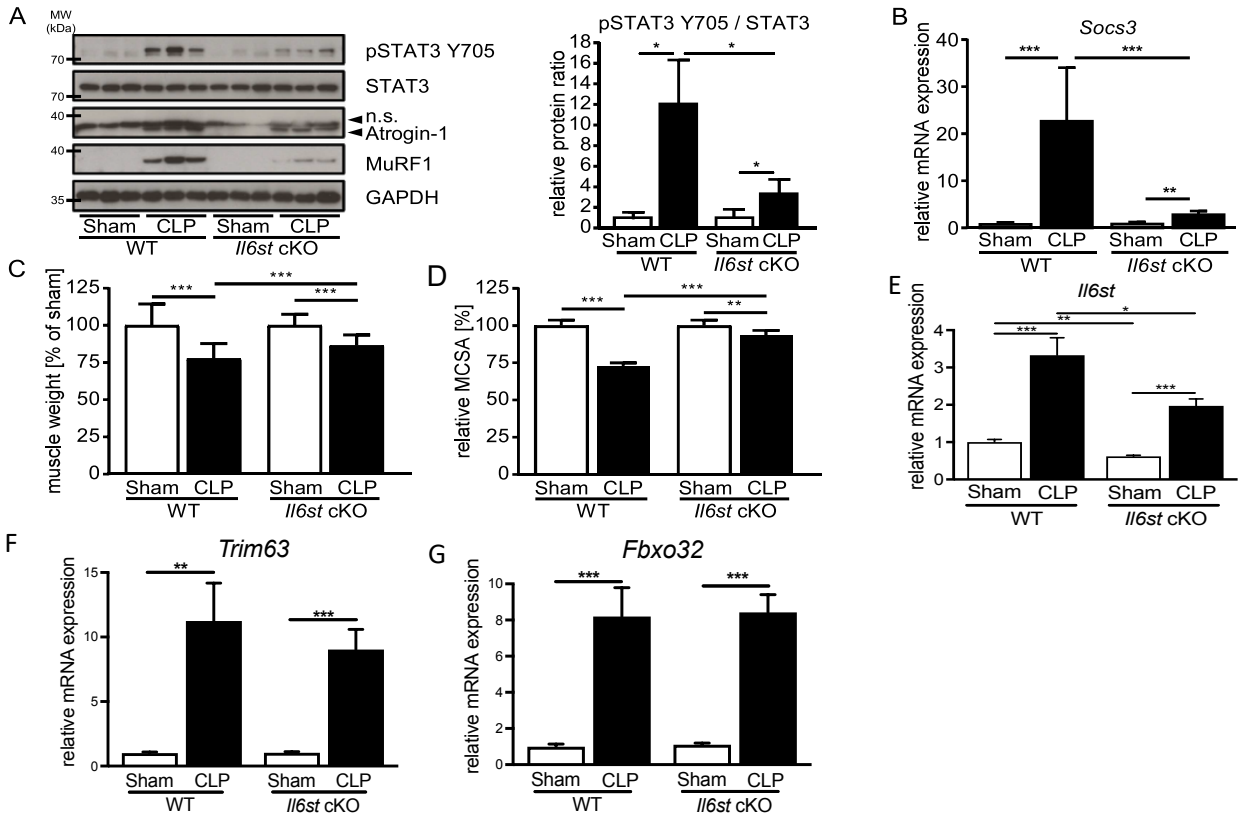

Figure 12. Analyses of muscle atrophy, signaling pathways and *atrogene* expression in tibialis anterior muscle of septic mice with a deletion of *Il6st* in myocytes. Mice bearing a specific deletion of *Il6st* in myocytes and according WT controls were subjected to CLP or sham surgery, sacrificed and tibialis anterior muscles harvested 24 (WT sham: n = 4, WT CLP: n = 6, *Il6st*$^{-/-}$ sham: n = 4, *Il6st*$^{-/-}$ CLP: n = 4) or 96 hours (WT sham: n = 6, WT CLP: n = 10, *Il6st*$^{-/-}$ sham: n = 6, *Il6st*$^{-/-}$ CLP: n = 15) after surgery. **A**: Immunoblots from tibialis anterior muscle lysates 24 hours after CLP or sham surgery using primary antibodies against pSTAT Y705, STAT3, Atrogin-1, MuRF1 and GAPDH and according densitometry analyses of pSTAT Y705 signals. **B**: *Socs3* mRNA content in tibialis anterior muscles 96 hours after surgery. **C**: Tibialis anterior muscle weights 96 hours after surgery. **D**: MCSA of fast-twitch / type 2 myocytes 96 hours after surgery. **E-F**: mRNA contents of *Il6st*, *Trim63* and *Fbxo32* in tibialis anterior muscles 96 hours after surgery as determined by RT-qPCR. * $p < 0.05$, ** $p < 0.01$, *** $p < 0.001$ as determined by Mann-Whitney U test (A, B, E-G) or two-tailed t test (C, D). Data are presented as mean ± SEM (A, B, E-G) or mean ± SD (C, D). pSTAT3 Y705: phospho-Signal Transducer and Activator of Transcription 3 at tyrosine 705; STAT3: Signal Transducer and Activator of Transcription 3; MuRF1: Muscle Really Interesing New Gene Finger 1; GAPDH: Glyceraldehyde-3-Phosphate Dehydrogenase; *Socs3*: Suppressor of Cytokine Signaling 3; *Il6st*: Interleukin 6 signal transducer; *Trim63*: Tripartit Motif Containing 63; *Fbxo32*: F-Box Protein 32, MCSA: Myocyte Cross Sectional Area. Adapted from Zanders et al., J Cachexia Sarcopenia Muscle. 2022 Feb;13(1):713-727 with permission under a Creative Commons Attribution 4.0 International License [49].

While protein levels of Atrogin-1 were not altered by loss of muscular *Il6st*, 24 hours after CLP, those of MuRF1 were reduced in septic *Il6st*$^{-/-}$ mice (WT sham: n = 4, WT CLP: n =

6, *Il6st*$^{-/-}$ sham: n = 4, *Il6st*$^{-/-}$ CLP: n = 4; Fig. 12A). Muscular *Trim63* and *Fbxo32* mRNA expression were not different between septic WT and *Il6st*$^{-/-}$ mice.

3.7 gp130 mediates the activation of the JAK/STAT signaling pathway in muscles of septic mice

After 24 hours of sepsis an induction of STAT3 phosphorylation at tyrosine 715 in TA and GP muscles was observed when compared to controls (Fig. 12A). This induction was attenuated in mice with loss of *Il6st* in myocytes. The upregulation of *Socs3* mRNA expression in muscles of septic WT animals was attenuated in *Il6st*$^{-/-}$ mice (Fig. 12B).

3.8 Inhibition of JAK2 attenuates sepsis-induced muscle atrophy in mice

WT animals were injected with the JAK2 inhibitor Tyrphostin AG490 or solvent and subsequently subjected to CLP or Sham procedure. Treatment with Tyrphostin AG490 did not result in different survival rates in septic mice (solvent sham: n = 5; solvent CLP: n = 11; AG490 sham: n = 5; AG 490 CLP: n = 12; Fig. 13).

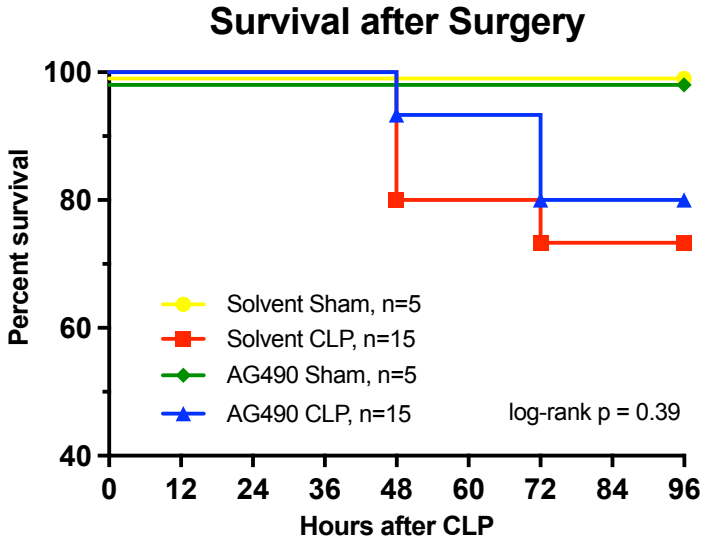

Figure 13. Survival rates after CLP- or sham-surgery according to treatment with solvent or Tyrphostin AG490. C57BL/6 mice were injected with Tyrphostin AG490 or solvent and subsequently subjected to CLP or sham surgery. Survival was monitored for 96 hours. The graph shows Kaplan-Meier-Curves for survival. The log-rank test was used for survival analysis. Animal numbers indicate mice entering the experiment.

At 96 hours after CLP, mice that received solvent infections exhibited a significant reduction in muscle weights, with a decrease of 19.2% in TA muscle and 17.4% in GP muscle. Mice treated with AG490 showed a reduction in muscle weights of 13.5% in TA muscle and 11.6% in GP muscle. This corresponds to a relative reduction in muscle weight loss of 29.7% in TA and 33.3% in GP muscle compared to solvent treated septic mice (Fig. 14C, GP data not shown).

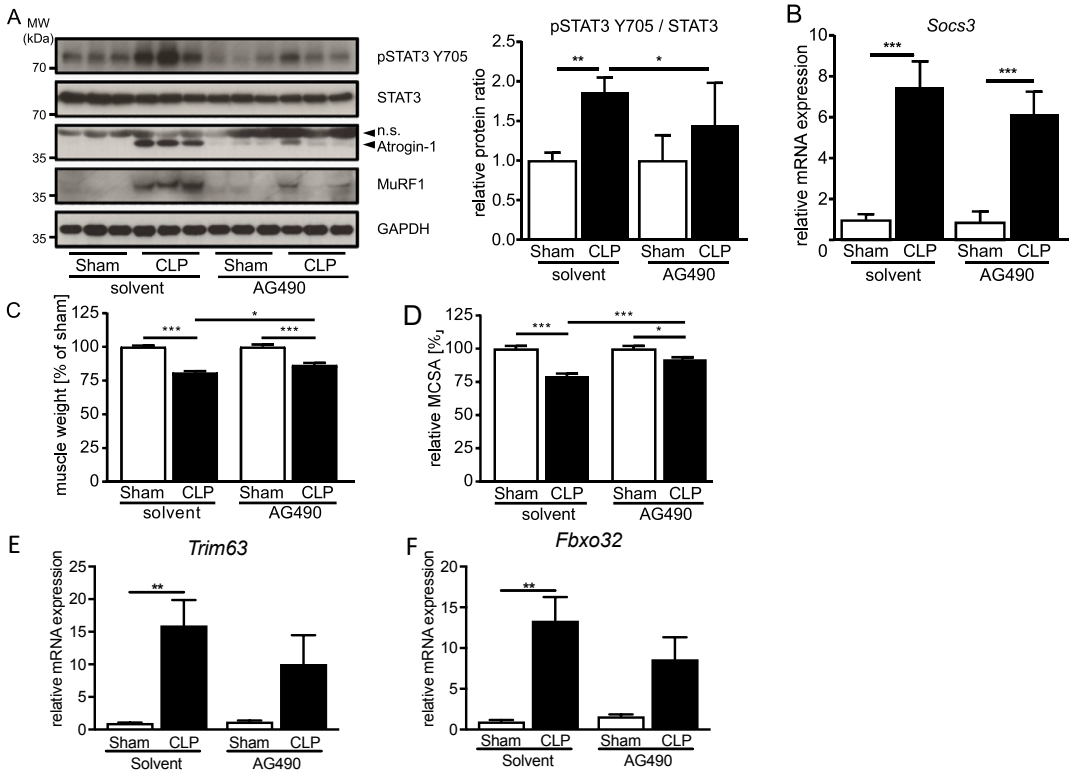

Figure 14. Analyses of muscle atrophy, signaling pathways and *atrogene* expression in tibialis anterior muscle of septic mice treated with solvent or Tyrphostin AG490. C57BL/6J mice were intraperitoneally injected with the Januskinase 2 inhibitor Tyrphostin AG490 or solvent, subjected to CLP or sham surgery and sacrificed 96 hours later. Tibialis anterior muscles were harvested (Solvent sham: n = 5, solvent CLP = 11, AG490 sham = 5, AG490 CLP = 12). **A**: Immunoblot analyses from tibialis anterior muscle lysates using primary antibodies against pSTAT3 Y705, STAT3, Atrogin-1, MuRF1 and GAPDH with according densitometry analyses for pSTAT Y705 signals. **B**: *Socs3* mRNA expression in tibialis anterior muscles as determined by RT-qPCR. **C**: Tibialis anterior muscle weights. **D**: Fast twitch / type 2 MCSA from tibialis anterior muscles. **E** *Trim63* mRNA expression in tibialis anterior muscles. **F** *Fbxo32* mRNA expression in tibialis anterior muscles. * $p < 0.05$, ** $p < 0.01$, *** $p < 0.001$ as determined by Mann-Whitney U test (A, B) or two-tailed t test (C, D). Bar graphs show mean ± SEM (A, B) or mean ± SD (C, D). pSTAT3 Y705: phospho-Signal Transducer and Activator of Transcription 3 at tyrosine 705; STAT3: Signal Transducer and Activator of Transcription 3; MuRF1: Muscle Really Interesting New Gene Finger 1; GAPDH: Glyceraldehyde-3-Phosphate Dehydrogenase; *Socs3*: Suppressor of Cytokine Signaling 3, MCSA: Myocyte Cross Sectional Area; *Trim63*: Tripartite Motif Containing 63; *Fbxo32*: F-Box Containing Protein 32 Adapted from Zanders et al., J Cachexia Sarcopenia Muscle. 2022 Feb;13(1):713-727 with permission under a Creative Commons Attribution 4.0 International License [49].

Solvent-treated mice with polymicrobial sepsis exhibited a significant reduction in MCSA, with a decrease of 20.7% in TA and 31.2% in GP muscle. Mice treated with AG490 showed a MCSA decrease of 8.6% in TA muscle and 25.5% in GP muscle. This corresponds to a relative reduction of 58.5% in TA muscle and 18.3% in GP muscle compared to solvent-treated septic mice (Fig. 14D, GP data not shown).
Treatment with AG490 resulted in a reduction in the mRNA expression of *Fbxo32* and *Trim63* as well as protein levels of Atrogin-1 and MuRF1 in septic mice (Fig. 14A, data on mRNA expression not shown). Solvent-treated septic mice exhibited an increase in STAT3 phosphorylation, which was attenuated by treatment with AG490 (Fig. 14A). No changes in *Socs3* mRNA expression were observed (Fig. 14B).

3.9 IL-6-induced signaling interferes with insulin signaling

Twenty-four hours following CLP, WT mice exerted reduced muscular AKT phosphorylation when compared to sham controls. This reduction was blocked by loss of muscular *Il6st* (Fig. 15A).
Five days differentiated C2C12 myotubes were treated with insulin with or without rIL-6 for one hour. Insulin-treatment resulted in an increase in phosphorylation of pIRS1 S636/639 and AKT S473. rIL-6 treatment induced STAT3 phosphorylation at Y705. Co-treatment with insulin and rIL-6 blocked the insulin-induced phosphorylation of IRS1 and AKT (Fig. 15B)

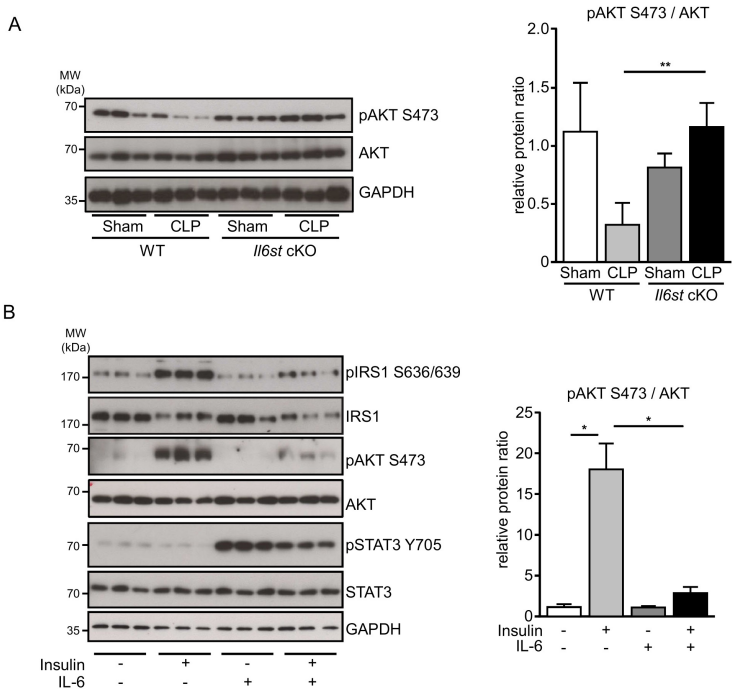

Figure 15. IL-6 induced signaling interferes with insulin signaling in myocytes. A: Mice bearing a conditional deletion of *Il6st* in the skeletal muscle cell lineage and WT controls were subjected to CLP or sham surgery, sacrificed 24 hours later and tibialis anterior muscles harvested (WT sham: n = 4, WT CLP: n = 6, *Il6st*$^{-/-}$ sham: n = 4, *Il6st*$^{-/-}$ CLP: n = 4). Depicted are immunoblots from tibialis anterior muscle lysates using primary antibodies targeting pAKT S473, AKT and GAPDH with according densitometry analyses of pAKT S473 signals. **B**: C2C12 myoblasts were differentiated into myotubes for five days and subsequently treated with IL-6 for 30 minutes and subsequently with solvent or insulin for another 60 minutes (n = 3 per group). Immunoblots of cell lysates using primary antibodies against pIRS1 S636/639, IRS1, pAKT S473, AKT, pSTAT3 Y705, STAT3 and GAPDH with according densitometry analyses of pAKT S473. * $p < 0.05$, ** $p < 0.01$ as determined by Mann-Whitney U test. Bar graphs show mean ± SEM. pIRS S636/639: phosphor-Insulin Receptor Substrate 1 at serines 636 and 639; IRS1: Insulin Receptor Substrate 1; pAKT S473: phospho-Protein Kinase B at serine 473; AKT: Protein Kinase B; pSTAT3 Y705: phospho-Signal Transducer and Activator of Transcription 3 at tyrosine 705; STAT3: Signal Transducer and Activator of Transcription 3; MuRF1: Muscle Really Interesting New Gene Finger 1; GAPDH: Glyceraldehyde-3-Phosphate Dehydrogenase; *Il6st*: Insulin 6 Signal Transducer. Reprinted from Zanders et al., J Cachexia Sarcopenia Muscle. 2022 Feb;13(1):713-727 with permission under a Creative Commons Attribution 4.0 International License [49].

4 Discussion

4.1 Brief summary of the findings

The data presented and published in Zanders et al. [49] demonstrate increased activation of the JAK/STAT signaling in skeletal muscles of critically ill patients. Bulk RNA sequencing of TA muscles from septic mice revealed higher expression levels of genes associated with IL-6-induced and JAK/STAT signaling, while genes associated with insulin- and PI3K/AKT-signaling were downregulated.

In vitro experiments showed that rIL-6-induced myocyte atrophy was mitigated by knockdown of *Il6st* or inhibition of either JAK2 or STAT3. Notably, rIL-6-induced myocyte atrophy was not associated with increased mRNA contents of *Trim63* or *Fbxo32*.

Loss of *Il6st* in myocytes reduced sepsis-induced muscle atrophy in mice and was associated with decreased JAK/STAT3 signaling pathway activation. While the expression of *Fbxo32*/Atrogin-1 remained unaffected by loss of *Il6st*, the content of MuRF1 was decreased without changes of *Trim63* in skeletal muscles of septic *Il6st*$^{-/-}$ mice.

Inhibiting JAK2 with the small molecule inhibitor Tyrphostin AG490 reduced the activation of JAK/STAT3-signaling, as well as the expression of *Trim63*/MuRF1 and *Fbxo32*/Atrogin-1 in muscles of septic mice.

Muscles of septic WT mice displayed signs of impaired insulin signaling, which was alleviated by loss of *Il6st* in skeletal myocytes. Co-treatment with rIL6 attenuated insulin-induced activation of the PI3K/AKT signaling pathway in myocytes *in vitro*.

4.2 Interpretation of the findings and integration with the current state of research

4.2.1 Cell type specificity of the observed effects

The experimental models employed in this study aimed to investigate the specific impact of gp130/JAK/STAT signaling on myocytes during sepsis-induced muscle atrophy. This approach was chosen, because breakdown of sarcomeric proteins is specific to myocytes, making them a potential target for therapeutic intervention.

Accordingly, a myocyte specific conditional knockout model of *Il6st* was used. In whole tissue lysates of skeletal muscles, *Il6st* mRNA was still detectable in *Il6st*$^{-/-}$ mice, as skeletal muscles contain various other cell types expressing *Il6st*, including pericytes, endothelial cells, immune and smooth muscle cells [52].

Considering the use of whole tissue samples in the *in vivo* experiments and the cohort study, contributions of other cell types to the observed effects have to be considered. Other cell types within skeletal muscles may undergo transcriptional and functional changes during sepsis, potentially contributing to inflammation-induced muscle atrophy through secondary effects, such as paracrine stimulation of myocytes. These cells also contain gp130 and JAK/STAT signaling in *Il6st*$^{-/-}$ mice, likely contributing to the remaining induction of STAT3 phosphorylation and *Socs3* mRNA expression in whole muscle lysates (Fig. 10 B, C) [53, 54]. Moreover, other receptors may have induced the JAK/STAT signaling pathway in myocytes.

It is essential to consider cellular heterogeneity, especially in the interpretation of mRNA analyses using RT-qPCR and bulk RNA-Seq. While myocytes constitute the large majority of skeletal muscle by volume, the number of nuclei belonging to other cell types is more relevant due to their smaller cell size. Nuclei contain substantial amounts of mRNA, which influences expression profiles in whole tissue samples.

However, since the deletion of *Il6st* was specific to myocytes, and gp130-mediated effects in other cell types would have attenuated the observed effects on mRNA and protein contents, it is reasonable to attribute the effects to gp130 in myocytes.

4.2.2 Specificity of the *in vivo* models for interleukin 6

Gp130 acts as a signal transducer for all members of the IL-6 cytokine family, raising the possibility that these other cytokines may contribute to the activation of gp130-mediated signaling and hence muscle atrophy.
During sepsis, circulating levels of the pro-inflammatory cytokines OSM, CNTF and LIF are elevated [55]. Interestingly, treatment with an OSM-receptor II antibody improved survival rates in septic mice, indicating a role of OSM in sepsis [56, 57]. Conversely, anti-

inflammatory members of the IL-6 family, such as CT-1 and IL-10, have demonstrated protective effects during sepsis [58, 59].

However, there are data suggesting IL-6 as the primary contributor to the observed effects. Plasma kinetics of IL-6 during sepsis are more pronounced than most of the other cytokines signaling through gp130 [55]. Additionally, the detrimental effects of IL-6 on skeletal muscle are well established, while other members of the IL-6 family have been associated with muscle regeneration and MSC differentiation [35, 60, 61]. Furthermore, the observed atrophic *in vivo* effects were replicated *in vitro* through rIL-6 treatment of myocytes. However, further research is needed to elucidate the role of individual members of the IL-6 cytokine family in inflammation-induced muscle atrophy, especially considering the potential involvement of OSM in muscle plasticity and inflammatory conditions [56, 60].

The utilized *Il6st* cKO model, while lacking specificity for IL-6-mediated effects, offers several advantages over alternative models. The expression level of membrane-bound IL-6R in skeletal myocytes remains uncertain, and myocyte-specific deletion of *Il6ra* would likely have minimal impact on systemic sIL-6R levels, while a global deletion could introduce secondary effects on myocytes. On the other hand, choosing a myocyte-specific *Il6* deletion would likely have minimal relevant effects on circulating plasma levels, while global deletion would blunt myocyte-specific effects.

Considering that the aim of the study was to investigate IL-6-induced signaling pathways, a myocyte-specific deletion of *Il6st* was employed to investigate the role of IL-6-mediated signaling in sepsis-induced muscle atrophy.

4.2.3 Sepsis model

The cecal ligation and puncture (CLP) model was utilized to induce peritonitis and subsequent polymicrobial sepsis [62]. However, there are other modelsto investigate the effects of sepsis in mice.

An alternative approach is Colon Ascendens Stent Peritonitis (CASP), which involves puncturing of the cecum and placement of a plastic stent into the cecal wall to facilitate

intraluminal content spillage into the abdominal cavity. CASP produces a more severe septic phenotype, with mortality rates reaching up to 100% after 48 hours [63].
A modification of this technique is the Colon Ascendens Stent Peritonitis with Intervention (CASPI), which adds stent removal after a given time and closure of the induced perforation to simulate the treatment course of intraabdominal sepsis [64].

CASP and CASPI offer better standardization through the selection of different stent sizes and explantation timepoints in the case of CASPI. In CLP, the severity of peritonitis can be controlled through the position of cecal ligation and the puncturing size [41, 63]. However, the CASP procedure is more time-consuming and, in the case of CASPI, requires an additional surgical intervention, which increases the likelihood of introducing confounding effects related to the procedures itself. Both CLP and CASP require large numbers of animals due to high mortality rates and interindividual variability in inflammatory responses [62].

Another commonly used model in sepsis research is endotoxin injection. This model induces endotoxemia, an inflammatory response and hemodynamic dysregulation, resembling septic shock [65]. However, since LPS signals through well-characterized signaling pathways, primarily activating TLR2 and TLR4 and does not induce bacteremia, it is to be considered more representative of septic shock rather than sepsis. LPS injection does not capture the complexity of sepsis as observed in the CLP and CASP techniques [66].

The CLP procedure is well-established in the host lab. Given the reliability of CLP in inducing sepsis and muscle atrophy and its established use in CIM research, it was selected for this project [15, 31, 67].

The CLP model can elicit varying phenotypes in different mouse strains. Mice used for the pharmacologic inhibitor experiment exhibited higher mortality compared to the *Il6st* cKO experiments. This difference is likely attributed to the distinct genetic backgrounds utilized in generating the loxP allele, whereby E14 embryonic stem cells from the 1290Ia mouse strain were implanted into C57BL/6 mice [40]. For the inhibitor experiment, C57BL/6J mice were used.

4.2.4 Mechanisms of muscle atrophy in different models

In mice bearing a myocyte-specific *Il6st* deletion and those systemically treated with the JAK2-inhibitor AG490, distinct expression patterns of *Fbxo32*/Atrogin-1 and *Trim63*/MuRF1 mRNA and protein levels were observed.
While no differences between mRNA expression levels were observed between muscles of septic WT and *Il6st*$^{-/-}$ mice, septic *Il6st*$^{-/-}$ mice exerted decreased protein levels of MuRF1 compared to WT littermates (Fig. 12A). Systemic inhibition of JAK2 on the other hand resulted in attenuated muscular mRNA expression levels of *Trim63* and *Fbxo32* as well as protein contents of MuRF1 and Atrogin-1 compared to solvent-treated controls (Fig. 14A).

Given the myocyte specificity of *Il6st* loss and the systemic administration of AG490, it is expected, that global JAK2 inhibition introduces in secondary effects on skeletal muscles (Fig. 14A). This model lacks the specificity to distinguish between secondary and primary muscular effects. The observed expression profiles of atrogenes resemble those observed in other models investigating systemic regulatory factors of sepsis-induced muscle atrophy, such as global *Nlrp3* KO or systemic NF-κB inhibition. This suggests that the observed muscular effects are partly attributable to attenuated systemic inflammation [31, 33].

While the JAK2/STAT3 signaling pathway plays a role in mediating muscle atrophy during sepsis, its inhibition by loss of *Il6st* in myocytes did not block skeletal muscle atrophy entirely [4, 18, 37, 49]. Signaling pathways induced by other upstream regulators with known atrophic effects, such as IL-1β, LPS and SAA1, likely contribute to muscle atrophy in the absence of *Il6st* [15, 31, 33]. Moreover, while inhibition of JAK2 and phosphorylation of STAT3 was investigated, other members of the JAK/STAT signaling pathway might still be active and contribute to muscle atrophy.

The most likely effector of the attenuated JAK2/STAT3 activation and muscle atrophy in *Il6st*$^{-/-}$ mice is MuRF1, which shows decreased protein contents despite unchanged *Trim63* mRNA levels.
This phenotype has not been reported previously and might be caused by post-translational mRNA silencing by noncoding RNAs, as seen in a model of chronic kidney

disease (CKD)-induced muscle atrophy, where overexpression of the microRNAs (miRNA) 23a and 27a resulted in an attenuation of muscle weight loss and MuRF1 protein levels [68]. CKD is associated with increased Angiotensin II serum levels, which exerts skeletal muscle atrophy primarily through IL-6 [69].
Treating C2C12 myotubes with rIL-6 results in increased MuRF1 protein content without affecting *Trim63* mRNA expression, supporting the idea of a post-transcriptional mechanism [4]. Investigating these post-transcriptional mechanisms might elucidate targeted therapies not only for CIM, but also other types of muscle atrophy.
Another potential explanation of the distinct *Trim63*/MuRF1 expression profile is an inhibitory effect of gp130-mediated signaling on MuRF1 protein degradation, although specific mechanisms of targeted MuRF1 proteolysis remain speculative.

In myocytes of septic mice, loss of *Il6st* did not alter Atrogin-1 content in contrast to a previous study of cancer cachexia, in which loss of gp130 in skeletal myocytes attenuated Atrogin-1 contents in skeletal muscles [18]. In accordance with the here presented data, global deletion of *Il6* did not affect *Fbxo32* mRNA or Atrogin-1 levels in an intestinal cancer model [61]. In denervation-induced muscle atrophy, treatment with an IL-6R antibody attenuated *Fbxo32* and Atrogin-1 induction [4].
The effects of global *Il6* KO and systemic IL-6R blockade introduce secondary effects and are not comparable to myocyte-specific deletions [4, 31, 33]. The different effects of myocyte *Il6st* loss in cancer cachexia and sepsis might indicate distinct mechanisms of gp130-mediated signaling on Atrogin-1 expression in these conditions. These differences might arise from different cytokine concentrations and expression patterns within the IL-6 family [18, 49].

There is limited data on the expression profiles of *Trim63* and MuRF1 in association with JAK/STAT signaling. While global deletion of *Il6* does not alter *Trim63* expression in an intestinal cancer model, treatment with an antibody targeting IL-6R reduced both *Trim63* mRNA and MuRF1 protein content in denervation atrophy [4, 61].

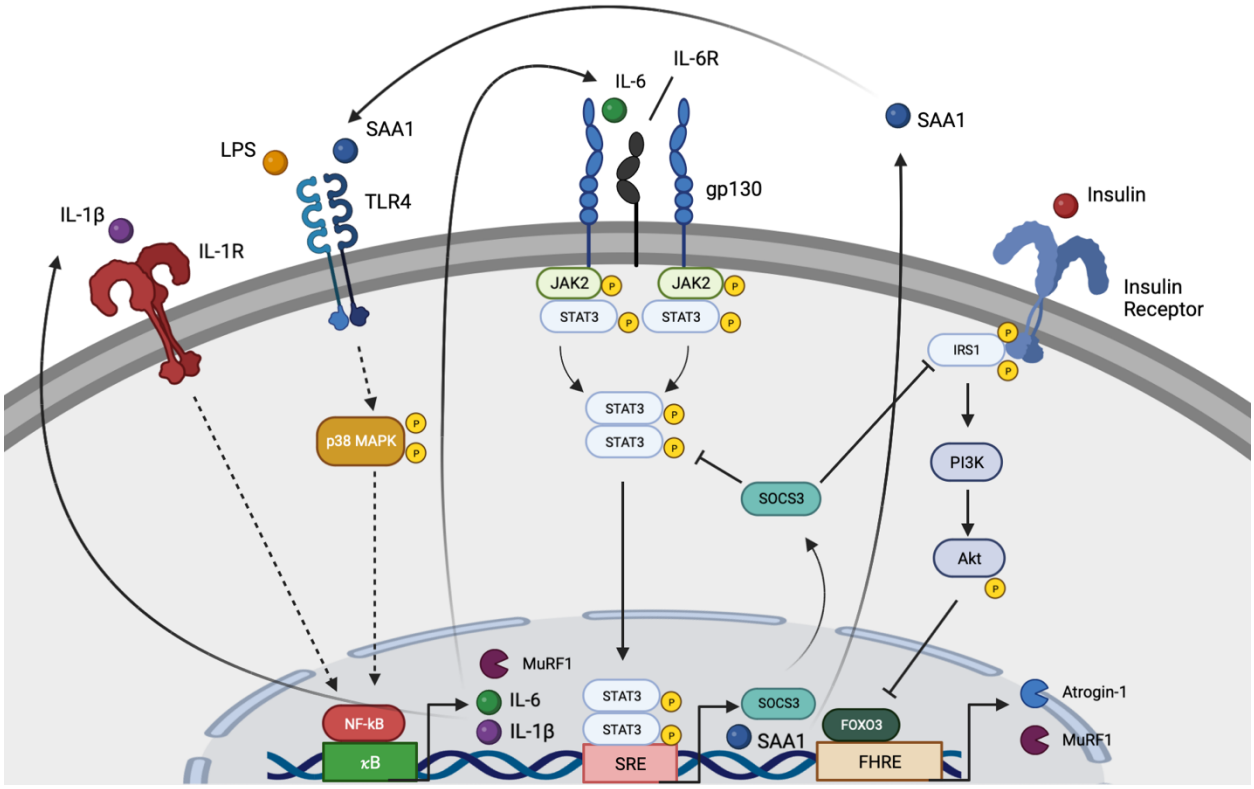

Figure 16. Suggested interactions of gp130-mediated intracellular signaling with other signaling pathways involved in sepsis-induced muscle atrophy. The depicted DNA binding sites (κB, SRE and FHRE) are examples of possible binding sites for NF-κB, STAT3 and FOXO3. gp130: glycoprotein 130; IL-6: Interleukin 6; IL-6R: Interleukin 6 receptor; IRS1: Insulin Receptor Substrate 1; PI3K: phosphoinositide-3-kinase; AKT: protein kinase B; FOXO3: Forkhead Box O3; FHRE: Forkhead Response Element; JAK2: Januskinase 2; STAT3: Signal transducer and activator of Transcription 3; SRE: Serum Response Element; LPS: Lipopolysaccharide; SAA1: Serum Amyloid A1; TLR4: Toll-Like Receptor 4; p38 MAPK: p38 Mitogen-Activated Protein Kinase; IL-1β : Interleukin 1 beta; IL-1R: Interleukin 1 Receptor; NF-κB: Nuclear Factor kappa-light-chain-enhancer of activated B cells, κB: Kappa B binding site; MuRF1: Muscle Really Interesting New Gene Finger 1. Created with biorender.com.

4.2.5 The PI3K/AKT signaling pathway in Critical Illness Myopathy

In skeletal muscles from septic WT mice, a reduced phosphorylation of AKT at S473 was observed, which was blocked by loss of *Il6st* in myocytes (Fig. 15A). Additionally, insulin-treatment of C2C12 myotubes led to induced AKT-phosphorylation, which was attenuated by co-treatment with rIL-6 (Figs. 15B, 16).

Previous studies have shown that the synergistic signaling of SAA1 and IL-6 can reduce AKT phosphorylation through IRS-1 degradation. During muscle atrophy, activation of AKT phosphorylation is suppressed [27, 28, 69]. The IL-6 target gene *SOCS3* has been implicated in UPS-mediated degradation of IRS-1 *in vitro* (Fig. 16) [30]. *In vivo*, loss of

Il6st resulted in rescued AKT phosphorylation, which is in line with these reports. However, rIL-6 alone attenuated insulin-induced AKT phosphorylation without affecting IRS1 protein content but reducing IRS-1 phosphorylation *in vitro*, suggesting a distinct mechanism by which IL-6 interferes with the PI3K-AKT signaling pathway in myocytes.

These findings are in contrast to the observation, that IL-6 can induce PI3K/AKT signaling itself [34, 70], which might be caused by differences in models or synergistic effects with other cytokines, as demonstrated for SAA1 [69].

Notably, in a clinical cohort of critically ill patients, increased AKT-phosphorylation was observed in skeletal muscle biopsies, along with increased IL-6 plasma concentrations. However, given the decreased insulin sensitivity and high insulin doses administered to these patients, the increase in AKT phosphorylation might be a result therapeutic interventions [29].

A more comprehensive study including different IL-6 dosages, co-stimulation and inhibition of components of the signaling pathways involved are needed to further elucidate the underlying mechanisms.

4.3 Strengths & Limitations

The presented data, for the first time, show a pivotal role of muscular JAK/STAT signaling in sepsis-induced muscle atrophy. Using a comprehensive translational approach, including patient's samples, *in vivo* and *in vitro* data, the study substantially contributes to the understanding of CIM. Using a small molecule inhibitor of JAK2 and demonstrating protective effects against muscle atrophy, the study provides a possible therapeutic approach in the treatment of ICUAW.

However, the conducted experiments have certain limitations. With the exception of the analyses performed on the clinical cohort, all other experiments were conducted using mice and murine cell lines. Therefore, the applicability of these models to humans may be restricted and requires further validation using human cell lines and tissues.
It should be noted that the *in vivo* experiments only utilized male mice aged between 12 and 20 weeks, which limits the generalizability of the findings to females and older

subjects. Furthermore, the exact cytokine or combination of cytokines from the IL-6 family that induce the observed effects could not be determined conclusively.

The small molecule inhibitors employed in the study exhibit high specificity at the dosages used. Tyrphostin AG490 does have off-target effects on JAK3 only at higher dosages than those administered in the experiments. C188-9 on the other hand, does not exert any known off-target effects. Although clinical inhibitors targeting the JAK/STAT signalling pathway possess less selective target profiles, the selected inhibitors were chosen in this study to specifically investigate the effects of the JAK2/STAT3 signaling pathway. However, further research is necessary to validate these findings using substances that are approved for clinical use.

The analytic approach of muscle atrophy chosen in this study was an anatomic one and no functional assays, such as grip strength, have been performed. These measurements would have added valuable functional data and should be considered in future experiments in this field.

4.4 Perspectives for clinical applications

The data presented are in line with previous studies indicating that gp130 plays a role in different models of muscle atrophy, including cancer and denervation [18, 37, 71, 72]. Mice with these conditions demonstrate elevated phosphorylation of skeletal muscle STAT3. While these models show distinct atrogene expression profiles, inhibition of the JAK/STAT signaling pathway consistently showed anti-atrophic effects.

Considering the involvement of the gp130/JAK2/STAT3 signaling pathway in cancer-, denervation-, and sepsis-induced muscle atrophy, it is tempting to speculate that these findings may have broader implications also for other forms of muscle atrophy and might represent a therapeutic target for use in patients.

The presented data indicate that inhibition of JAK2 attenuates sepsis-induced skeletal muscle atrophy *in vivo*. Previous studies have shown that inhibition of JAK2 improved

survival rates after CLP and reduced signs of acute liver damage after LPS injections in mice [73-75].

In human umbilical vein endothelial cells (HUVEC), STAT3-inhibition after LPS stimulation resulted in lower expression levels of vascular cell adhesion molecule 1 (VCAM-1) and intracellular adhesion molecule 1 (ICAM-1), which are key factors in the pathomechanism of sepsis-induced multi organ failure [51]. These data indicate that JAK2-inhibition may elicit beneficial effects beyond the attenuation of muscle atrophy in sepsis.

Over the past years, several small molecule inhibitors of different JAK isoforms have entered clinical practice. For example, inhibition of JAK1 and 2 resulted in improved clinical outcomes in rheumatoid arthritis and better survival in primary myelofibrosis and polycythemia vera, while being well tolerated [76-78].
Patients with severe Covid-19 show similar cytokine storm dynamics as patients with sepsis [79]. A central role for IL-6/gp130/JAK/STAT3-signaling in Covid-19 has been elucidated [79]. In the ACTT-2 trial of patients with Covid-19, inhibition of JAK1 and JAK2 using baricitinib in addition to remdesevir resulted in a shorter time to recovery and a trend towards lower mortality [80]. Notably, this effect was more pronounced in patients with more severe disease. In the COV-BARRIER trial, treatment of hospitalized Covid-19 patients with or without baseline treatment with remdesevir resulted in a lower mortality in the baricitinib group, while showing a good safety profile. Again, the beneficial effect was more pronounced in patients on high-flow oxygen or non-invasive ventilation when compared to the overall cohort also including patients without need for oxygen supplementation or on normal flow oxygen supplementation [81]. These data implicate a more pronounced benefit in patients with higher inflammatory activity, which has been shown in more severe cases of Covid-19 [79].

The clinically available inhibitors lack specificity for JAK2 that is observed with AG490. However, because of the partial functional redundancy between the different JAKs as well as the more specific inhibitors under development for clinical use, there is an opportunity of JAK-inhibition for the prevention of intensive care unit acquired weakness in critically ill patients.

5 Conclusion

The presented data provides evidence for a key role of gp130/JAK2/STAT3-signaling in sepsis-induced muscle atrophy both *in vivo* and *in vitro*. Activation of the JAK/STAT signaling pathway was observed in skeletal muscle biopsies from critically ill patients and septic mice. Interference with this signaling pathway, either by deletion of *Il6st* or inhibition of JAK2 attenuated muscle atrophy in septic mice.

This study adds a causal explanation for the effects of IL-6 on skeletal muscle during sepsis and introduces potential novel therapeutic approaches for critical illness myopathy.

References

1. Luis, N.M. and F. Schnorrer, *Mechanobiology of muscle and myofibril morphogenesis.* Cells Dev, 2021. **168**: p. 203760.
2. Plotkin, D.L., M.D. Roberts, C.T. Haun, and B.J. Schoenfeld, *Muscle Fiber Type Transitions with Exercise Training: Shifting Perspectives.* Sports (Basel), 2021. **9**(9).
3. Adams, G.R., *Satellite cell proliferation and skeletal muscle hypertrophy.* Appl Physiol Nutr Metab, 2006. **31**(6): p. 782-90.
4. Huang, Z., L. Zhong, J. Zhu, H. Xu, W. Ma, L. Zhang, Y. Shen, B.Y. Law, F. Ding, X. Gu, and H. Sun, *Inhibition of IL-6/JAK/STAT3 pathway rescues denervation-induced skeletal muscle atrophy.* Ann Transl Med, 2020. **8**(24): p. 1681.
5. Weber-Carstens, S., M. Deja, S. Koch, J. Spranger, F. Bubser, K.D. Wernecke, C.D. Spies, S. Spuler, and D. Keh, *Risk factors in critical illness myopathy during the early course of critical illness: a prospective observational study.* Crit Care, 2010. **14**(3): p. R119.
6. Schefold, J.C., T. Wollersheim, J.J. Grunow, M.M. Luedi, W.J. Z'Graggen, and S. Weber-Carstens, *Muscular weakness and muscle wasting in the critically ill.* J Cachexia Sarcopenia Muscle, 2020. **11**(6): p. 1399-1412.
7. Bodine, S.C., E. Latres, S. Baumhueter, V.K. Lai, L. Nunez, B.A. Clarke, W.T. Poueymirou, F.J. Panaro, E. Na, K. Dharmarajan, Z.Q. Pan, D.M. Valenzuela, T.M. DeChiara, T.N. Stitt, G.D. Yancopoulos, and D.J. Glass, *Identification of ubiquitin ligases required for skeletal muscle atrophy.* Science, 2001. **294**(5547): p. 1704-8.
8. Gomes, M.D., S.H. Lecker, R.T. Jagoe, A. Navon, and A.L. Goldberg, *Atrogin-1, a muscle-specific F-box protein highly expressed during muscle atrophy.* Proc Natl Acad Sci U S A, 2001. **98**(25): p. 14440-5.
9. Olguin, H.C., *The Gentle Side of the UPS: Ubiquitin-Proteasome System and the Regulation of the Myogenic Program.* Front Cell Dev Biol, 2021. **9**: p. 821839.
10. Sandri, M., C. Sandri, A. Gilbert, C. Skurk, E. Calabria, A. Picard, K. Walsh, S. Schiaffino, S.H. Lecker, and A.L. Goldberg, *Foxo transcription factors induce the atrophy-related ubiquitin ligase atrogin-1 and cause skeletal muscle atrophy.* Cell, 2004. **117**(3): p. 399-412.
11. Hirano, T., K. Yasukawa, H. Harada, T. Taga, Y. Watanabe, T. Matsuda, S. Kashiwamura, K. Nakajima, K. Koyama, A. Iwamatsu, and et al., *Complementary*

DNA for a novel human interleukin (BSF-2) that induces B lymphocytes to produce immunoglobulin. Nature, 1986. **324**(6092): p. 73-6.

12. Schmidt, S., N. Schumacher, J. Schwarz, S. Tangermann, L. Kenner, M. Schlederer, M. Sibilia, M. Linder, A. Altendorf-Hofmann, T. Knosel, E.S. Gruber, G. Oberhuber, J. Bolik, A. Rehman, A. Sinha, J. Lokau, P. Arnold, A.S. Cabron, F. Zunke, C. Becker-Pauly, A. Preaudet, P. Nguyen, J. Huynh, S. Afshar-Sterle, A.L. Chand, J. Westermann, P.J. Dempsey, C. Garbers, D. Schmidt-Arras, P. Rosenstiel, T. Putoczki, M. Ernst, and S. Rose-John, *ADAM17 is required for EGF-R-induced intestinal tumors via IL-6 trans-signaling.* J Exp Med, 2018. **215**(4): p. 1205-1225.
13. Cressman, D.E., L.E. Greenbaum, R.A. DeAngelis, G. Ciliberto, E.E. Furth, V. Poli, and R. Taub, *Liver failure and defective hepatocyte regeneration in interleukin-6-deficient mice.* Science, 1996. **274**(5291): p. 1379-83.
14. Poli, V., R. Balena, E. Fattori, A. Markatos, M. Yamamoto, H. Tanaka, G. Ciliberto, G.A. Rodan, and F. Costantini, *Interleukin-6 deficient mice are protected from bone loss caused by estrogen depletion.* EMBO J, 1994. **13**(5): p. 1189-96.
15. Langhans, C., S. Weber-Carstens, F. Schmidt, J. Hamati, M. Kny, X. Zhu, T. Wollersheim, S. Koch, M. Krebs, H. Schulz, D. Lodka, K. Saar, S. Labeit, C. Spies, N. Hubner, J. Spranger, S. Spuler, M. Boschmann, G. Dittmar, G. Butler-Browne, V. Mouly, and J. Fielitz, *Inflammation-induced acute phase response in skeletal muscle and critical illness myopathy.* PLoS One, 2014. **9**(3): p. e92048.
16. Begue, G., A. Douillard, O. Galbes, B. Rossano, B. Vernus, R. Candau, and G. Py, *Early activation of rat skeletal muscle IL-6/STAT1/STAT3 dependent gene expression in resistance exercise linked to hypertrophy.* PLoS One, 2013. **8**(2): p. e57141.
17. Ebisui, C., T. Tsujinaka, T. Morimoto, K. Kan, S. Iijima, M. Yano, E. Kominami, K. Tanaka, and M. Monden, *Interleukin-6 induces proteolysis by activating intracellular proteases (cathepsins B and L, proteasome) in C2C12 myotubes.* Clin Sci (Lond), 1995. **89**(4): p. 431-9.
18. Puppa, M.J., S. Gao, A.A. Narsale, and J.A. Carson, *Skeletal muscle glycoprotein 130's role in Lewis lung carcinoma-induced cachexia.* FASEB J, 2014. **28**(2): p. 998-1009.
19. Rose-John, S., *IL-6 trans-signaling via the soluble IL-6 receptor: importance for the pro-inflammatory activities of IL-6.* Int J Biol Sci, 2012. **8**(9): p. 1237-47.

20. Riedemann, N.C., T.A. Neff, R.F. Guo, K.D. Bernacki, I.J. Laudes, J.V. Sarma, J.D. Lambris, and P.A. Ward, *Protective effects of IL-6 blockade in sepsis are linked to reduced C5a receptor expression.* J Immunol, 2003. **170**(1): p. 503-7.
21. Barkhausen, T., T. Tschernig, P. Rosenstiel, M. van Griensven, R.P. Vonberg, M. Dorsch, A. Mueller-Heine, A. Chalaris, J. Scheller, S. Rose-John, D. Seegert, C. Krettek, and G.H. Waetzig, *Selective blockade of interleukin-6 trans-signaling improves survival in a murine polymicrobial sepsis model.* Crit Care Med, 2011. **39**(6): p. 1407-13.
22. Bierbrauer, J., S. Koch, C. Olbricht, J. Hamati, D. Lodka, J. Schneider, A. Luther-Schroder, C. Kleber, K. Faust, S. Wiesener, C.D. Spies, J. Spranger, S. Spuler, J. Fielitz, and S. Weber-Carstens, *Early type II fiber atrophy in intensive care unit patients with nonexcitable muscle membrane.* Crit Care Med, 2012. **40**(2): p. 647-50.
23. Herridge, M.S., C.M. Tansey, A. Matte, G. Tomlinson, N. Diaz-Granados, A. Cooper, C.B. Guest, C.D. Mazer, S. Mehta, T.E. Stewart, P. Kudlow, D. Cook, A.S. Slutsky, A.M. Cheung, and G. Canadian Critical Care Trials, *Functional disability 5 years after acute respiratory distress syndrome.* N Engl J Med, 2011. **364**(14): p. 1293-304.
24. de Jonghe, B., J.C. Lacherade, T. Sharshar, and H. Outin, *Intensive care unit-acquired weakness: risk factors and prevention.* Crit Care Med, 2009. **37**(10 Suppl): p. S309-15.
25. Bolton, C.F., J.J. Gilbert, A.F. Hahn, and W.J. Sibbald, *Polyneuropathy in critically ill patients.* J Neurol Neurosurg Psychiatry, 1984. **47**(11): p. 1223-31.
26. Patel, B.K., A.S. Pohlman, J.B. Hall, and J.P. Kress, *Impact of early mobilization on glycemic control and ICU-acquired weakness in critically ill patients who are mechanically ventilated.* Chest, 2014. **146**(3): p. 583-9.
27. Bodine, S.C., T.N. Stitt, M. Gonzalez, W.O. Kline, G.L. Stover, R. Bauerlein, E. Zlotchenko, A. Scrimgeour, J.C. Lawrence, D.J. Glass, and G.D. Yancopoulos, *Akt/mTOR pathway is a crucial regulator of skeletal muscle hypertrophy and can prevent muscle atrophy in vivo.* Nat Cell Biol, 2001. **3**(11): p. 1014-9.
28. Sacheck, J.M., A. Ohtsuka, S.C. McLary, and A.L. Goldberg, *IGF-I stimulates muscle growth by suppressing protein breakdown and expression of atrophy-related ubiquitin ligases, atrogin-1 and MuRF1.* Am J Physiol Endocrinol Metab, 2004. **287**(4): p. E591-601.

29. Weber-Carstens, S., J. Schneider, T. Wollersheim, A. Assmann, J. Bierbrauer, A. Marg, H. Al Hasani, A. Chadt, K. Wenzel, S. Koch, J. Fielitz, C. Kleber, K. Faust, K. Mai, C.D. Spies, F.C. Luft, M. Boschmann, J. Spranger, and S. Spuler, *Critical illness myopathy and GLUT4: significance of insulin and muscle contraction.* Am J Respir Crit Care Med, 2013. **187**(4): p. 387-96.
30. Rui, L., M. Yuan, D. Frantz, S. Shoelson, and M.F. White, *SOCS-1 and SOCS-3 block insulin signaling by ubiquitin-mediated degradation of IRS1 and IRS2.* J Biol Chem, 2002. **277**(44): p. 42394-8.
31. Hahn, A., M. Kny, C. Pablo-Tortola, M. Todiras, M. Willenbrock, S. Schmidt, K. Schmoeckel, I. Jorde, M. Nowak, E. Jarosch, T. Sommer, B.M. Broker, S.B. Felix, C. Scheidereit, S. Weber-Carstens, C. Butter, F.C. Luft, and J. Fielitz, *Serum amyloid A1 mediates myotube atrophy via Toll-like receptors.* J Cachexia Sarcopenia Muscle, 2020. **11**(1): p. 103-119.
32. Cannon, J.G., R.G. Tompkins, J.A. Gelfand, H.R. Michie, G.G. Stanford, J.W. van der Meer, S. Endres, G. Lonnemann, J. Corsetti, B. Chernow, and et al., *Circulating interleukin-1 and tumor necrosis factor in septic shock and experimental endotoxin fever.* J Infect Dis, 1990. **161**(1): p. 79-84.
33. Huang, N., M. Kny, F. Riediger, K. Busch, S. Schmidt, F.C. Luft, H. Slevogt, and J. Fielitz, *Deletion of Nlrp3 protects from inflammation-induced skeletal muscle atrophy.* Intensive Care Med Exp, 2017. **5**(1): p. 3.
34. Serrano, A.L., B. Baeza-Raja, E. Perdiguero, M. Jardi, and P. Munoz-Canoves, *Interleukin-6 is an essential regulator of satellite cell-mediated skeletal muscle hypertrophy.* Cell Metab, 2008. **7**(1): p. 33-44.
35. Tsujinaka, T., J. Fujita, C. Ebisui, M. Yano, E. Kominami, K. Suzuki, K. Tanaka, A. Katsume, Y. Ohsugi, H. Shiozaki, and M. Monden, *Interleukin 6 receptor antibody inhibits muscle atrophy and modulates proteolytic systems in interleukin 6 transgenic mice.* J Clin Invest, 1996. **97**(1): p. 244-9.
36. Weber-Carstens, S., S. Koch, S. Spuler, C.D. Spies, F. Bubser, K.D. Wernecke, and M. Deja, *Nonexcitable muscle membrane predicts intensive care unit-acquired paresis in mechanically ventilated, sedated patients.* Crit Care Med, 2009. **37**(9): p. 2632-7.
37. Bonetto, A., T. Aydogdu, X. Jin, Z. Zhang, R. Zhan, L. Puzis, L.G. Koniaris, and T.A. Zimmers, *JAK/STAT3 pathway inhibition blocks skeletal muscle wasting*

downstream of IL-6 and in experimental cancer cachexia. Am J Physiol Endocrinol Metab, 2012. **303**(3): p. E410-21.

38. Strassmann, G., M. Fong, J.S. Kenney, and C.O. Jacob, *Evidence for the involvement of interleukin 6 in experimental cancer cachexia.* J Clin Invest, 1992. **89**(5): p. 1681-4.
39. Trenerry, M.K., P.A. Della Gatta, A.E. Larsen, A.P. Garnham, and D. Cameron-Smith, *Impact of resistance exercise training on interleukin-6 and JAK/STAT in young men.* Muscle Nerve, 2011. **43**(3): p. 385-92.
40. Betz, U.A., W. Bloch, M. van den Broek, K. Yoshida, T. Taga, T. Kishimoto, K. Addicks, K. Rajewsky, and W. Muller, *Postnatally induced inactivation of gp130 in mice results in neurological, cardiac, hematopoietic, immunological, hepatic, and pulmonary defects.* J Exp Med, 1998. **188**(10): p. 1955-65.
41. Rittirsch, D., M.S. Huber-Lang, M.A. Flierl, and P.A. Ward, *Immunodesign of experimental sepsis by cecal ligation and puncture.* Nat Protoc, 2009. **4**(1): p. 31-6.
42. Dobin, A., C.A. Davis, F. Schlesinger, J. Drenkow, C. Zaleski, S. Jha, P. Batut, M. Chaisson, and T.R. Gingeras, *STAR: ultrafast universal RNA-seq aligner.* Bioinformatics, 2013. **29**(1): p. 15-21.
43. Liao, Y., G.K. Smyth, and W. Shi, *featureCounts: an efficient general purpose program for assigning sequence reads to genomic features.* Bioinformatics, 2014. **30**(7): p. 923-30.
44. Love, M.I., W. Huber, and S. Anders, *Moderated estimation of fold change and dispersion for RNA-seq data with DESeq2.* Genome Biol, 2014. **15**(12): p. 550.
45. Kanehisa, M., S. Goto, S. Kawashima, Y. Okuno, and M. Hattori, *The KEGG resource for deciphering the genome.* Nucleic Acids Res, 2004. **32**(Database issue): p. D277-80.
46. Liebermeister, W., E. Noor, A. Flamholz, D. Davidi, J. Bernhardt, and R. Milo, *Visual account of protein investment in cellular functions.* Proc Natl Acad Sci U S A, 2014. **111**(23): p. 8488-93.
47. Huang da, W., B.T. Sherman, and R.A. Lempicki, *Systematic and integrative analysis of large gene lists using DAVID bioinformatics resources.* Nat Protoc, 2009. **4**(1): p. 44-57.

48. Huang da, W., B.T. Sherman, and R.A. Lempicki, *Bioinformatics enrichment tools: paths toward the comprehensive functional analysis of large gene lists.* Nucleic Acids Res, 2009. **37**(1): p. 1-13.
49. Zanders, L., M. Kny, A. Hahn, S. Schmidt, S. Wundersitz, M. Todiras, I. Lahmann, A. Bandyopadhyay, T. Wollersheim, L. Kaderali, F.C. Luft, C. Birchmeier, S. Weber-Carstens, and J. Fielitz, *Sepsis induces interleukin 6, gp130/JAK2/STAT3, and muscle wasting.* J Cachexia Sarcopenia Muscle, 2021.
50. Yoo, J.Y., D.L. Huso, D. Nathans, and S. Desiderio, *Specific ablation of Stat3beta distorts the pattern of Stat3-responsive gene expression and impairs recovery from endotoxic shock.* Cell, 2002. **108**(3): p. 331-44.
51. Cho, Y.S., C.H. Kim, T.S. Ha, and H.Y. Ahn, *Inhibition of STAT3 phosphorylation by sulforaphane reduces adhesion molecule expression in vascular endothelial cell.* Can J Physiol Pharmacol, 2016. **94**(11): p. 1220-1226.
52. Rubenstein, A.B., G.R. Smith, U. Raue, G. Begue, K. Minchev, F. Ruf-Zamojski, V.D. Nair, X. Wang, L. Zhou, E. Zaslavsky, T.A. Trappe, S. Trappe, and S.C. Sealfon, *Single-cell transcriptional profiles in human skeletal muscle.* Sci Rep, 2020. **10**(1): p. 229.
53. Rose-John, S., *Interleukin-6 signalling in health and disease.* F1000Res, 2020. **9**.
54. Hu, X., J. Li, M. Fu, X. Zhao, and W. Wang, *The JAK/STAT signaling pathway: from bench to clinic.* Signal Transduct Target Ther, 2021. **6**(1): p. 402.
55. Guillet, C., M. Fourcin, S. Chevalier, A. Pouplard, and H. Gascan, *ELISA detection of circulating levels of LIF, OSM, and CNTF in septic shock.* Ann N Y Acad Sci, 1995. **762**: p. 407-9.
56. Gong, Y., X. Yan, X. Sun, T. Chen, Y. Liu, and J. Cao, *Oncostatin M Is a Prognostic Biomarker and Inflammatory Mediator for Sepsis.* J Infect Dis, 2020. **221**(12): p. 1989-1998.
57. Waring, P., K. Wycherley, D. Cary, N. Nicola, and D. Metcalf, *Leukemia inhibitory factor levels are elevated in septic shock and various inflammatory body fluids.* J Clin Invest, 1992. **90**(5): p. 2031-7.
58. Carneros, D., E.M. Santamaria, E. Larequi, J.M. Velez-Ortiz, M. Reboredo, U. Mancheno, M.J. Perugorria, P. Navas, M. Romero-Gomez, J. Prieto, S. Hervas-Stubbs, and M. Bustos, *Cardiotrophin-1 is an anti-inflammatory cytokine and promotes IL-4-induced M2 macrophage polarization.* FASEB J, 2019. **33**(6): p. 7578-7587.

59. Latifi, S.Q., M.A. O'Riordan, and A.D. Levine, *Interleukin-10 controls the onset of irreversible septic shock.* Infect Immun, 2002. **70**(8): p. 4441-6.
60. Xiao, F., H. Wang, X. Fu, Y. Li, K. Ma, L. Sun, X. Gao, and Z. Wu, *Oncostatin M inhibits myoblast differentiation and regulates muscle regeneration.* Cell Res, 2011. **21**(2): p. 350-64.
61. Baltgalvis, K.A., F.G. Berger, M.M. Pena, J.M. Davis, J.P. White, and J.A. Carson, *Muscle wasting and interleukin-6-induced atrogin-I expression in the cachectic Apc (Min/+) mouse.* Pflugers Arch, 2009. **457**(5): p. 989-1001.
62. Schabbauer, G., *Polymicrobial sepsis models: CLP versus CASP.* Drug Discovery Today: Disease Models, 2012. **9**(1): p. e18-e21.
63. Maier, S., T. Traeger, M. Entleutner, A. Westerholt, B. Kleist, N. Huser, B. Holzmann, A. Stier, K. Pfeffer, and C.D. Heidecke, *Cecal ligation and puncture versus colon ascendens stent peritonitis: two distinct animal models for polymicrobial sepsis.* Shock, 2004. **21**(6): p. 505-11.
64. Traeger, T., P. Koerner, W. Kessler, K. Cziupka, S. Diedrich, A. Busemann, C.D. Heidecke, and S. Maier, *Colon ascendens stent peritonitis (CASP)--a standardized model for polymicrobial abdominal sepsis.* J Vis Exp, 2010(46).
65. Ehrentraut, S., S. Frede, H. Stapel, T. Mengden, C. Grohe, J. Fandrey, R. Meyer, and G. Baumgarten, *Antagonism of lipopolysaccharide-induced blood pressure attenuation and vascular contractility.* Arterioscler Thromb Vasc Biol, 2007. **27**(10): p. 2170-6.
66. Remick, D.G., D.E. Newcomb, G.L. Bolgos, and D.R. Call, *Comparison of the mortality and inflammatory response of two models of sepsis: lipopolysaccharide vs. cecal ligation and puncture.* Shock, 2000. **13**(2): p. 110-6.
67. Schmidt, F., M. Kny, X. Zhu, T. Wollersheim, K. Persicke, C. Langhans, D. Lodka, C. Kleber, S. Weber-Carstens, and J. Fielitz, *The E3 ubiquitin ligase TRIM62 and inflammation-induced skeletal muscle atrophy.* Crit Care, 2014. **18**(5): p. 545.
68. Wang, B., C. Zhang, A. Zhang, H. Cai, S.R. Price, and X.H. Wang, *MicroRNA-23a and MicroRNA-27a Mimic Exercise by Ameliorating CKD-Induced Muscle Atrophy.* J Am Soc Nephrol, 2017. **28**(9): p. 2631-2640.
69. Zhang, L., J. Du, Z. Hu, G. Han, P. Delafontaine, G. Garcia, and W.E. Mitch, *IL-6 and serum amyloid A synergy mediates angiotensin II-induced muscle wasting.* J Am Soc Nephrol, 2009. **20**(3): p. 604-12.

70. Gao, S., J.L. Durstine, H.J. Koh, W.E. Carver, N. Frizzell, and J.A. Carson, *Acute myotube protein synthesis regulation by IL-6-related cytokines.* Am J Physiol Cell Physiol, 2017. **313**(5): p. C487-C500.
71. Silva, K.A., J. Dong, Y. Dong, Y. Dong, N. Schor, D.J. Tweardy, L. Zhang, and W.E. Mitch, *Inhibition of Stat3 activation suppresses caspase-3 and the ubiquitin-proteasome system, leading to preservation of muscle mass in cancer cachexia.* J Biol Chem, 2015. **290**(17): p. 11177-87.
72. Baltgalvis, K.A., F.G. Berger, M.M. Pena, J.M. Davis, S.J. Muga, and J.A. Carson, *Interleukin-6 and cachexia in ApcMin/+ mice.* Am J Physiol Regul Integr Comp Physiol, 2008. **294**(2): p. R393-401.
73. Pena, G., B. Cai, E.A. Deitch, and L. Ulloa, *JAK2 inhibition prevents innate immune responses and rescues animals from sepsis.* J Mol Med (Berl), 2010. **88**(8): p. 851-9.
74. Hui, L., Y. Yao, S. Wang, Y. Yu, N. Dong, H. Li, and Z. Sheng, *Inhibition of Janus kinase 2 and signal transduction and activator of transcription 3 protect against cecal ligation and puncture-induced multiple organ damage and mortality.* J Trauma, 2009. **66**(3): p. 859-65.
75. Gyurkovska, V. and N. Ivanovska, *Tyrosine kinase inhibitor tyrphostin AG490 reduces liver injury in LPS-induced shock.* Eur J Pharmacol, 2015. **751**: p. 118-26.
76. Taylor, P.C., E.C. Keystone, D. van der Heijde, M.E. Weinblatt, L. Del Carmen Morales, J. Reyes Gonzaga, S. Yakushin, T. Ishii, K. Emoto, S. Beattie, V. Arora, C. Gaich, T. Rooney, D. Schlichting, W.L. Macias, S. de Bono, and Y. Tanaka, *Baricitinib versus Placebo or Adalimumab in Rheumatoid Arthritis.* N Engl J Med, 2017. **376**(7): p. 652-662.
77. Vannucchi, A.M., J.J. Kiladjian, M. Griesshammer, T. Masszi, S. Durrant, F. Passamonti, C.N. Harrison, F. Pane, P. Zachee, R. Mesa, S. He, M.M. Jones, W. Garrett, J. Li, U. Pirron, D. Habr, and S. Verstovsek, *Ruxolitinib versus standard therapy for the treatment of polycythemia vera.* N Engl J Med, 2015. **372**(5): p. 426-35.
78. Verstovsek, S., J. Gotlib, R.A. Mesa, A.M. Vannucchi, J.J. Kiladjian, F. Cervantes, C.N. Harrison, R. Paquette, W. Sun, A. Naim, P. Langmuir, T. Dong, P. Gopalakrishna, and V. Gupta, *Long-term survival in patients treated with ruxolitinib for myelofibrosis: COMFORT-I and -II pooled analyses.* J Hematol Oncol, 2017. **10**(1): p. 156.

79. Hojyo, S., M. Uchida, K. Tanaka, R. Hasebe, Y. Tanaka, M. Murakami, and T. Hirano, *How COVID-19 induces cytokine storm with high mortality.* Inflamm Regen, 2020. **40**: p. 37.

80. Kalil, A.C., T.F. Patterson, A.K. Mehta, K.M. Tomashek, C.R. Wolfe, V. Ghazaryan, V.C. Marconi, G.M. Ruiz-Palacios, L. Hsieh, S. Kline, V. Tapson, N.M. Iovine, M.K. Jain, D.A. Sweeney, H.M. El Sahly, A.R. Branche, J. Regalado Pineda, D.C. Lye, U. Sandkovsky, A.F. Luetkemeyer, S.H. Cohen, R.W. Finberg, P.E.H. Jackson, B. Taiwo, C.I. Paules, H. Arguinchona, N. Erdmann, N. Ahuja, M. Frank, M.D. Oh, E.S. Kim, S.Y. Tan, R.A. Mularski, H. Nielsen, P.O. Ponce, B.S. Taylor, L. Larson, N.G. Rouphael, Y. Saklawi, V.D. Cantos, E.R. Ko, J.J. Engemann, A.N. Amin, M. Watanabe, J. Billings, M.C. Elie, R.T. Davey, T.H. Burgess, J. Ferreira, M. Green, M. Makowski, A. Cardoso, S. de Bono, T. Bonnett, M. Proschan, G.A. Deye, W. Dempsey, S.U. Nayak, L.E. Dodd, J.H. Beigel, and A.-S.G. Members, *Baricitinib plus Remdesivir for Hospitalized Adults with Covid-19.* N Engl J Med, 2021. **384**(9): p. 795-807.

81. Marconi, V.C., A.V. Ramanan, S. de Bono, C.E. Kartman, V. Krishnan, R. Liao, M.L.B. Piruzeli, J.D. Goldman, J. Alatorre-Alexander, R. de Cassia Pellegrini, V. Estrada, M. Som, A. Cardoso, S. Chakladar, B. Crowe, P. Reis, X. Zhang, D.H. Adams, E.W. Ely, and C.-B.S. Group, *Efficacy and safety of baricitinib for the treatment of hospitalised adults with COVID-19 (COV-BARRIER): a randomised, double-blind, parallel-group, placebo-controlled phase 3 trial.* Lancet Respir Med, 2021.

Eidesstattliche Versicherung

Ich, Lukas Zanders, versichere an Eides statt durch meine eigenhändige Unterschrift, dass ich die vorgelegte Dissertation mit dem Thema „The role of glycoprotein 130 and the JAK/STAT-pathway in sepsis-induced muscle atrophy“ - „Die Rolle von Glykoprotein 130 und dem JAK/STAT-Signalweg in der sepsisinduzierten Muskelatrophie“ selbstständig und ohne nicht offengelegte Hilfe Dritter verfasst und keine anderen als die angegebenen Quellen und Hilfsmittel genutzt habe.
Alle Stellen, die wörtlich oder dem Sinne nach auf Publikationen oder Vorträgen anderer Autoren/innen beruhen, sind als solche in korrekter Zitierung kenntlich gemacht. Die Abschnitte zu Methodik (insbesondere praktische Arbeiten, Laborbestimmungen, statistische Aufarbeitung) und Resultaten (insbesondere Abbildungen, Graphiken und Tabellen) werden von mir verantwortet.

Ich versichere ferner, dass ich die in Zusammenarbeit mit anderen Personen generierten Daten, Datenauswertungen und Schlussfolgerungen korrekt gekennzeichnet und meinen eigenen Beitrag sowie die Beiträge anderer Personen korrekt kenntlich gemacht habe (siehe Anteilserklärung). Texte oder Textteile, die gemeinsam mit anderen erstellt oder verwendet wurden, habe ich korrekt kenntlich gemacht.

Meine Anteile an etwaigen Publikationen zu dieser Dissertation entsprechen denen, die in der untenstehenden gemeinsamen Erklärung mit dem/der Erstbetreuer/in, angegeben sind. Für sämtliche im Rahmen der Dissertation entstandenen Publikationen wurden die Richtlinien des ICMJE (International Committee of Medical Journal Editors; www.icmje.og) zur Autorenschaft eingehalten. Ich erkläre ferner, dass ich mich zur Einhaltung der Satzung der Charité – Universitätsmedizin Berlin zur Sicherung Guter Wissenschaftlicher Praxis verpflichte.

Weiterhin versichere ich, dass ich diese Dissertation weder in gleicher noch in ähnlicher Form bereits an einer anderen Fakultät eingereicht habe.

Die Bedeutung dieser eidesstattlichen Versicherung und die strafrechtlichen Folgen einer unwahren eidesstattlichen Versicherung (§§156, 161 des Strafgesetzbuches) sind mir bekannt und bewusst.“

Datum Unterschrift

Ausführliche Anteilserklärung an der erfolgten Publikation als Top-Journal im Rahmen der Promotionsverfahren zum PhD bzw. MD/PhD

Publikation 1: Zanders L, Kny M, Hahn A, Schmidt S, Wundersitz S, Todiras M, et al. Sepsis induces interleukin 6, gp130/JAK2/STAT3, and muscle wasting. *J Cachexia Sarcopenia Muscle.* 2021.

Beitrag im Einzelnen:
Die Konzeption, eigenständige Durchführung und molekularbiologische, histologische und statistische Analysen der humanen und *in vitro* Versuche mit Ausnahme der Insulin / IL-6 Kostimulationsversuche (Abb. 15) erfolgten durch Lukas Zanders. Die Ergebnisse sind in Abb. 5, 9 und 10 dargestellt. Die Konzeption und Durchführung der Tiersuche mit *Il6st*$^{-/-}$ und AG490 behandelten Mäusen erfolgte durch Lukas Zanders und Jens Fielitz. Die Analysen, die in den Abb. 11-14 dargestellt sind, erfolgten eigenständig durch Lukas Zanders. Die Protein-Expressionsanalysen in Abb. 15 erfolgten durch Melanie Kny. Die *in vivo* Versuche für das RNA-Seq erfolgten durch Jens Fielitz und Sebastian Wundersitz. Die bioinformatische Analyse erfolgte durch Arnab Bandyopadhyay und Lars Kaderali (Abb. 6-8). Teile der statistischen Analyse und Visualisierung dieser Versuche erfolgten durch Lukas Zanders (Publikation Abb. 1E, S4, S5).

_____
Unterschrift, Datum und Stempel des/der erstbetreuenden Hochschullehrers/in

_____

Unterschrift des Doktoranden/der Doktorandin

Authors' contributions

The observational cohort study was conducted under the supervision of Steffen Weber-Carstens and Maria Deja.
Lukas Zanders conceptualized and conducted the analyses from the clinical cohort study (Fig. 5). Cell culture experiments, including the cultivation and differentiation of C2C12 myocytes, cytokine stimulation, small molecule inhibition, and siRNA transfection, were planned and carried out by Lukas Zanders. Subsequent analyses, such as myocyte diameter measurements, protein and RNA isolation, cDNA synthesis, RT-qPCR, and immunoblotting, which resulted in the data presented in figures 9 and 10, were also performed by Lukas Zanders. The co-stimulation experiments with IL-6 and insulin were conceptualized by Lukas Zanders, Melanie Kny and Jens Fielitz, and conducted by Melanie Kny (Fig. 15).

The 96-hour sepsis experiment using *Il6st* cKO mice was conceptualized as part of a Berlin Institute of Health Twining Grant (TRG3-1.2.3 400219) prior to Lukas Zanders joining the host lab. The 24-hour sepsis experiment using *Il6st* cKO mice was planned by Lukas Zanders and Jens Fielitz. The CLP and sham surgeries were performed by Jens Fielitz and assisted by Lukas Zanders. The JAK2 in vivo inhibition experiment was planned by Lukas Zanders. Analyses from in vivo experiments, including survival monitoring and analysis, tissue lysis, RNA and protein extraction, cDNA synthesis, RT-qPCR, immunoblotting, and muscle weight and MCSA measurements were performed by Lukas Zanders (Fig. 11 - 14). Immunoblotting for IRS, pIRS, AKT and pAKT was performed by Melanie Kny (Fig. 15).

Next generation sequencing and statistical analyses of sequencing data was conducted by Arnab Banyopadhyay and Lars Kaderali (Fig. 6-8). Visualization of GO-Term Analyses were performed by Lukas Zanders (Zanders et al., Fig. 1E, S4, S5). All other statistical analyses and graph designs were performed by Lukas Zanders (Fig. 5, 9-14). The manuscript for publication was prepared and by Lukas Zanders under the supervision of Melanie Kny, Jens Fielitz, Carmen Birchmeier, Ines Lahman and Friedrich C. Luft.

Excerpt of the Journal Summary List (ISI Web of Knowledge℠

Journal Data Filtered By: **Selected JCR Year: 2021** Selected Editions: SCIE,SSCI
Selected Categories: **"MEDICINE, GENERAL and INTERNAL"**
Selected Category Scheme: WoS
Gesamtanzahl: 171 Journale

Rank	Full Journal Title	Total Cites	Journal Impact Factor	Eigenfaktor
1	LANCET	403,221	202.731	0.56608
2	NEW ENGLAND JOURNAL OF MEDICINE	506,069	176.079	0.75350
3	JAMA-JOURNAL OF THE AMERICAN MEDICAL ASSOCIATION	242,479	157.335	0.38221
4	BMJ-British Medical Journal	183,681	93.333	0.20057
5	Nature Reviews Disease Primers	21,565	65.038	0.04754
6	ANNALS OF INTERNAL MEDICINE	83,711	51.598	0.09934
7	JAMA Internal Medicine	31,254	44.409	0.09195
8	JOURNAL OF TRAVEL MEDICINE	6,380	39.194	0.01202
9	Lancet Digital Health	3,373	36.615	0.00949
10	Military Medical Research	3,830	34.915	0.00649
11	JOURNAL OF THE ROYAL SOCIETY OF MEDICINE	5,569	18.000	0.00302
12	EClinicalMedicine	8,029	17.033	0.02095
13	CANADIAN MEDICAL ASSOCIATION JOURNAL	21,959	16.859	0.01853
14	QJM-AN INTERNATIONAL JOURNAL OF MEDICINE	8,176	14.040	0.00555
15	JAMA Network Open	31,821	13.353	0.10663
16	JOURNAL OF INTERNAL MEDICINE	15,804	13.068	0.01512
17	MEDICAL JOURNAL OF AUSTRALIA	14,683	12.776	0.01443
18	Journal of Cachexia Sarcopenia and Muscle	7,461	12.063	0.01164

Printed copy of the Publication

ORIGINAL ARTICLE

Journal of Cachexia, Sarcopenia and Muscle (2021)
Published online in Wiley Online Library (wileyonlinelibrary.com) **DOI:** 10.1002/jcsm.12867

Sepsis induces interleukin 6, gp130/JAK2/STAT3, and muscle wasting

Lukas Zanders[1,2,3], Melanie Kny[1], Alexander Hahn[1], Sibylle Schmidt[1], Sebastian Wundersitz[1], Mihail Todiras[4,5], Ines Lahmann[6], Arnab Bandyopadhyay[7], Tobias Wollersheim[8,9], Lars Kaderali[7,10], Friedrich C. Luft[1], Carmen Birchmeier[6,9], Steffen Weber-Carstens[8,9] & Jens Fielitz[1,9,10,11]*

[1]*Experimental and Clinical Research Center (ECRC), Charité-Universitätsmedizin Berlin, Max Delbrück Center for Molecular Medicine in the Helmholtz Association (MDC), Berlin, Germany;* [2]*DZHK (German Center for Cardiovascular Research), partner site Berlin, Berlin, Germany;* [3]*Department of Cardiology, Charité Campus Benjamin Franklin, Berlin, Germany;* [4]*Cardiovascular hormones, Max Delbrück Center (MDC) for Molecular Medicine in the Helmholtz Association, Berlin, Germany;* [5]*Nicolae Testemiţanu State University of Medicine and Pharmacy, Chişinău, Moldova;* [6]*Developmental Biology/Signal Transduction, Max-Delbrück-Center for Molecular Medicine, Berlin, Germany;* [7]*Institute of Bioinformatics, University Medicine Greifswald, Greifswald, Germany;* [8]*Anesthesiology and operative Intensive Care Medicine, Charité Campus Virchow and Campus Mitte, Berlin, Germany;* [9]*Berlin Institute of Health (BIH), Berlin, Germany;* [10]*DZHK (German Center for Cardiovascular Research), partner site Greifswald, Greifswald, Germany;* [11]*Department of Internal Medicine B, Cardiology, University Medicine Greifswald, Greifswald, Germany*

Abstract

Background Sepsis and inflammation can cause intensive care unit-acquired weakness (ICUAW). Increased interleukin-6 (IL-6) plasma levels are a risk factor for ICUAW. IL-6 signalling involves the glycoprotein 130 (gp130) receptor and the JAK/STAT-pathway, but its role in sepsis-induced muscle wasting is uncertain. In a clinical observational study, we found that the IL-6 target gene, *SOCS3*, was increased in skeletal muscle of ICUAW patients indicative for JAK/STAT-pathway activation. We tested the hypothesis that the IL-6/gp130-pathway mediates ICUAW muscle atrophy.

Methods We sequenced RNA (RNAseq) from tibialis anterior (TA) muscle of cecal ligation and puncture-operated (CLP) and sham-operated wildtype (WT) mice. The effects of the IL-6/gp130/JAK2/STAT3-pathway were investigated by analysing the atrophy phenotype, gene expression, and protein contents of C2C12 myotubes. Mice lacking *Il6st*, encoding gp130, in myocytes (cKO) and WT controls, as well as mice treated with the JAK2 inhibitor AG490 or vehicle were exposed to CLP or sham surgery for 24 or 96 h.

Results Analyses of differentially expressed genes in RNAseq (≥2-log2-fold change, $P < 0.01$) revealed an activation of IL-6-signalling and JAK/STAT-signalling pathways in muscle of septic mice, which occurred after 24 h and lasted at least for 96 h during sepsis. IL-6 treatment of C2C12 myotubes induced STAT3 phosphorylation (three-fold, $P < 0.01$) and *Socs3* mRNA expression (3.1-fold, $P < 0.01$) and caused myotube atrophy. Knockdown of *Il6st* diminished IL-6-induced STAT3 phosphorylation (−30.0%; $P < 0.01$), *Socs3* mRNA expression, and myotube atrophy. JAK2 (− 29.0%; $P < 0.01$) or STAT3 inhibition (−38.7%; $P < 0.05$) decreased IL-6-induced *Socs3* mRNA expression. Treatment with either inhibitor attenuated myotube atrophy in response to IL-6. CLP-operated septic mice showed an increased STAT3 phosphorylation and *Socs3* mRNA expression in TA muscle, which was reduced in septic *Il6st*-cKO mice by 67.8% ($P < 0.05$) and 85.6% ($P < 0.001$), respectively. CLP caused a loss of TA muscle weight, which was attenuated in *Il6st*-cKO mice (WT: −22.3%, $P < 0.001$, cKO: −13.5%, $P < 0.001$; WT vs. cKO $P < 0.001$). While loss of *Il6st* resulted in a reduction of MuRF1 protein contents, Atrogin-1 remained unchanged between septic WT and cKO mice. mRNA expression of *Trim63*/MuRF1 and *Fbxo32*/Atrogin-1 were unaltered between CLP-treated WT and cKO mice. AG490 treatment reduced STAT3 phosphorylation (−22.2%, $P < 0.05$) and attenuated TA muscle atrophy in septic mice (29.6% relative reduction of muscle weight loss, $P < 0.05$). The reduction in muscle atrophy was accompanied by a reduction in *Fbxo32*/Atrogin-1-mRNA (−81.3%, $P < 0.05$) and *Trim63*/MuRF1-mRNA expression (−77.6%, $P < 0.05$) and protein content.

Conclusions IL-6 via the gp130/JAK2/STAT3-pathway mediates sepsis-induced muscle atrophy possibly contributing to ICUAW.

Keywords gp130; IL-6 signalling; Inflammation; Sepsis; Muscle atrophy; Intensive care unit acquired weakness

Received: 1 July 2021; Revised: 18 October 2021; Accepted: 20 October 2021
**Correspondence to: Jens Fielitz, Universitätsmedizin Greifswald, Klinik und Poliklinik für Innere Medizin B Forschungscluster III, Fleischmannstr. 41, 17475 Greifswald, Germany. Phone: +49 3834 86 80519; Fax: +49 3834 86 80502. Email: jens.fielitz@uni-greifswald.de*

Introduction

Intensive care unit-acquired weakness (ICUAW) affects up to 90% of patients with severe sepsis increasing their morbidity and mortality.[1,2] ICUAW is characterized by a loss of muscle mass, a reduction in myofibre size, and a decreased muscle strength leading to persisting physical impairment.[3] This phenotype results from a dysregulated protein homeostasis with increased protein degradation and decreased protein synthesis, eventually causing a decrease of muscle structural proteins.[4,5] In ICUAW, atrophy predominantly occurs in fast twitch/type II myofibres[6] and is mainly mediated by the ubiquitin-proteasome system. The E3 ligase muscle RING-finger protein-1 (MuRF1), encoded by *Trim63*, and the F-Box protein Atrogin-1, encoded by *Fbxo32*, are key factors for ubiquitin-proteasome system-mediated protein degradation in muscle atrophy.[7] Both MuRF1 and Atrogin-1 are increased early and persistently during critical illness and possibly mediate muscle atrophy in ICUAW patients.[4,6] Inflammation and sepsis are major risk factors for ICUAW.[8,9] Previously, we reported that interleukin 1β (IL-1β)[10] and the acute-phase protein serum amyloid A1 (SAA1)[11,12] promote muscle atrophy in sepsis, and that their inhibition attenuated sepsis-induced muscle atrophy in mice. Both IL-1β and SAA1 signalling converge on the transcription factor NF-κB (nuclear factor 'kappa-light-chain-enhancer' of activated B-cells) and increase the expression of interleukin 6 (IL-6).[10–12] IL-6 regulates protein homeostasis in the skeletal muscle.[13,14] While an acute increase in systemic IL-6 promotes muscle growth and hypertrophy, its sustained elevation, as occurring in cancer or diabetes, causes muscle atrophy.[15,16] However, the role of IL-6 signalling in sepsis-induced muscle atrophy is not well understood.

IL-6 can signal through the canonical pathway, where IL-6 binds to its α-receptor (IL-6R) on the cell surface, and induces homodimerization and association with the signal transducing β-receptor glycoprotein 130 (gp130, encoded by *Il6st*). Alternatively, IL-6 can use the trans-signalling pathway, where it binds to a soluble IL-6R, which associates with gp130. In both pathways, the activated IL-6R-gp130 complex binds and activates the Janus kinase (JAK) family of tyrosine kinases, primarily JAK1, JAK2, and TYK2, which phosphorylate the cytoplasmatic tail of gp130, enabling the association of the Signal Transducer and Activator of Transcription (STAT), mainly STAT1 and STAT3. Phosphorylated STAT (i.e. STAT3 Y705) proteins dimerize and translocate to the nucleus where they control the expression of their target genes, such as Suppressor of Cytokine Signalling 3 (*SOCS3*).[17,18] SOCS3 acts as a negative feedback inhibitor of cytokine signalling by inhibition of JAK1, JAK2, and Tyk2.[19] *In vitro*, SOCS3 also inhibits the Insulin/PI3K/Akt pathway as a substrate recognition component of an E3 ubiquitin ligase complex, degrading Insulin Receptor Substrate 1 (IRS-1) that is essential for insulin signalling.[20] Insulin increases protein synthesis[21] and decreases atrogene expression and protein degradation[22] via the PI3K/Akt pathway in mice. This promotes muscle growth and inversely perturbations can aggravate muscle atrophy that is frequently seen in critically ill patients.[23] Based on these data and together with our observation that increased IL-6 plasma level is a risk factor for Critical Illness Myopathy (CIM) in patients,[8] we hypothesized that the IL-6/gp130/JAK/STAT pathway plays a role in sepsis-induced muscle atrophy.

Methods

Patient samples

The institutional review board of the *Charité Universitätsmedizin Berlin*, Germany, approved the study, and written informed consent was obtained from legal proxy [intensive care unit (ICU) patients], or the patients themselves before inclusion in the study (*Charité* EA2/061/06; http://www.controlled-trials.com, ISRCTN77569430). Clinical data were reported previously.[11] We analysed mRNA expression in biopsy specimens obtained from the *vastus lateralis* muscle of patients at high risk to develop ICUAW. Accordingly, these patients (n = 5) were critically ill, mechanically ventilated with a SOFA score ≥8 on three consecutive days within the first 5 days after ICU admission. Biopsy specimens were taken at Day 5 and Day 15 after ICU admission. Five age-matched and gender-matched patients undergoing elective orthopaedic surgery permitted muscle biopsies and were used as controls. For more details on the clinical data, please refer to Wollersheim *et al*. and Langhans *et al*.[4,11]

Animal model of polymicrobial sepsis

All animal procedures were performed in accordance with the guidelines of the Max-Delbrück Center for Molecular Medicine and the *Charité-Universitätsmedizin Berlin*, and were approved by the *Landesamt für Gesundheit und Soziales* (LAGeSo, Berlin, Germany; permit number G 207/13). The investigation conforms to the *Guide for the Care and Use of Laboratory Animals* published by the US National Institutes of Health (NIH Publication No. 85-23, revised 1985), as well as the current version of German Law on the Protection of Animals.

Klaus Rajewsky kindly provided conditional *Il6st* knockout (KO) mice.[24] *Il6st*$^{loxP/loxP}$ mice were crossed with Cre carrying mice controlled by myoblast-specific Pax7-promotor (Pax7-Cre) (cKO, Il6st$^{loxP/loxP;\ Pax7\text{-}Cre}$). Pax7-Cre-negative littermates were used as controls (WT, *Il6st*$^{loxP/loxP}$). Genotyping was performed as recently described[10] using primer pairs shown in *Supporting information Table* S1.

Cecal ligation and puncture (CLP) surgery was performed in 12- to 16-week-old male *Il6st c*KO mice and WT littermate controls, as recently described.[10,25] Sham mice were treated identically except for the ligation and puncture of the cecum. The effects of AG490 treatment on sepsis-induced muscle atrophy were investigated in 20-week-old male C57BL/6J mice. Animals received vehicle (10 μL DMSO in 240 μL normal saline) or AG490 (16 mg/kg in 250 μL vehicle) 60 min prior to, and every 24 h after surgery for 96 h.

Mice were sacrificed 24 or 96 h after surgery, as indicated, and *tibialis anterior* (TA) and *gastrocnemius/plantaris* (GP) muscles were harvested for analysis. Body, muscle, and organ weight was measured and normalized to tibia length. Measurements of plasma IL-6 were performed using the Mouse ELISA Quantikine Kit for IL-6 (R&D Systems, MN, USA) according to the manufacturers' protocol.

RNA sequencing and statistical analyses

Three biological replicates of WT sham and WT CLP 24 and 96 h after surgery were sequenced. Total RNA analyses were evaluated by an Agilent 2100 Bioanalyzer (Agilent Technologies, Inc., CA, USA). Library preparation of 500 ng RNA was performed using the Illumina TruSeq Stranded mRNA Kit. cDNA was evaluated and sequencing was performed using an Illumina HiSeq 4000 sequencer. The transcriptome data can be found under EBI Annotare v.2.0 (E-MTAB-10960). Pathway enrichment analysis was performed using DAVID (Database for Annotation, Visualization and Integrated Discovery) Bioinformatics Resources 6.8 (https://david.ncifcrf.gov) using the outputs BP_ALL (all biological process terms). For further information, please refer to the supporting information.

Histological analyses

Tibialis anterior and *gastrocnemius/plantaris* muscles were flash frozen in liquid nitrogen with gum tragacanth (Merck KGaA, Germany), cut with a thickness of 5 μm and stained with metachromatic ATPase. One hundred myocyte cross-sectional areas (MCSAs) were measured per mouse, muscle and condition in a blinded fashion.

Myoblast culture, differentiation, and atrophy assay

Cell culture experiments were performed in 5 days differentiated C2C12 cells (American Type Culture Collection, Manassas, VA, USA). Myocytes were treated with 10 ng/mL of recombinant IL-6 (R&D Systems, MN, USA) or solvent (0.1% bovine serum albumin in phosphate-buffered saline) for the indicated times. The JAK2 inhibitor AG490 (10 μM, Sigma-Aldrich, MO, USA), and two STAT3 inhibitors (C188-9; 10 μM, Merck-Millipore, Germany; S3i-201, 10 μM, Selleckchem) were added 60 min prior to IL-6 treatment. For siRNA transfection we used the Dharmacon SmartPool siRNA targeting Il6st (J-040007-09-0005, Dharmacon/Fisher Scientific; control siRNA D-001810-10-05). Transfection was performed as per the manufacturer's protocol. Light microscopy pictures were analysed using the Leica CTR 6500 microscope and the Leica DFC 360 FX digital camera. Out of 100 myotubes per condition, three diameters per myotube were measured and averaged using the ImageJ software in a blinded fashion.

RNA isolation, cDNA synthesis, and quantitative real-time-polymerase chain reaction

RNA isolation was performed using TRIzol® Reagent (Invitrogen™, Life Technologies Corporation, CA, USA) and the FastPrep-24™ instrument (MP Biomedicals GmbH). SuperScript® First-Strand Synthesis System (Invitrogen™, Life Technologies Corporation, CA, USA) was used for cDNA synthesis. Quantitative real-time polymerase chain reaction (qRT-PCR) was performed using *Power* SYBR® Green PCR Master Mix (Thermo Fischer Scientific Inc., MA, USA) and self-designed primers (for primer sequences, refer to *Table* S2). PCR reactions were performed in a StepOnePlus™ thermocycler (Applied Biosystems). Gene expression was normalized to glyceraldehyde-3-phosphate dehydrogenase (*Gapdh*).

Protein extraction and Western blot assay

Muscle tissue was homogenized in lysis buffer using the FastPrep-24™ instrument. Lysates were separated by

DOI: 10.1002/jcsm.12867

SDS-PAGE and transferred to PVDF or nitrocellulose membranes (GE Healthcare, Germany). Membranes were incubated with the indicated primary and secondary antibodies. The antibodies used are indicated in the supporting information. GAPDH was used as loading control. We used the SuperSignal® West Pico Chemiluminescent substrate (Thermo Fischer Scientific Inc., MA, USA) and Chemiluminescence detection films (GE Amersham, UK) for protein visualization.

Statistics

All experiments were performed independently and at least three times using biological triplicates each. For mRNA expression, myotube diameter and MCSA data from cell culture experiments, a paired *t* test was used. Data on muscle weight and mRNA expression were analysed using the Mann–Whitney *U* test. *In vitro* data are shown as mean ± SD and *in vivo* data are mean ± SEM. Frequency-distribution histograms plotting myotube width or MCSA against its frequency. Differences were considered statistically significant at $P \leq 0.05$. The GraphPad Prism® 8 program (GraphPad Software, La Jolla, CA, USA), Adobe Illustrator CS6, version 16.0.0, and Photoshop CS6, version 13.0 were used to perform statistics and draw graphics, respectively.

Results

Interleukin 6 signalling is activated in skeletal muscle during sepsis

We analysed *SOCS3* mRNA expression in muscle biopsy specimens of ICUAW patients and control subjects. qRT-PCR analysis showed an increased *SOCS3* mRNA expression in the vastus lateralis of critically ill patients at day five and day 15 after ICU-admission compared to controls (*Figure* 1A) indicative for an activation of the IL-6/JAK/STAT pathway.

To confirm that the IL-6/JAK/STAT pathway is activated in muscle during sepsis, we performed next generation sequencing of RNAs (RNAseq) isolated from TA muscles of CLP and sham operated WT mice and analysed these data for changes in the expression of the IL-6 cytokine family and its receptors. *Il6*, *Il6st*, and *Il6ra* expression was significantly increased in muscle after 24 and 96 h of sepsis, whereas the other IL-6 family members showed only minor changes (i.e. *Ctf1* and *Cntf*) or a reduction of gene expression (i.e. *Lif* and *Lifr*) (*Figure* 1B). Analyses of all differentially expressed genes (DEG; ≥2-log2-fold change, adjusted *P* value <0.01) by Voronoi plots showed an enrichment of IL-6 and IL-6 related genes after 24 h, which was even more pronounced after 96 h of sepsis (*Figure* 1C, *Figure* S1). These data show that IL-6 signalling is activated in the TA muscle of septic mice.

Further, gene ontology (GO) term analysis (biological process) revealed a significant enrichment of genes belonging to transcription, translation, autophagy, and proteasomal protein degradation and a decrease in genes involved in TGFβ-signalling and skeletal system development after 24 but not 96 h (*Figure* S2). Kyoto Encyclopedia of Genes and Genomes (KEGG)-pathway analysis showed that insulin resistance and tumour necrosis factor-signalling were increased and TGFβ and insulin signalling were decreased after 24 h but not 96 h (*Figure* S2). Next, we defined a subgroup encompassing 1036 genes that were up-regulated (*Figure* 1D) and 1621 genes that were down-regulated at both time points in sepsis (*Figure* S3). GO term analysis of up-regulated DEG showed an enrichment of ubiquitin-dependent protein degradation. In accordance with our previous data,[10,11] we found an increase in cellular response to IL-1 and acute-phase response, as well as IL-6 signalling and positive regulation of JAK/STAT signalling. KEGG pathway analysis revealed an increase in DEG involved in proteasomal protein degradation, TNF-signalling and JAK/STAT-signalling, and insulin resistance (*Figure* 1D). A strong deregulation of DEG contained in 'cellular response to IL6' (GO:0071354) (*Figure* 1E), 'IL-6 production' (GO:0032635) (*Figure* S4), and 'receptor signalling pathway via JAK-STAT' (GO:0007259) (*Figure* S5) indicated an activation of IL-6 signalling in muscle of septic mice after 24 and 96 h. Collectively, our data indicate that the IL-6 and JAK/STAT pathways are activated in muscle of septic mice after 24 and 96 h.

Interleukin 6 induces atrophy via the gp130/JAK/STAT pathway in C2C12 myotubes

To analyse IL-6 signalling in myocytes, we treated differentiated murine C2C12 myotubes with recombinant IL-6 or solvent. Western blot analysis showed an increased STAT3 Y705 phosphorylation after 5 to 60 min of IL-6 treatment (*Figure* 2A). qRT-PCR revealed that IL-6 increased *Socs3* mRNA expression after 24 to 72 h (*Figure* 2B). IL-6 induced a reduction in myotube diameter by 11.1%, 9.7%, and 7.1% at 24, 48, and 72 h, respectively (*Figure* 2C and 2D). These data indicate that IL-6 activates the JAK/STAT3 pathway and causes atrophy of myocytes *in vitro*.

We next reduced gp130, encoded by *Il6st*, by siRNA prior to IL-6 treatment in C2C12 myotubes. Knockdown was confirmed by qRT-PCR (relative reduction 69%, $P < 0.005$; *Figure* 3A) and immunoblotting (*Figure* 3B). Knockdown of *Il6st* attenuated IL-6-induced STAT3 Y705 phosphorylation (*Figure* 3B), *Socs3* expression (*Figure* 3C) and IL-6-mediated reduction of myotube diameters compared to siRNA controls (8.3% vs. 28.3%, $P < 0.01$; *Figure* 3D). C2C12 myotubes were treated with the JAK2 inhibitor AG490 or the STAT3 inhibitor C188-9 prior to IL-6 treatment. Both inhibitors attenuated IL-6-induced STAT3 Y705 phosphorylation (*Figure* 3E) and *Socs3*

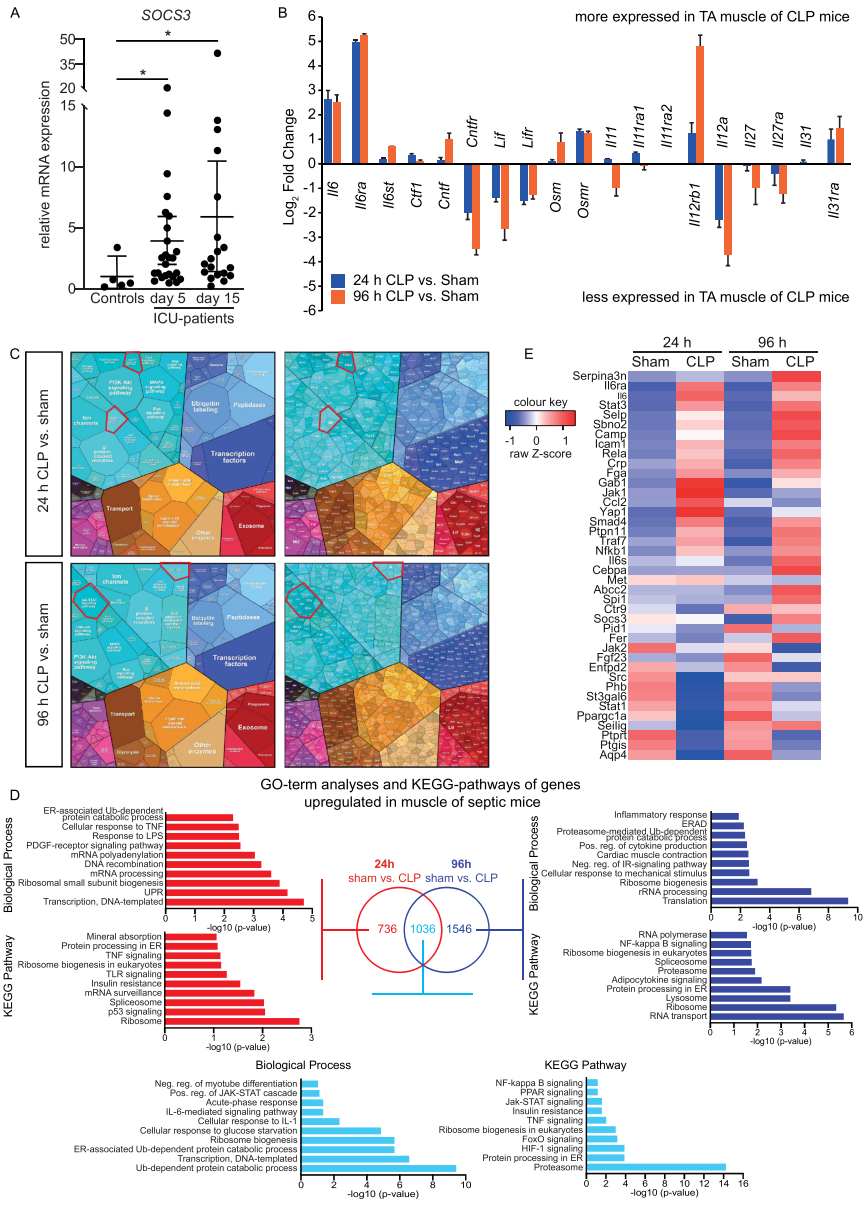

Figure 1 The IL-6 pathway is activated in skeletal muscle during sepsis. (*A*) *SOCS3* mRNA expression in muscle of critically ill patients. Muscle biopsy specimens from critically ill patients were obtained from the *vastus lateralis* muscle on Day 5 (n = 25) and Day 15 (n = 19) in intensive care unit (ICU). Healthy individuals (n = 5) served as controls. Data are presented as fold change (mean ± SEM). *$P < 0.05$. (*B–E*) WT mice were subjected to cecal ligation and puncture (CLP) or sham surgery. RNA sequencing analyses were performed 24 and 96 h after surgery (WT sham, n = 3; WT CLP, n = 3, for both time points). (*B*) Gene expression of known IL6-family members and their receptors in TA muscle of sham- and CLP-operated mice after 24 and 96 h. (*C*) Voronoi plot of differentially expressed genes (log2 fold change≥2, adjusted P value <0.05) from RNA sequencing analysis is shown. Voronoi-plots show the respective GO terms (left panels) and the enriched genes (right panel) per time point (top panels 24 h, bottom panels 96 h) as indicated. Insets localize IL-6- and JAK/STAT pathway. (*D*) Venn diagram showing the number of genes that were increased (log2 fold change≥2, adjusted P value <0.01) in the tibialis anterior muscle compared with sham treated mice after 24 h, 96 h or at both time points. The DAVID functional annotation tool was used for gene ontology (GO) term-pathway and Kyoto Encyclopedia of Genes and Genomes (KEGG)-pathway analyses of each individual time point, and 10 of the most enriched biological processes and pathways are shown. (*E*) Heat map of genes contained in GO-term 0071354 cellular response to IL-6 that were significantly regulated (P value <0.05) in TA muscle of septic mice 24 and 96 h after surgery when compared to TA of sham operated mice.

DOI: 10.1002/jcsm.12867

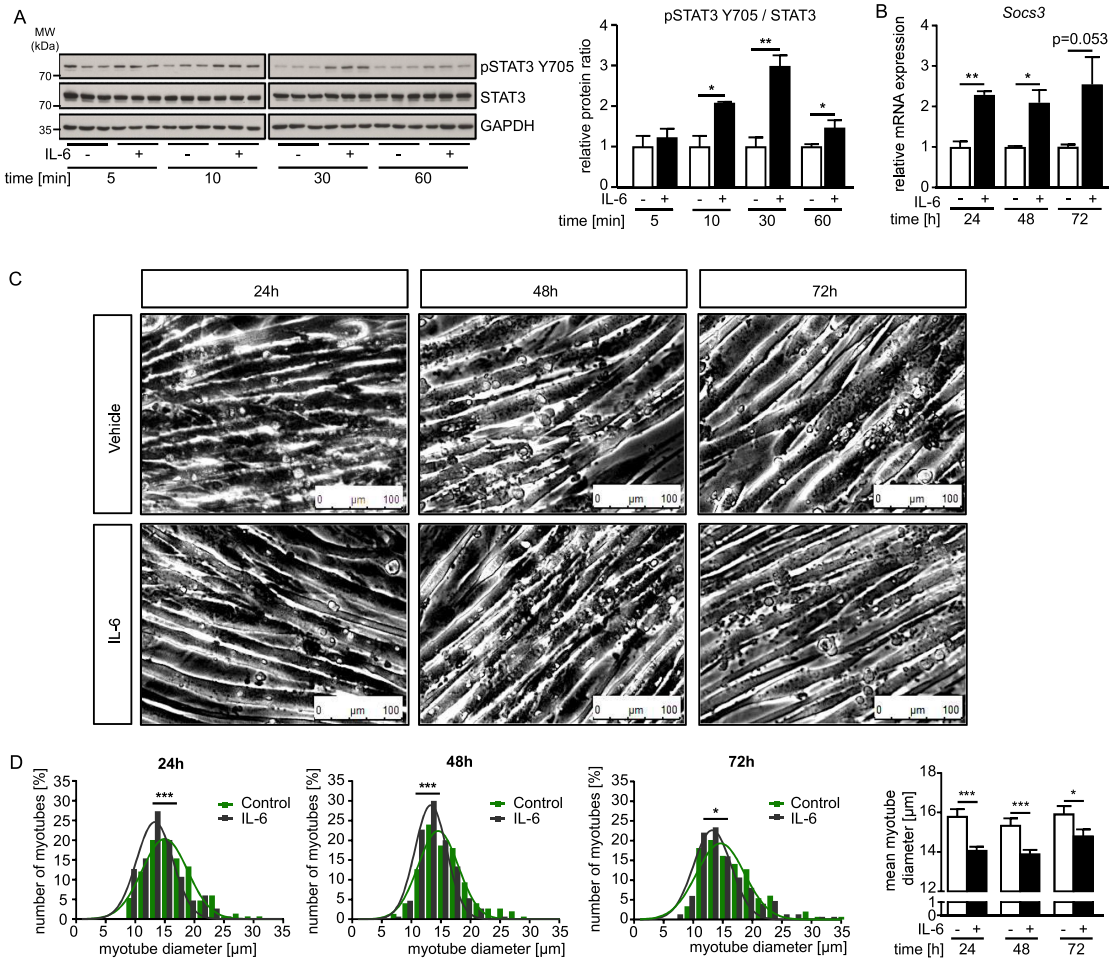

Figure 2 Interleukin 6 activates the JAK/STAT signalling pathway and induces atrophy in myocytes. Five days differentiated C2C12 myotubes were treated with interleukin 6 (IL-6, 10 ng/mL, *n* = 3) or solvent control (0.1% bovine serum albumin in phosphate-buffered saline, *n* = 3) for the indicated time points. (*A*) Western blot analysis with anti-phospho-STAT3-Tyr705 (pSTAT3 Y705), anti-STAT3 and anti-GAPDH antibodies, *n* = 3. GAPDH was used as loading control. Bar graph showing the ratio of the relative densities of pSTAT3 Y705 and STAT3 protein contents as detected C. (*B*) Quantitative real-time polymerase chain reaction (qRT-PCR) analysis of *Socs3* expression. mRNA expression was normalized to *Gapdh*. Data are presented as mean ± SD. $*P < 0.05$, $**P < 0.01$, $***P < 0.001$. MW, molecular weight; min, minutes; IL-6, interleukin 6. (*C*) Representative light microscopy pictures. Scale bar = 100 µm. (*D*) Frequency distribution histograms of cell width of IL-6 and solvent treated myotubes, *n* = 100 cells per condition. Mean myotube width.

expression (*Figure* 3F). IL-6-induced atrophy was attenuated by AG490, C188-9, and S3i-201 (*Figure*s 3G, 3H and S6). These findings reveal that the gp130/JAK2/STAT3 pathway mediates IL-6-induced myotube atrophy.

Skeletal muscle specific deletion of Il6st attenuates sepsis-induced muscle atrophy in mice

To verify our data *in vivo*, we generated mice deficient in *Il6st* in the myocyte lineage. Mice bearing a conditional *Il6st*$^{loxP/loxP}$ allele were bred with mice expressing the Cre-recombinase under the control of the Pax7 promoter (*Il6st*$^{loxP/loxP//Pax7Cre}$, cKO). *Il6st*$^{loxP/loxP}$ littermates not expressing Pax7-Cre served as controls (WT). We performed CLP surgery to induce polymicrobial sepsis for 24 h (to analyse gp130 signalling; WT: *n* = 6; cKO: *n* = 4) and 96 h (to analyse muscle atrophy; WT: *n* = 15; cKO: *n* = 10). Sham operated littermates (24 h: WT: *n* = 4; cKO: *n* = 4; 96 h: WT: *n* = 6; cKO: *n* = 6) served as controls. qRT-PCR analysis confirmed *Il6st* deletion in TA of cKO mice (*Figure* S7A). At baseline, cKO mice showed no differences in survival, body

DOI: 10.1002/jcsm.12867

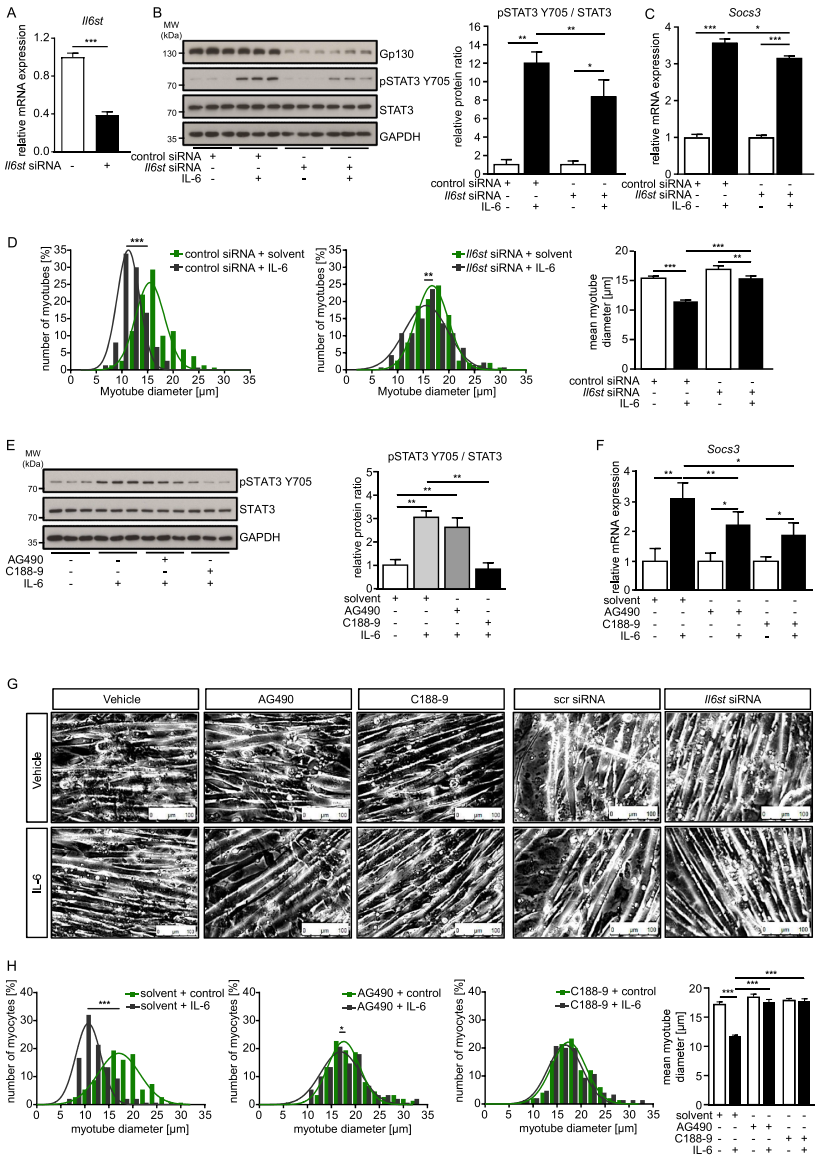

Figure 3 Interleukin 6 mediates atrophy through gp130/JAK2/STAT3 signalling in myocytes. (*A–D*) Five days differentiated C2C12 myotubes were transfected with control siRNA (control siRNA, 50 nM) (*n* = 6) or siRNA targeting Il6st/gp130 (Il6st siRNA, 50 nM) (*n* = 6) followed by treatment with IL-6 (10 ng/mL) or vehicle control, as indicated, for 24 h. (*A*) Quantitative real-time polymerase chain reaction (qRT-PCR) analysis of *Il6st* expression. mRNA expression was normalized to *Gapdh*. (*B*) Western blot analysis with anti-gp130, anti-phospho-STAT3-Tyr705 (pSTAT3 Y705), anti-STAT3, and anti-GAPDH antibodies, *n* = 3. GAPDH was used as loading control. Bar graph showing the ratio of the relative densities of pSTAT3 Y705 and STAT3 protein contents as detected in (*B*). (*C*) qRT-PCR analysis of *Socs3* expression. mRNA expression was normalized to *Gapdh*. (*D*) Frequency distribution histograms of cell width of IL-6 and vehicle-treated myotubes, *n* = 100 cells per condition. Bar graph showing mean myotube width. (*E–H*) Five days differentiated C2C12 myotubes were treated with the JAK2 inhibitor AG490 (*n* = 6), the STAT3 inhibitor C188-9 (*n* = 6) or vehicle control prior to treatment with IL-6 (10 ng/mL) or solvent control, as indicated, for 24 h. (*E*), Western blot analysis with anti-phospho-STAT3-Tyr705 (pSTAT3 Y705), anti-STAT3, and anti-GAPDH antibodies, *n* = 3. GAPDH was used as loading control. Bar graph showing the ratio of the relative densities of pSTAT3 Y705 and STAT3 protein contents as detected (*E*). Data are shown as mean ± SD. (*F*) qRT-PCR analysis of *Socs3* expression. mRNA expression was normalized to *Gapdh*. (*G*) Representative light microscopy pictures. Scale bar = 100 μm. Data are presented as mean ± SD. $*P < 0.05$, $**P < 0.01$, $***P < 0.001$. MW, molecular weight, IL-6, interleukin 6. (*H*) Frequency distribution histograms of cell width of IL-6 and vehicle-treated myotubes in the absence or presence of JAK2 and STAT3 inhibitors, and *Il6st* siRNA or scrambled siRNA control, as indicated, *n* = 100 cells per condition. Bar graph showing mean myotube width.

DOI: 10.1002/jcsm.12867

weight, and IL-6 plasma levels (*Table* S3, *Figure* S7B). Septic WT mice showed an increased STAT3 Y705 phosphorylation in the TA, which was diminished in septic cKO mice 24 h after CLP (*Figure* 4A). *Socs3* expression was increased in the TA of WT CLP, and this increase was attenuated in cKO after 24 h (22-fold vs. 6-fold, $P < 0.01$; *Figure* S8A) and 96 h (22-fold vs. 3.0-fold, $P < 0.001$; *Figure* 4B). These data indicate that gp130 mediates STAT3 activation and *Socs3* expression in TA of septic mice. The observed reduction in TA (WT: −22.3%, cKO: −13.5%; $P < 0.001$; *Figure* 4C) and gastrocnemius/plantaris (GP) weights (WT: −19.7%, cKO: −7.7%; $P < 0.001$; *Figure* 4G, *Table* S3) after 96 h of sepsis, was less pronounced for both muscles in cKO mice ($P < 0.001$ for both). ATPase-stained histological cross sections showed a reduction in MCSA of fast twitch/type II myofibres of septic WT mice that was attenuated in TA (WT: −26.7%, cKO: −6.0%; $P < 0.001$; *Figure* 4D–4F) and GP (WT: −39.1%, cKO: −21.5%; $P < 0.001$; *Figure* 4H–4J) of septic cKO mice. Immunoblotting of muscle protein lysates showed an increase in MuRF1 protein levels in septic WT that was abolished in cKO mice after 24 h (*Figure* S8B) and 96 h (*Figure* 4A). In contrast, we found no differences between the induction of *Trim63* and *Fbxo32*-mRNA expression in TA of WT CLP (*Trim63*: 11.2-fold, $P < 0.01$; *Fbxo32*: 8.2-fold, $P < 0.001$) and cKO CLP mice (*Trim63*: 9-fold, $P < 0.001$; *Fbxo32*: 8.4-fold, $P < 0.001$) after 96 h of sepsis (*Figure* 4K and 4L). Expression of *Myh2*, encoding MyHC2a, was increased in TA of septic cKO but not WT mice when compared with sham animals (*Figure* 4M). In contrast, expression of *Myh4*, encoding MyHC2b, was equally and significantly decreased in TA of WT and cKO mice after 96 h of sepsis (*Figure* 4N). In summary, these data indicate that gp130 activates STAT3/*Socs3* in muscle during sepsis and that *Il6st* deletion prevents sepsis-induced muscle atrophy. This was associated with a reduction of MuRF1 protein levels in cKO mice.

JAK2 inhibition attenuates sepsis-induced muscle atrophy in mice

To investigate the effect of pharmaceutical inhibition of the JAK2/STAT3 pathway, we treated C57BL/6J mice with AG490 or solvent 1 h prior to CLP (AG490: $n = 15$; solvent: $n = 15$) or sham surgery (AG490: $n = 5$; solvent: $n = 5$) and every 24 h until the experimental endpoint at 96 h after surgery. Treatment with AG490 attenuated sepsis-induced STAT3 Y705 phosphorylation ($P < 0.01$, *Figure* 5A) and *Socs3* expression (*Figure* 5B) in TA muscle. AG490 treatment reduced sepsis-induced muscle weight loss (relative reduction 29.6%, $P < 0.05$ in the TA, *Figure* 5C; relative reduction in GP 33.6%, $P < 0.01$, *Figure* 5G, *Table* S4) and reduction in MCSA of fast twitch/type II myofibres (relative reduction 58.3%, $P < 0.001$, in the TA, *Figure* 5D–5F; relative reduction 18.3%, $P < 0.001$ in GP, *Figure* 5H–5J). AG490-treatment attenuated sepsis-induced increase in MuRF1 and Atrogin-1 protein contents (*Figure* 5A). *Trim63* and *Fbxo32* mRNA expression was increased in TA of vehicle-treated CLP mice (CLP vs. sham: *Trim63*: 16.0-fold, $P < 0.01$; *Fbxo32*: 13.4-fold, $P < 0.001$), which was attenuated by AG490 (CLP vs. sham: *Trim63*: 3.0-fold; *Fbxo32*: 3.0-fold; both $P < 0.05$ vs. vehicle CLP) (*Figure* 5K and 5L). Comparable results were obtained in GP muscle (*Figure* S9A–S9D). Neither sepsis nor AG490 treatment had an effect on *Myh2* mRNA expression in TA or GP muscles (*Figure* 5M, *Figure* S9F). In contrast, sepsis decreased *Myh4* mRNA expression in TA and GP, which was attenuated by AG490 treatment (*Figure*s 5N and S9G). In summary, these data indicate that JAK2 inhibition attenuates sepsis-induced skeletal muscle atrophy, which coincides with *Trim63*/MuRF1, *Fbxo32*/Atrogin-1 and Myosin expression in mice.

Interleukin 6 interferes with insulin-induced IRS-1/Akt-signalling

RNAseq data from TA of septic WT mice showed a down-regulation of the gene signature of PI3K/Akt signalling (*Figure* S2). Immunoblotting confirmed a decreased Akt S473 phosphorylation in TA of septic WT but not cKO mice (*Figure* 6A). To investigate the interaction between the IL-6 and insulin pathways, we co-treated C2C12 myocytes with IL-6 and insulin. Insulin treatment resulted in increased insulin receptor substrate 1 (IRS-1) S636/639 and Akt S473 phosphorylation, which was blocked by pretreatment with IL-6 (*Figure* 6B). These data indicate that IL-6 inhibits insulin signalling, suggesting that IL-6-induced atrophy is mediated by both an increased protein degradation and a decreased protein synthesis.

Discussion

Our novel findings are as follows. First, the IL-6/gp130/JAK2/STAT3 target gene *SOCS3* was increased in muscle of ICUAW patients when compared with controls. Second, IL-6 caused atrophy of C2C12 myotubes, which was attenuated by knockdown of *Il6st*/gp130 and treatment with JAK2 or STAT3 inhibitors. Third, skeletal muscle specific deletion of *Il6st* and pharmacological JAK2 inhibition by AG490 attenuated sepsis-induced muscle atrophy in mice *in vivo*. Fourth, IL-6 promoted protein degradation and inhibited insulin signalling, which might reduce muscular protein synthesis and therefore protein homeostasis.

Recently, we showed that IL-1β and SAA1 are crucial for muscle atrophy in sepsis and that both increased the mRNA and protein expression of IL-6 as well as MuRF1/*Trim63* and Atrogin-1/*Fbxo32*.[11,12,26] Together with our novel data, we

DOI: 10.1002/jcsm.12867

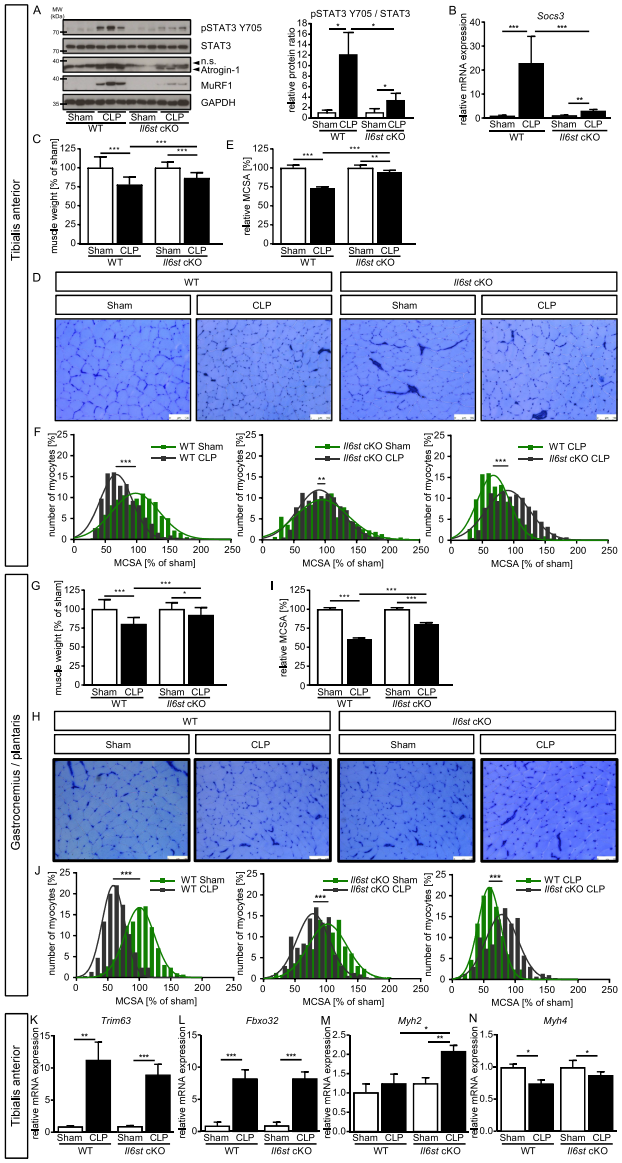

Figure 4 Deletion of *Il6st* in skeletal myocytes attenuates sepsis-induced muscle atrophy in mice. Twelve- to 16-week-old male *Il6st* cKO mice and wildtype (WT) littermates were subjected to cecal ligation and puncture (CLP) or sham surgery. Analyses were performed 24 h (for Western blot: WT sham, $n = 4$; WT CLP, $n = 6$; KO sham, $n = 4$; KO CLP, $n = 4$) or 96 h (for qRT PCR and morphological analyses: WT sham, $n = 6$; WT CLP, $n = 15$; KO sham, $n = 6$; KO CLP, $n = 10$) after surgery in *tibialis anterior* (TA) and *gastrocnemius and plantaris* (GP). (*A*) Western blot analysis with anti-phospho-STAT3-Tyr705 (pSTAT3 Y705), anti-STAT3, anti-Atrogin-1, anti-MuRF1, and anti-GAPDH antibodies, $n = 3$. GAPDH was used as loading control. Bar graph showing the ratio of the relative densities of pSTAT3 Y705 and STAT3 protein contents as detected in (*A*) as mean ± SD. Arrow denotes non-specific (*n*.s.) signal. (*B*) Quantitative real-time polymerase chain reaction (qRT-PCR) analysis of *Socs3*. mRNA expression was normalized to *Gapdh*. Data are presented as mean ± SEM; $^{**}P < 0.01$, $^{***}P < 0.001$. (*C*, *G*) Analyses of TA and GP muscle weights normalized to tibia length of the same animal. (*D*, *H*) Metachromatic ATPase staining of histological cross-sections from TA and GP of sham or CLP operated WT and *Il6st* cKO mice. (*E*, *I*) Mean myofibre cross-sectional area (MCSA) of TA and GP muscle. (*F*, *J*) Frequency distribution histograms of fast/type II MCSA of sham-treated and CLP-treated *Il6st* cKO and WT mice of TA and GP muscle. Data are presented as mean ± SEM; $^{*}P < 0.05$, $^{**}P < 0.01$, $^{***}P < 0.001$. (*K*–*N*) qRT-PCR analysis of *Trim63*, *Fbxo32*, *Myh2*, and *Myh4*. mRNA expression was normalized to *Gapdh*. Data are presented as mean ± SEM; $^{*}P < 0.05$, $^{**}P < 0.01$, $^{***}P < 0.001$.

DOI: 10.1002/jcsm.12867

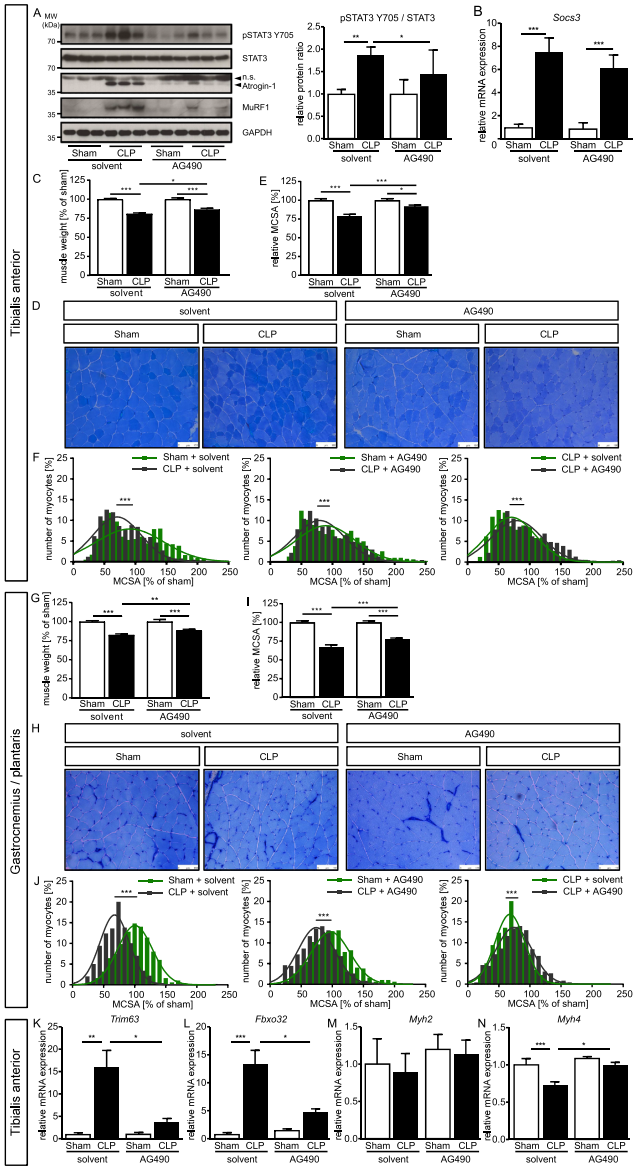

Figure 5 The JAK2 inhibitor AG490 attenuates sepsis-induced muscle atrophy in mice. Twelve- to 16-week-old male *Il6st* cKO and wildtype (WT) mice were treated with the JAK2 inhibitor AG490 (n = 20, 10 μM) or vehicle (n = 20) and then subjected to cecal ligation and puncture (CLP) or sham surgery (solvent sham, n = 5; solvent CLP, n = 15; AG490 sham, n = 5; AG490 CLP, n = 15). Analyses were performed 96 h after surgery in *tibialis anterior* (TA) and *gastrocnemius and plantaris* (GP) of sham-treated and CLP-treated AG490 and vehicle-treated animals. (*A*) Western blot analysis with anti-phospho-STAT3-Tyr705 (pSTAT3 Y705), anti-STAT3, anti-Atrogin-1, anti-MuRF1, and anti-GAPDH antibodies, n = 3. GAPDH was used as loading control. Bar graph showing the ratio of the relative densities of pSTAT3 Y705 and STAT3 protein contents as detected in (*A*) as mean ± SD. Arrow denotes non-specific (n.s.) signal. (*B*) Quantitative real-time polymerase chain reaction (qRT-PCR) analysis of *Socs3*. mRNA expression was normalized to *Gapdh*. Data are presented as mean ± SEM; $^{***}P < 0.001$. (*C*, *G*) Analyses of TA and GP muscle weights normalized to tibia length of the same animal. (*D*, *H*) Metachromatic ATPase staining of histological cross-sections from TA and GP of sham and CLP operated AG490- and solvent-treated mice. (*E*, *I*) Mean myofibre cross-sectional area (MCSA) of TA and GP muscle. (*F*, *J*) Frequency distribution histograms of fast/type II MCSA of sham-operated and CLP-operated AG490-treated and solvent-treated mice. Data are presented as mean ± SEM; $^{*}P < 0.05$, $^{**}P < 0.01$, $^{***}P < 0.001$. (*K*–*N*) Quantitative real-time polymerase chain reaction (qRT-PCR) analysis of *Trim63*, *Fbxo32*, *Myh2*, and *Myh4*. mRNA expression was normalized to *Gapdh*. Data are presented as mean ± SEM; $^{*}P < 0.05$, $^{**}P < 0.01$, $^{***}P < 0.001$.

DOI: 10.1002/jcsm.12867

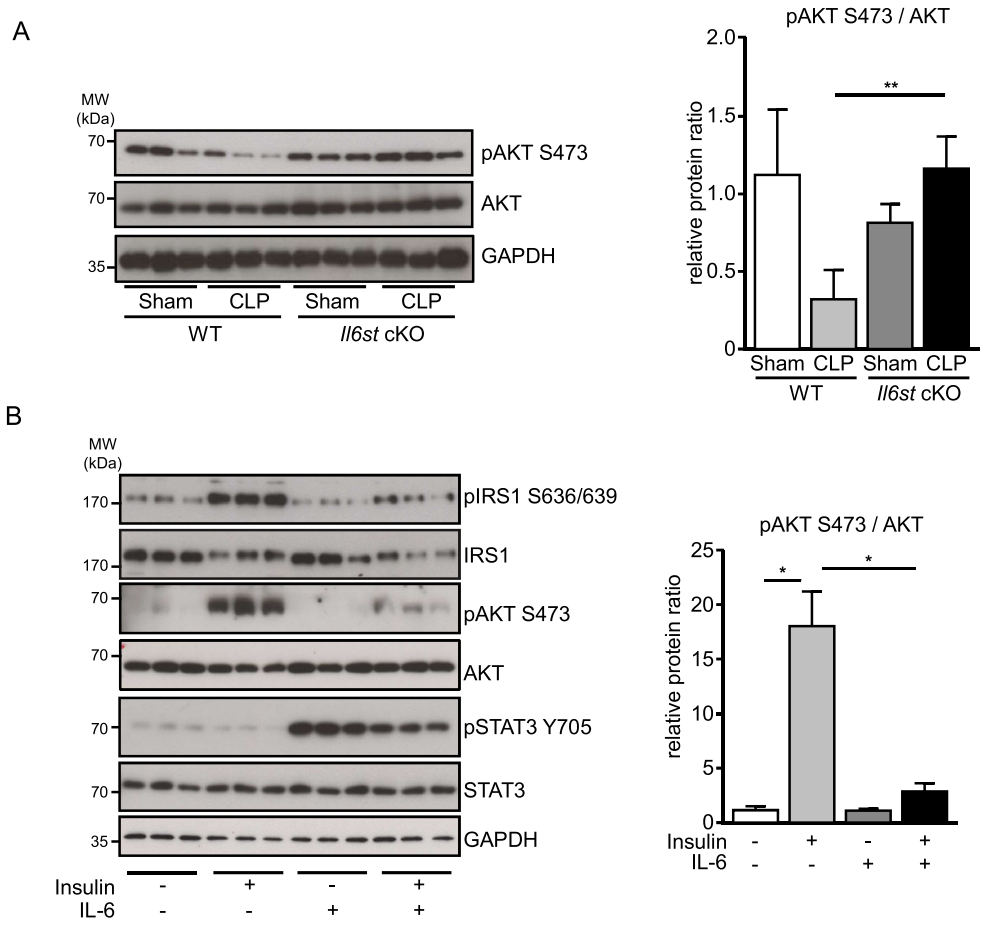

Figure 6 IL-6 inhibits insulin signalling in myocytes *in vitro*. (*A*) Twelve- to 16-week-old male *Il6st* cKO and wildtype (WT) mice were subjected to cecal ligation and puncture (CLP) or sham surgery (WT sham, $n = 4$; WT CLP, $n = 6$; KO sham, $n = 4$; KO CLP, $n = 4$). Analyses were performed 24 h after surgery. Western blot analysis with anti-Akt, anti-pAkt S473, and anti-GAPDH antibodies, $n = 3$. GAPDH was used as loading control. Bar graph showing the ratio of the relative densities of pAkt S473 and Akt protein contents as detected in (*A*) as mean ± SD. (*B*) Five days differentiated C2C12 myotubes were treated with IL-6 (10 ng/mL) or vehicle for 30 min ($n = 6$) before insulin-treatment for 1 h ($n = 3$). Western blot analysis with anti-Akt, anti-pAkt S473, anti-STAT3, anti-pSTAT3 Y705, anti-pIRS1 S636/639, anti-IRS1, and anti-GAPDH antibodies, $n = 3$. GAPDH was used as loading control. Bar graph showing the ratio of the relative densities of pAkt S473 and Akt as well as pSTAT3 Y705 and STAT3 protein contents mean ± SD; $^{*}P < 0.05$, $^{**}P < 0.01$, $^{***}P < 0.001$.

propose that the atrophic effect of IL-1β and SAA1 is partially mediated by IL-6. Our data are in accordance with previous reports showing that gp130 via the JAK/STAT pathway mediates muscle atrophy in a cancer cachexia mouse model.[15,27,28] Specifically, increased IL-6 plasma levels are associated with cachexia in various models of cancer, such as Lewis lung carcinoma, colon cancer, and melanoma. In accordance with our data, STAT3 inhibition attenuated cancer-associated muscle wasting in mice bearing colon-26 carcinoma.[16] Mice devoid of *Il6st* in myocytes were protected from cancer cachexia, which was attributed to a reduced Atrogin-1 expression, while MuRF1 was not analysed.[27] However, compared with this cancer-cachexia model where only mildly elevated IL-6 plasma levels were reported,[27] we measured 10 times higher IL-6 levels in septic mice. In addition, while cancer is a chronic condition, the cytokine storm in sepsis is acute. These differences may explain the different kinetics of muscle wasting that develops gradually in cancer but occurs rapidly in sepsis.

The JAK2 inhibitor AG490 attenuated sepsis-induced muscle atrophy *in vitro* and *in vivo*. This was associated with a reduced *Trim63*/MuRF1 and *Fbxo32*/Atrogin-1 expression. Peña *et al*. showed that AG490 leads to a reduction in TNF plasma levels in septic mice.[29] In addition,

DOI: 10.1002/jcsm.12867

Gyurkovska and Ivanovska found decreased IL-6 and IL-12 plasma levels as well as decreased numbers of T-cells and monocytes in the peritoneal lavage of AG490 treated mice with LPS-induced toxic shock.[30] AG490 treatment protected against liver and lung injury and improved survival in CLP-induced sepsis and LPS-induced toxic shock in mice.[29–31] Therefore, we suggest that the anti-atrophic effects of AG490 are not only mediated by inhibition of muscular gp130 signalling but also by its systemic anti-inflammatory effect. Based on our data, JAK2 inhibition might be useful to treat or prevent muscle atrophy in sepsis. Indeed, different JAK inhibitors received approval for clinical use in patients with polycythemia vera and primary myelofibrosis, in which somatic *JAK2* mutations are common. Treatment with the JAK1/2 inhibitor ruxolitinib resulted in clinical improvements in polycythemia vera and an increased survival in primary myelofibrosis.[32,33] Because of the good tolerability of JAK inhibitors and the improved outcomes of JAK inhibitor-treated septic mice, it seems feasible to investigate their effects in septic patients.

Our RNAseq data revealed an increased expression of genes involved in insulin resistance and a decreased expression of genes involved in insulin signalling, suggesting that insulin resistance also occurs in skeletal muscle of septic mice. Our data presented here indicate that insulin resistance in sepsis occurs at the post-insulin receptor level. IL-6 attenuated insulin-induced IRS-1- and Akt-phosphorylation indicative for insulin resistance. We also found that sepsis-mediated Akt-inactivation was prevented in muscle of cKO mice. This indicates improved insulin signalling and suggests that gp130 signalling contributes to insulin resistance in muscle of septic mice. Our findings are in accordance with previous reports that IL-6 induces insulin resistance in hepatocytes and skeletal muscle cells.[34] However, contradictory results have been reported about the effects of IL-6 on Akt phosphorylation. For example, IL-6 was shown to increase Akt phosphorylation and protein synthesis in muscle and myeloma cells.[34,35] Others showed that the combined treatment of HepG2 cells with insulin and IL-6 had no effect on Akt phosphorylation.[36] These discrepancies could be explained

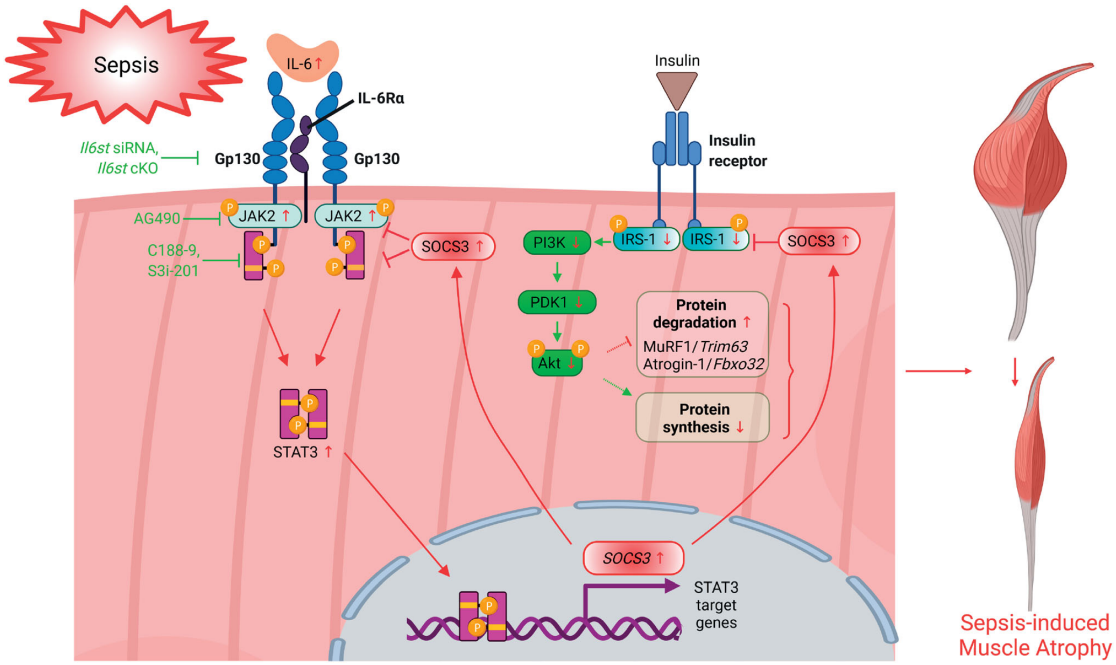

Figure 7 The IL-6/gp130/JAK2/STAT3-pathway mediates sepsis-induced muscle atrophy. IL-6 plasma levels are increased in critically ill human patients and mice with polymicrobial sepsis. IL-6 acts on myocytes via the gp130 and IL-6Rα-complex and activates JAK2- and STAT3-signalling, which leads to an increased expression of *SOCS3*. SOCS3 functions as a negative regulator of cytokine signalling and inhibits the growth promoting insulin/insulin-receptor/Akt pathway by degradation of IRS-1. Reduction of IRS-1 is paralleled by a decreased Akt-activity that results in a reduced protein synthesis and an increased protein degradation, which eventually mediate muscle atrophy. Inhibition of IL-6/gp130 signalling by *IL6st*-knockdown (e.g. *Il6st* siRNA and *Il6st* cKO), JAK2 (e.g. AG490), or STAT3 inhibition (e.g. C188-9 and S3i-201) prevents IL-6-induced *SOCS3* expression as well as myocyte atrophy *in vitro* and skeletal muscle atrophy in vivo. Red arrows indicate changes related to increased IL-6 plasma levels. Fbxo32 indicates F-box protein 32; Gp130, glycoprotein 130; IRS-1, insulin receptor substrate-1; IL-6, interleukin 6; IL-6Rα, interleukin 6 receptor alpha; JAK2, Janus kinase-2; MuRF1, muscle-specific RING finger protein 1; PDK1, 3-phosphoinositide-dependent protein kinase 1; PI3K, phosphatidylinositol 3-kinase; SOCS3, suppressor of cytokine signalling 3; STAT3, signal transducer and activator of transcription 3; Trim63, tripartite motif containing 63. Created with BioRender.com.

by the sensitivity of the model systems, the cell types and the experimental setup used. In our hands, Akt phosphorylation was significantly inhibited in the skeletal muscle of septic mice. In addition, when we preincubated myocytes with IL-6 prior to insulin treatment, insulin-induced IRS-1 and Akt phosphorylation were attenuated, suggesting that IL-6 interferes with insulin signalling in myocytes. Further studies are needed to examine the mechanisms behind IL-6-induced insulin resistance. Based on our data and the body of literature, we conclude that in sepsis, IL-6 via the gp130/JAK2/STAT3/SOCS3 pathway mediates skeletal muscle atrophy by increasing protein degradation and decreasing protein synthesis.

Interestingly, we found a discrepancy between *Trim63* mRNA expression and MuRF1 protein levels in muscle of septic cKO mice. Our data implicate that IL-6 does not increase *Trim63* expression, but possibly increases its translation or its protein stability, or reduces its degradation. Further studies are needed to address this observation.

As a beta-receptor, gp130 is shared by the IL-6 cytokine family consisting of IL-6, IL-11, CNF, LIF, OSM, CT-1, CLCF1, and IL-27.[37] Our RNAseq data showed that the expression of genes involved in IL-6 signalling were increased in muscle of septic mice, whereas the expression of the other IL-6 family members and their receptors was not as much increased or even reduced. Increased IL-6 plasma levels are a risk factor for CIM, and IL-6 strongly induces the JAK/STAT pathway and induces myocyte atrophy *in vitro*. We therefore suggest that IL-6 plays the predominant role among the IL-6 family for sepsis-induced muscle atrophy. However, the involvement of other IL-6 family members in ICUAW warrants further studies.

Conclusion

IL-6 plasma levels are increased in critically ill human patients and mice with polymicrobial sepsis. IL-6 acts on myocytes via the gp130 and IL-6Rα-complex and activates JAK2- and STAT3-signalling, which leads to an increased expression of *SOCS3* (*Figure* 7). SOCS3 functions as a negative regulator of cytokine signalling and inhibits the growth promoting insulin/insulin-receptor/Akt pathway by degradation of IRS-1. Reduction of IRS-1 is paralleled by a decreased Akt-activity that results in a reduced protein synthesis and an increased protein degradation, which eventually mediate muscle atrophy. Inhibition of IL-6/gp130 signalling by *IL6st*-knockdown (e.g. *Il6st* siRNA and *Il6st* cKO), JAK2 (e.g. AG490) or STAT3 inhibition (e.g. C188-9 and S3i-201) prevents IL-6-induced *SOCS3* expression as well as myocyte atrophy in vitro and skeletal muscle atrophy *in vivo* (*Figure* 7). In summary, IL-6 via the gp130/JAK2/STAT3-pathway mediates sepsis-induced muscle atrophy and possibly contributes to ICUAW. An inhibition of this pathway in muscle could be beneficial to prevent sepsis-induced muscle wasting.

Limitations

Our in vitro experiments were performed in murine C2C12 myotubes. Further analyses of primary murine and/or human myocytes are needed to independently confirm our observations about the role of IL-6/gp130/JAK2/STAT3 signalling in myocyte atrophy *in vitro*. In human patients, sepsis frequently occurs at the extremes of ages, especially in elderly patients. Here, we have used 12–20-week-old mice, which relates to a young age in human patients. Although our data are informative for a younger age, further studies on mature (12-month-old) and aged mice (24-month-old) are needed[38] to provide data that are more relevant to the elderly population. Because, we have used only male mice for our experiments, further sex-specific studies are needed to elucidate if IL-6 signalling is equally important for sepsis-induced muscle atrophy in female mice.

Acknowledgements

We thank Claudia Langnick for excellent technical assistance. We are grateful to Klaus Rajewsky for providing the conditional *Il6st* knockout mice, Daniele Sunaga-Franze for help with bioinformatics, and Wei Chen and Bin Zhang for performing RNA sequencing. This study was supported by the *Deutsche Forschungsgemeinschaft* [FI 965/5-1, FI 965/5-2, FI 965/9-1 (to J.F.)] and the German Center for Cardiovascular Research, partner site Greifswald [DZHK 81Z5400153 (to J. F.)] and the Berlin Institute of Health [TRG3-1.2.3 400219 to (J.F., C.B., and S.W.C.)]. The authors of this manuscript certify that they comply with the ethical guidelines for authorship and publishing in the *Journal of Cachexia, Sarcopenia and Muscle*.[39]

Online supplementary material

Additional supporting information may be found online in the Supporting Information section at the end of the article.

Table S1. Primer pairs for genotyping of *Il6st* cKO and *Il6st* WT mice.
Table S2. Primer pairs for quantitative real-time-PCR.
Table S3. Body and organ weights 96 hours after CLP or sham surgery of *Il6st* WT and *Il6st* KO mice
Table S4. Body and organ weights 96 hours after CLP or sham surgery of AG490 and solvent treated WT mice

Figure S1. Differentially expressed genes in muscle of septic mice. Voronoi tree map of differentially expressed genes (**log$_2$** fold change $\geq$2, adjusted p-value$<$0.05) in TA muscles

of WT mice after 24 (left) or 96 hours (right) after CLP surgery compared to sham treated controls (n = 3 for each condition). Every tile (small polygon) represents one gene. Tiles are arranged and coloured according to the hierarchical KEGG pathway maps (larger regions correspond to functional categories). The diagrams show three hierarchical KEGG pathway levels (top three panels) and the level of individual genes (bottom panel) per time point (24 hours: left panels, 96 hours: right panels). Tile sizes represent changes in gene expression.

Figure S2. Genes up- and downregulated in muscle of septic mice. Significantly up (top) or down (bottom) regulated genes in TA muscle of WT mice 24 (left) or 96 hours (right) after sham or CLP surgery. Analyses for GO-terms and KEGG-pathways are shown (n = 3 for each condition). Data are p-values and presented as $-\log_{10}$

Figure S3. Decreased Genes in muscle of septic mice. Venn Diagram showing the number of genes that were decreased ($\log_2$ fold change ≥ 2, adjusted p-value<0.01) in the tibialis anterior muscle of CLP-treated compared to sham treated mice after 24 (left) or 96 hours (right) or at both time points (bottom) (n = 3 for each condition). Data are p-values and presented as $-\log_{10}$.

Figure S4. Regulated genes involved in IL-6 production. Heat map of genes contained in GO:0032635-IL-6 production that were significantly regulated ($p<0.05$) in TA muscle of WT mice 24 hours and 96 hours after CLP or sham surgery (n = 3 for each condition).

Figure S5. Regulated genes involved in JAK-STAT signalling. Heat map of genes contained in GO:0007259-receptor signalling pathway via JAK-STAT that were significantly regulated ($p<0.05$) in TA muscle of WT mice 24 hours and 96 hours after CLP or sham surgery (n = 3 for each condition).

Figure S6. Inhibition of STAT3 attenuates IL-6 induced myotube atrophy *in vitro*. Frequency distribution histograms showing the width of differentiated C2C12 myocytes after 24 hours of treatment with solvent or IL6 after preincubation with DMSO or S3i-201 (n = 100 cells for each condition). Bar graph showing mean myotube width ± SEM. *P <0.05 (Student's t-test).

Figure S7. Deletion of *Il6st* in myocytes does not affect interleukin 6 plasma levels in septic mice. (A) Quantitative RT-PCR analysis of Il6st mRNA expression in TA muscle of WT and Il6st cKO mice 96 hours after sham or CLP surgery (WT: Sham n=6, CLP: n=15; cKO: Sham: n=6; CLP: n=10). **(B)** IL-6 plasma concentrations from the same mice. Data information: Data are presented as mean ± SEM. **P <0.01, ***P <0.001 (Mann-Whitney U test).

Figure S8. Deletion of *Il6st* in myocytes attenuates sepsis-induced *Socs3* expression and MuRF1 protein content. **(A)** Quantitative RT-PCR analysis of Socs3 mRNA content in TA muscle of Il6st cKO and WT mice 96 hours after CLP or sham operation (WT Sham, n=6; WT CLP, n=15; KO Sham, n=6; KO CLP, n=10). Data are presented as mean ± SEM **P < 0.01, ***P < 0.001 (Mann-Whitney U test). **(B)** Immunoblots with anti-Atrogin-1, anti-MuRF1 and anti-GAPDH antibodies in TA muscle of Il6st cKO and WT mice 24 hours after CLP or sham operation (n = 3 for each condition).

Figure S9. Inhibition of JAK2 attenuates sepsis-induced *Socs3* and *Trim63* expression and MuRF1 protein content in gastrocnemius and plantaris muscle. (A) Immunoblots with anti-pSTAT3 Y705, anti-STAT3, anti-Atrogin-1, anti-MuRF1 and anti-GAPDH antibodies in GP muscle of AG490 or solvent treated WT mice 96 hours after CLP or sham surgery (n = 3 for each condition). Bar graph showing the ratio of the relative densities of pSTAT3 Y705 and STAT3 protein contents as detected in B. B-F Quantitative RT-PCR analysis of *Socs3* **(B)**, *Trim63* **(C)**, *Fbxo32* **(D)**, *Myh2* **(E)** and *Myh4* **(F)** mRNA expression in GP muscle of AG490 or solvent treated WT mice 96 hours after CLP or sham surgery (AG490: sham: n=5, CLP: n=15; solvent: sham: n=5, CLP: n=15). Data information: (B-F) Data are presented as mean ± SEM. *P $<$ 0.05, **P $<$ 0.01 (Mann-Whitney U test).

Conflict of interest

Lukas Zanders, Melanie Kny, Alexander Hahn, Sibylle Schmidt, Sebastian Wundersitz, Mihail Todiras, Ines Lahmann, Arnab Bandyopadhyay, Tobias Wollersheim, Lars Kaderali, Friedrich C. Luft, Carmen Birchmeier, Steffen Weber-Carstens, and Jens Fielitz declare that they have no conflict of interest.

References

1. Ali NA, O'Brien JM Jr, Hoffmann SP, Phillips G, Garland A, Finley JC, et al. Acquired weakness, handgrip strength, and mortality in critically ill patients. *Am J Respir Crit Care Med* 2008;**178**:261–268.
2. Sharshar T, Bastuji-Garin S, Stevens RD, Durand MC, Malissin I, Rodriguez P, et al. Presence and severity of intensive care unit-acquired paresis at time of awakening are associated with increased intensive care unit and hospital mortality. *Crit Care Med* 2009;**37**:3047–3053.
3. Herridge MS, Tansey CM, Matte A, Tomlinson G, Diaz-Granados N, Cooper A, et al. Functional disability 5 years after acute respiratory distress syndrome. *N Engl J Med* 2011;**364**:1293–1304.
4. Wollersheim T, Woehlecke J, Krebs M, Hamati J, Lodka D, Luther-Schroeder A, et al. Dynamics of myosin degradation in intensive care unit-acquired weakness

during severe critical illness. *Intensive Care Med* 2014;**40**:528–538.
5. Puthucheary ZA, Rawal J, McPhail M, Connolly B, Ratnayake G, Chan P, et al. Acute skeletal muscle wasting in critical illness. *JAMA* 2013;**310**:1591–1600.
6. Bierbrauer J, Koch S, Olbricht C, Hamati J, Lodka D, Schneider J, et al. Early type II fiber atrophy in intensive care unit patients with nonexcitable muscle membrane. *Crit Care Med* 2012;**40**:647–650.
7. Bodine SC, Latres E, Baumhueter S, Lai VK, Nunez L, Clarke BA, et al. Identification of ubiquitin ligases required for skeletal muscle atrophy. *Science* 2001;**294**:1704–1708.
8. Weber-Carstens S, Deja M, Koch S, Spranger J, Bubser F, Wernecke KD, et al. Risk factors in critical illness myopathy during the early course of critical illness: a prospective observational study. *Crit Care* 2010;**14**:R119.
9. Winkelman C. The role of inflammation in ICU-acquired weakness. *Crit Care* 2010;**14**: 186.
10. Huang N, Kny M, Riediger F, Busch K, Schmidt S, Luft FC, et al. Deletion of Nlrp3 protects from inflammation-induced skeletal muscle atrophy. *Intensive Care Med Exp* 2017;**5**:3.
11. Langhans C, Weber-Carstens S, Schmidt F, Hamati J, Kny M, Zhu X, et al. Inflammation-induced acute phase response in skeletal muscle and critical illness myopathy. *PLoS One*. 2014;**9**:e92048, https://doi.org/10.1371/journal.pone.0092048
12. Hahn A, Kny M, Pablo-Tortola C, Todiras M, Willenbrock M, Schmidt S, et al. Serum amyloid A1 mediates myotube atrophy via Toll-like receptors. *J Cachexia Sarcopenia Muscle* 2020;**11**:103–119.
13. Tierney MT, Aydogdu T, Sala D, Malecova B, Gatto S, Puri PL, et al. STAT3 signaling controls satellite cell expansion and skeletal muscle repair. *Nat Med* 2014;**20**: 1182–1186.
14. Hoene M, Runge H, Haring HU, Schleicher ED, Weigert C. Interleukin-6 promotes myogenic differentiation of mouse skeletal muscle cells: role of the STAT3 pathway. *Am J Physiol Cell Physiol* 2013;**304**:C128–C136.
15. Bonetto A, Aydogdu T, Kunzevitzky N, Guttridge DC, Khuri S, Koniaris LG, et al. STAT3 activation in skeletal muscle links muscle wasting and the acute phase response in cancer cachexia. *PLoS One* 2011;**6**:e22538, https://doi.org/10.1371/journal.pone.0022538
16. Bonetto A, Aydogdu T, Jin X, Zhang Z, Zhan R, Puzis L, et al. JAK/STAT3 pathway inhibition blocks skeletal muscle wasting downstream of IL-6 and in experimental cancer cachexia. *Am J Physiol Endocrinol Metab* 2012;**303**:E410–E421.
17. Wen Z, Zhong Z, Darnell JE Jr. Maximal activation of transcription by Stat1 and Stat3 requires both tyrosine and serine phosphorylation. *Cell* 1995;**82**:241–250.
18. Heinrich PC, Behrmann I, Muller-Newen G, Schaper F, Graeve L. Interleukin-6-type cytokine signalling through the gp130/Jak/STAT pathway. *Biochem J* 1998;**334**: 297–314.
19. Babon JJ, Kershaw NJ, Murphy JM, Varghese LN, Laktyushin A, Young SN, et al. Suppression of cytokine signaling by SOCS3: characterization of the mode of inhibition and the basis of its specificity. *Immunity* 2012;**36**:239–250.
20. Rui L, Yuan M, Frantz D, Shoelson S, White MF. SOCS-1 and SOCS-3 block insulin signaling by ubiquitin-mediated degradation of IRS1 and IRS2. *J Biol Chem* 2002;**277**: 42394–42398.
21. Rommel C, Bodine SC, Clarke BA, Rossman R, Nunez L, Stitt TN, et al. Mediation of IGF-1-induced skeletal myotube hypertrophy by PI(3)K/Akt/mTOR and PI(3)K/Akt/GSK3 pathways. *Nat Cell Biol* 2001;**3**:1009–1013.
22. Yoshida T, Delafontaine P. Mechanisms of IGF-1-mediated regulation of skeletal muscle hypertrophy and atrophy. *Cells* 2020; **9**:1970, https://doi.org/10.3390/cells9091970
23. Weber-Carstens S, Schneider J, Wollersheim T, Assmann A, Bierbrauer J, Marg A, et al. Critical illness myopathy and GLUT4: significance of insulin and muscle contraction. *Am J Respir Crit Care Med* 2013;**187**:387–396.
24. Betz UA, Bloch W, van den Broek M, Yoshida K, Taga T, Kishimoto T, et al. Postnatally induced inactivation of gp130 in mice results in neurological, cardiac, hematopoietic, immunological, hepatic, and pulmonary defects. *J Exp Med* 1998;**188**: 1955–1965.
25. Busch K, Kny M, Huang N, Klassert TE, Stock M, Hahn A, et al. Inhibition of the NLRP3/IL-1beta axis protects against sepsis-induced cardiomyopathy. *J Cachexia Sarcopenia Muscle* 2021;https://doi.org/10.1002/jcsm.12763
26. Haberecht-Muller S, Kruger E, Fielitz J. Out of control: the role of the ubiquitin proteasome system in skeletal muscle during inflammation. *Biomolecules* 2021;**11**:1327, https://doi.org/10.3390/biom11091327
27. Puppa MJ, Gao S, Narsale AA, Carson JA. Skeletal muscle glycoprotein 130's role in Lewis lung carcinoma-induced cachexia. *FASEB J* 2014;**28**:998–1009.
28. Silva KA, Dong J, Dong Y, Dong Y, Schor N, Tweardy DJ, et al. Inhibition of Stat3 activation suppresses caspase-3 and the ubiquitin-proteasome system, leading to preservation of muscle mass in cancer cachexia. *J Biol Chem* 2015;**290**: 11177–11187.
29. Peña G, Cai B, Deitch EA, Ulloa L. JAK2 inhibition prevents innate immune responses and rescues animals from sepsis. *J Mol Med (Berl)* 2010;**88**:851–859.
30. Gyurkovska V, Ivanovska N. Tyrosine kinase inhibitor tyrphostin AG490 reduces liver injury in LPS-induced shock. *Eur J Pharmacol* 2015;**751**:118–126.
31. Hui L, Yao Y, Wang S, Yu Y, Dong N, Li H, et al. Inhibition of Janus kinase 2 and signal transduction and activator of transcription 3 protect against cecal ligation and puncture-induced multiple organ damage and mortality. *J Trauma* 2009;**66**: 859–865.
32. Vannucchi AM. Ruxolitinib versus standard therapy for the treatment of polycythemia vera. *N Engl J Med* 2015;**372**:1670–1671.
33. Verstovsek S, Gotlib J, Mesa RA, Vannucchi AM, Kiladjian JJ, Cervantes F, et al. Long-term survival in patients treated with ruxolitinib for myelofibrosis: COMFORT-I and -II pooled analyses. *J Hematol Oncol* 2017;**10**:156.
34. Hideshima T, Nakamura N, Chauhan D, Anderson KC. Biologic sequelae of interleukin-6 induced PI3-K/Akt signaling in multiple myeloma. *Oncogene* 2001;**20**:5991–6000.
35. Gao S, Durstine JL, Koh HJ, Carver WE, Frizzell N, Carson JA. Acute myotube protein synthesis regulation by IL-6-related cytokines. *Am J Physiol Cell Physiol* 2017;**313**: C487–C500.
36. Kortylewski M, Feld F, Kruger KD, Bahrenberg G, Roth RA, Joost HG, et al. Akt modulates STAT3-mediated gene expression through a FKHR (FOXO1a)-dependent mechanism. *J Biol Chem* 2003;**278**: 5242–5249.
37. Tanaka T, Narazaki M, Kishimoto T. IL-6 in inflammation, immunity, and disease. *Cold Spring Harb Perspect Biol* 2014;**6**:a016295, https://doi.org/10.1101/cshperspect.a016295
38. Turnbull IR, Wlzorek JJ, Osborne D, Hotchkiss RS, Coopersmith CM, Buchman TG. Effects of age on mortality and antibiotic efficacy in cecal ligation and puncture. *Shock* 2003;**19**:310–313.
39. von Haehling S, Morley JE, Coats AJS, Anker SD. Ethical guidelines for publishing in the *Journal of Cachexia, Sarcopenia and Muscle*: update 2017. *J Cachexia Sarcopenia Muscle* 2019;**10**:1143–1145.

Mein Lebenslauf wird aus datenschutzrechtlichen Gründen in der elektronischen Version meiner Arbeit nicht veröffentlicht.

Publication List

Publications

1. **Zanders L**, Kny M, Hahn A, Schmidt S, Wundersitz S, Todiras M, et al. Sepsis induces interleukin 6, gp130/JAK2/STAT3, and muscle wasting. *J Cachexia Sarcopenia Muscle.* 2021. (Impact Factor 12.06)

2. Abdelwahed YS, **Zanders L**, Landmesser U, and Leistner DM. Acute coronary syndrome by two different spontaneous coronary artery dissection types in two different vessels. *Cardiovasc Interv Ther.* 2021. (Impact Factor 1.61)

Congress reports

1. **Zanders L**, Kny M, McShane E, Lahmann I, Selbach M, Birchmeier, Fielitz J. Muscular glycoprotein 130 mediates inflammation-induced muscle atrophy in mice. *Hans-Blöhmer Young Investigator Award, German Association of Cardiology*, Mannheim 2017

2. **Zanders L**, Kny M, McShane E, Lahmann I, Schmidt S, Selbach M, Birchmeier, Fielitz J. Muscular glycoprotein 130 mediates inflammation-induced muscle atrophy in mice. *Scientific Sessions, European Students' Conference* Berlin 2017

3. **Zanders L,** Kny M, McShane E, Lahmann I, Schmidt S, Selbach M, Birchmeier, Fielitz J. Muscular glycoprotein 130 mediates inflammation-induced muscle atrophy in mice. *Poster Sessions, Leopoldina Symposium Evolution in Intensive Care Medicine,* Berlin 2017

Acknowledgements

This work would not have been possible without the input, help and support of people, to who I am deeply grateful:

Prof. Jens Fielitz MD for his excellent supervision, approachability and productive discussions throughout the lab time with all its ups and downs.

Melanie Kny PhD for her accurate teaching and supervision of crucial techniques, theoretical and practical support during and after the wet lab work. Dörte Lodka PhD for her support, interesting discussions and productive input.

Sebastian Wundersitz MD for the important and entertaining discussions, long evenings and weekends in the lab and shared suffering. Alexander Hahn PhD and Cristina Pablo Tortola PhD for their input and methodological support.

Sibylle Schmidt for her excellent technical assistance and really interesting lunch breaks.

My family, first and foremost Stefanie Breining for their enduring support and open ears.